Simulations of Complex Synergies in bcc-Fe under Multi-Ion Irradiation Using Stochastic Cluster Dynamics

by

Tuan Luong Hoang

A dissertation submitted in partial satisfaction of the

requirements for the degree of

Doctor of Philosophy

in

Engineering - Nuclear Engineering

in the

Graduate Division

of the

University of California, Berkeley

Committee in charge:

Professor Peter Hosemann, Chair

Professor Daryl C. Chrzan, Co-Chair

Doctor Vasily V. Bulatov (LLNL)

Fall 2014

Simulations of Complex Synergies in bcc-Fe under Multi-Ion Irradiation Using Stochastic Cluster Dynamics

by

Tuan Luong Hoang

Abstract

Simulations of Complex Synergies in bcc-Fe under Multi-Ion Irradiation Using Stochastic Cluster Dynamics

by

Tuan Luong Hoang

Doctor of Philosophy in Engineering - Nuclear Engineering

University of California, Berkeley

Professor Peter Hosemann, Chair

Professor Daryl C. Chrzan, Co-Chair

The objective of the reported study is to develop the much-needed computational bridge for connecting the accelerated irradiation tests to the expected material performance in the future fission/fusion reactors. This new computational model serves as an alternative to traditional mean-field ODE-based reaction rate theory (RT) models which come with intrinsic disadvantages that cause simulations of complex microstructure evolution under multi-ion irradiation conditions to become prohibitively expensive to handle. Our stochastic cluster dynamics (SCD) model enables efficient simulation of complex damage accumulation in materials irradiated to practical damage doses with reasonable computing time and resources. SCD obviates the need to solve the exceedingly large sets of ODEs and relies instead on the sparse stochastic sampling from the underlying kinetic Master Equation (ME). We then apply the SCD model to simulate multi-ion irradiation experiments of Fe^{3+}, He^{+} and H^{+} on bcc-Fe and provide explanation to the synergistic effects observed in the triple-beam experiments carried out at the Japanese Takasaki Ion Accelerator for Advanced Radiation Application (TIARA) facility. We also propose the employment of pulsed single/dual-beam irradiations as possible alternatives to steady triple-beam irradiation for investigation of materials used for nuclear applications.

To my family ...

for their love and support

Contents

List of Algorithms

List of Figures

List of Tables

Acknowledgements

I would like to dedicate this work to my grandfather. Without his service and sacrifice for his mother country, South Vietnam, I would not have the opportunity to come to America, where all exciting things happen. My grandfather did the tough job planting the seeds that I now simply harvest the sweet fruits. I want to thank America, my adopted country, for giving me the opportunity to reunite with my big family, start a new life and make dreams come true. I also want to thank UC Berkeley, especially the Nuclear Engineering Department for admitting me as a graduate student in 2008. For me, it is a true honor to be a part of such a wonderful community. I appreciate the financial supports from the UC Berkeley Chancellor's Fellowship, the Nuclear Regulatory Commission Fellowship and the Lawrence Scholar Program at Lawrence Livermore National Laboratory, which gave me complete freedom to pursue the research that I was most excited about.

I would like to thank my advisors and mentors, Prof. Peter Hosemann, Prof. Daryl C. Chrzan, Prof. Jaime Marian, and Dr. Vasily V. Bulatov, for their valuable advice, outstanding guidance, constant encouragement and constructive criticism during my tenure at UC Berkeley and LLNL. It has been my privilege and great pleasure to work with such exceptional scholars. Their knowledge, insight and vision played a tremendous role in the successful completion of this dissertation. I am also grateful for the opportunities to work or discuss with Prof. Brian D. Wirth, Dr. Athanasios Arsenlis, Dr. Babak Sadigh, Dr. Alexander Stukowski, Dr. Sylvain Queyreau, Dr. Donghua Xu, Dr. Hyon-Jee Lee Voigt, and soon-to-be Dr. David Cereceda. Brian made me change my mind and decide to come to Berkeley in the last minute, yet it turned out that I would never wish to leave this area ever since. This university, this environment has helped me better understand my inner self, and my true passion and has given me the inspiration and courage to keep exploring, learning, or trying and breaking things. I guess that what is called the Golden Bear spirit. Tom was my host during my first summer internship at LLNL, and three months was enough for him to leave a long-lasting influence on me, personally and professionally. I also published my first scientific paper with Tom. Alex was extremely helpful with his programming expertise. With David, I shared the love for sailing, hiking and salsa dancing, I hope someday we will sail to New Zealand, Norway and the Mediterranean together, on our own boat.

I also wish to express my gratitude to Prof. Eric B. Norman for serving as the Chairman of my qualifying examination, and to Lisa Zemelman for her outstanding service to the department and the graduate students. I also want to thank Prof. Lin Shao, Prof. Marvin L. Adams and Prof. William H. Marlow for their support during my wonderful years at Texas A&M University. Lin showed me the beauty of condensed matter physics and materials science, and has always been a great mentor, and a great friend.

I want to thank my friends: Cuong Nguyen, Dai Bui, Ned Nguyen, Long Tran, Hanh-Phuc Le, and Thuan Bao for spending time working with me on several start-up ideas. I have learnt and improved tremendously from these precious experiences, especially on what I should not do. My thanks also go to my dear friends at UC Berkeley and LLNL, who make me feel like home away from home.

I would like to thank all the members of the Wirth's, Hosemann's and Chrzan's research groups at UC Berkeley and everyone in the Computational Materials Science Group at LLNL for their help and company.

Last but not least, I want to express my overwhelming thank to my big family in Texas, for their love and support, and to my beautiful girlfriend, Khuong Nou, who makes me become a better man. I love you all.

Chapter 1

Introduction

1.1 Concerns on simulation of materials used for nuclear applications

The Catch-22 in the design of Advanced Nuclear Energy Systems (ANES) is that they must be built with materials whose performance over long periods of time can be fully assessed only after the reactor is built and operated over those periods. The unknown limits of material performance constrain the parameter space and introduce perhaps unnecessary conservatism into the design. To break this circular dependence, materials R&D for ANES can and should employ accelerated material testing and not rely exclusively on reactor over-design and periodic surveillance. Multi-ion beam irradiation facilities in Japan, Europe and the US combine several ion accelerators to generate high particle fluxes to impart the same total damage in a matter of days as the material would receive over its entire work life in a nuclear reactor [13]. What remains unclear is whether the material degradation (or lack of thereof) observed over six hours of an accelerated violent irradiation test can be used to predict the behavior of the same material over the much longer nuclear reactor exposures. The utility of ion-accelerator facilities for irradiation testing rests upon the premise that materials theory and numerical simulations can provide a reliable connection between accelerated tests and material nuclear performance limits.

For simulations to serve in this important role, two conditions must be in place: (1) the material models must be accurate and (2) the simulations should be able to extend to the time scales of accelerated irradiation tests ($\sim 10^4$ s) and the expected material working life in the reactor ($\sim 10^8$ s). As always, these two requirements of accuracy and computational efficiency are difficult to meet simultaneously – accuracy is often traded for efficiency. In the wide spectrum of existing theoretical approaches to irradiation damage kinetics, the Rate Theory (RT) has been the workhorse method for material simulations integrated in the reactor design practice for over 40 years. As is well known, RT achieves its unparalleled efficiency at a cost of drastic simplifications in the description of spatial distributions of defects (none) and treatment of defect sinks. The last 7-10 years have witnessed several breakthrough developments in computational materials sciences that

are particularly relevant for simulations of irradiated materials and can be brought to improve accuracy of the Rate Theory method. The two key advances are: (1) direct Dislocation Dynamics simulations of crystal strength and (2) Monte Carlo simulations of reaction-diffusion processes with full spatial resolution (beyond mean-field). The push is to replace the commonplace use of RT with its crude assumptions with a new generation of simulation methods of much higher fidelity (smaller uncertainty) and fewer assumptions. The work reported in this dissertation is an integral component of these on-going efforts.

Our ultimate goal is to obtain accurate and efficient prediction of material degradation on the reactor timescales benchmarked by accelerated irradiation tests. In order to establish and maintain a close connection to on-going irradiation research at LLNL that focuses on complex materials such as ODS steels, it is necessary to direct theoretical development to the RT method that covers the same time scales as in the irradiation tests. The specific technical challenges that we intend to overcome is the current inability of the RT method to deal with complex defect populations, such as multi-component particle-reinforced ferritic steels.

We develop a novel stochastic implementation of RT, to be referenced hereafter as Stochastic Cluster Dynamics (SCD) that overcomes a well-known limitation of the standard RT method in simulations of complex materials. Specifically, the major bottleneck in the standard RT method is that simulations of realistically complex materials require solving exceedingly large sets of ordinary differential equations for the different components of the defect cluster populations. Consequently, the RT simulations are presently limited to relatively simple materials in which defect populations can have no more than two size attributes. This limitation can be overcome by re-casting the Rate Theory into a discrete stochastic framework that operates with integer-valued defect populations in a finite material volume, rather than with fractional defect concentrations in an infinite material. The advantage of using the discrete population is that computational complexity of RT simulations is no longer defined by the complexity of defect species (clusters) but by the selected simulation volume. This very idea has been put forward by Dan Gillespie in 1976 [1] and has since gained wide acceptance in the bio-chemistry and cell biology fields [2, 3, 4]. Remarkably, this idea has been completely overlooked by the nuclear engineering community, and here we propose to remedy this unfortunate oversight.

1.2 The physics of radiation damages

Materials used in extremely hostile environments such as inside nuclear fission/fusion reactors are subject to high radiation fluxes. As a result, an extremely large number of non-equilibrium point defects are produced due to the collisions of the energetic incident particles with lattice atoms in the solids. Upon collisions, lattice atoms will be displaced from their original positions if the energies gained from these collisions are larger than the energies binding them to their lattice sites, namely the displacement threshold energies. We call those atoms that situate between perfect lattice sites interstitial atoms, and if these interstitial atoms are of the same nature with atoms of the matrix lattice, they

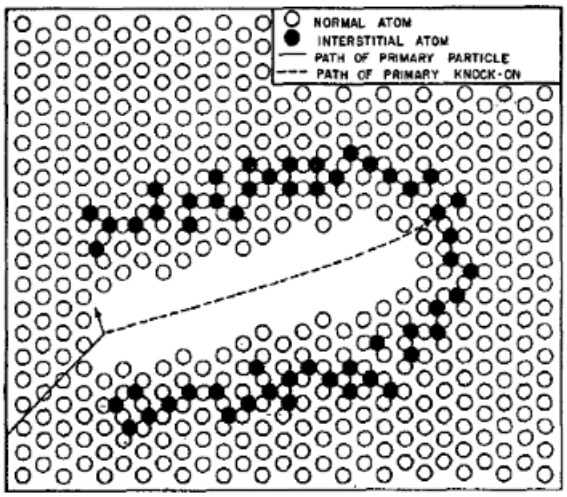

Figure 1.1: Simple version of a displacement spike caused by neutron bombardment on a material lattice [5].

are termed self interstitial atoms (SIAs). On the other hand, the empty spaces left behind by the displaced atoms are called vacancies. The combination of an interstitial and a vacancy is termed a Frenkel pair. The fate of these defects depends on various reactions that occur following production of the displacement cascades/sub-cascades such as annihilation, recombination, clustering or trapping of vacancies, interstitials and/or their clusters at microstructural features prior to long-range diffusion.

Fig. 1.1 shows a simple version of a thermal spike generated by the collisions of an initial incident particle with a matrix lattice. Such thermal spike normally lasts several ps, and the hot disordered core initially has some liquid-like characteristics. During this phase, most of the defects immediately (about less than 1 ps) annihilate after the formation of the collision cascades/sub-cascades, but strong disorder can stay for longer time (several ps). This process can be viewed as a short-term local melting of the matrix lattice followed by the rapid quenching of the liquid phase to form a damaged solid structure in the bombardment affected regions. During this final stage, the atoms that cannot regain their lattice sites become interstitial atoms at the periphery of the core, together with the vacancies produced when the core crystalizes while some atoms are mobile enough to depart from the depleted zone through thermally activated diffusion processes. The accumulation of mobile vacancies and vacancy-clusters consequently forms immobile cavities in the materials. This process directly competes with the migration of mobile vacancies to other defect sinks such as dislocations or grain boundaries which is dominant right after the formation of the radiation damage cascades [6]. The diffusional transport and evolution of defects and defect clusters will determine the effects of radiation on material microstructures and mechanical properties such as changes in creep rate, ductility, yield strength or fracture toughness. These changes significantly affect material

serviceability and lifetime in nuclear applications, as consequences [7].

Inside fission and fusion reactors, the combined effect of neutron-generated atomic displacements with He and H production from (n, α) and (n, p) transmutation reactions further degrades the mechanical and physical properties of the materials. Moreover, H isotopes are reactants of the fusion reactions while He is created as products, thus the effects on the structural materials due to these gas species are even more detrimental in fusion reactors.

1.3 Sources and effects of He in materials

In water-moderated fission reactors, He atoms are produced from the transmutation of $^{10}\mathrm{B}$, which comprises 19.9% of natural boron dissolved in the reactor coolant, or from the transmutation of nickel contained in reactor structural components through the $^{58}\mathrm{Ni}(\mathrm{n}, \gamma)\ ^{59}\mathrm{Ni}(\mathrm{n}, \alpha)$ two-step reaction sequence in amounts as low as a few parts per million (*appm*), or from the deuterium-tritium (D-T) reactions in fusion reactors [8, 76]. He is insoluble thus has the tendency to be absorbed at vacancy clusters, voids or other defect sinks, such as dislocations in the materials. In iron, He has been shown to have the ability to nucleate and stabilize He bubbles (i.e. He-V clusters) by suppressing the thermal vacancy emission and by promoting the thermal SIA emission, resulting in a significant increase of the lifetime of the clusters. Simulation studies have pointed out that He density, rather than the He-V cluster size determines the thermal emission rate of vacancy, He or SIA from the cluster [9]. Terentyev *et al.* went further and calculated the binding energies of vacancy and He atom to a $\mathrm{V_nHe_m}$ cluster as follows:

$$E_b\,(\mathrm{V}) = 1.59 + 3.01 log\left(\frac{\mathrm{m}}{\mathrm{n}}\right) + 2.70 log^2\left(\frac{\mathrm{m}}{\mathrm{n}}\right) \tag{1.1}$$

$$E_b\,(\mathrm{He}) = 2.20 - 1.55 log\left(\frac{\mathrm{m}}{\mathrm{n}}\right) - 0.53 log^2\left(\frac{\mathrm{m}}{\mathrm{n}}\right) \tag{1.2}$$

which apparently depend only on the density of He contained in the bubble [10].

Simulations using semi-empirical potentials done by Ventelon *et al.* revealed different interactions between He and SIA clusters, including a spontaneous SIA–substitutional He recombination and replacement mechanism that ejects He into interstitial positions and a strong interaction between He, in either interstitial or substitutional positions, with SIA and SIA clusters and also with other He atoms. These interactions are governed by elastic interactions between He atoms and SIA clusters. Ventelon's study also shows the relatively small interaction trapping radii of about 1 nm between interstitial He and SIA clusters, the binding energies between them are quite high from 1.3 to 4.4 eV, depending on cluster size and interaction geometry [11].

1.4 Sources and effects of H in materials

While He is relatively immobile and almost completely retained in the material, the retention of H is strongly influenced by the irradiation temperature, implantation rate

as well as the details of radiation-induced microstructures. H is also generated by the transmutation reactions in fission reactors, primarily from the various isotopes of nickel, especially ^{58}Ni. Besides, H can also be introduced into steels by other environmental processes such as corrosion, radiolytic decomposition of water, or direct injection from proton recoil following collisions of neutrons with H atoms in the water [8, 76].

H also has low solubility and diffuses throughout the material; it is known to be trapped at vacancy clusters, providing internal stabilization to these clusters. In most metals, H is attracted to defects that have associated regions of reduced electron densities and repelled where the electron densities are increased. The binding of H to SIA depends on the lattice distortions around the interstitial, however the binding energy is not as strong as that with a vacancy. H is quite mobile, e.g. at 300 °C, the average diffusion distances in austenitic steel are about 1 mm per day, 4 mm per month and 15 mm per year; for ferritic steels, these average distances increase by at least an order of magnitude. Protons born from (n, p) reactions may have a wide spectrum of energies with maximum energies of several MeV and maximum ranges of $6 - 16\,\mu m$. As a result, the loss of H at surfaces can be significant in some cases [8].

1.5 Synergistic effects developed in materials under multi-ion irradiation

To examine the physical and mechanical changes of materials due to irradiation, they are usually irradiated in nuclear reactors. However, this approach usually takes a very long time due to the unavailability of neutron sources that can accelerate the aging process. It is a traditional practice to define the irradiation dose in terms of "displacements per atom", or *dpa*. For example, an exposure to an irradiation dose of 50 *dpa* means that on average each atom in the materials has been displaced from its lattice site 50 times. In current operating nuclear reactors, the maximum dose for core internal structures of is limited to several *dpas* while, in order to reach maximum burn-up, fuel-cladding alloys must endure exposures that are significantly greater than 100 *dpa*. For some fast reactor applications, the component materials may be subjected to an irradiation dose of $200 - 250$ *dpa* [13, 55]. Besides, the irradiated samples are highly radioactive and require examination in hot cells. Since the material development normally takes several iterations of irradiation, testing and modification before an optimum material may be qualified for use in a reactor, this process can take up to several decades [55].

To overcome these adversities, charged particle irradiation has been widely employed to accelerate the testing process of materials used in nuclear applications. This approach has many advantages over neutron irradiation since it allows us to achieve higher damage rates and shorten the irradiation time. Beside the exclusion of radioactivity concerns, experimental conditions can be easily controlled in these ion-beam accelerators. However, charged particle irradiation in accelerated material testing facilities also comes with disadvantages. The biggest drawback is that the materials may not be subjected to simultaneous implantation of different element types as in actual nuclear reactors thus the

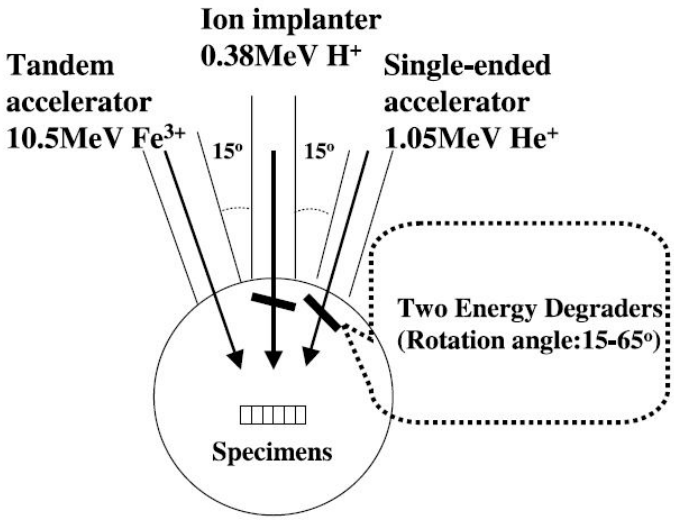

(A)

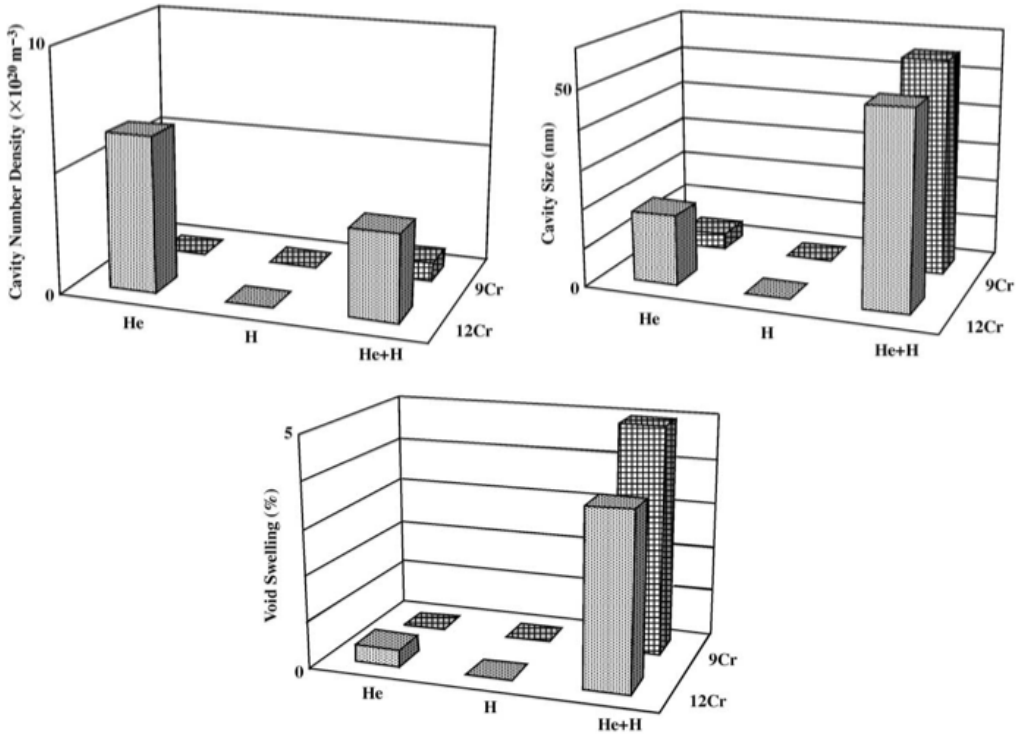

(B)

Figure 1.2: (A) Schematic configuration of the Japanese TIARA triple-ion beam facility. (B) Synergistic effects on cavity number density, size and swelling, developed in 9Cr and 12Cr alloys irradiated under various multi-beam conditions [14].

synergistic effects due to interactions between implanted species can be overlooked as a result.

Currently, a few multi-ion facilities around the world has enabled the simultaneous irradiation of materials by two or three different types of species [13]. Experimentally, it has been shown that sequential implantation of heavy ions, H and He does not produce conditions that are relevant to those observed in advanced nuclear energy systems. One example, experiments carried out at the TIARA triple-ion facility in Japan show that complex synergies are observed when Fe-Cr ferritic model alloys are irradiated with Fe^{3+}, He^{+} and H^{+} ions concurrently [14]. The swelling ratios measured in these alloys are significantly higher and noncumulative compared to those obtained from dual-ion experiments of Fe^{3+} with either He^{+} and H^{+} ion-implantation as shown in Fig. 1.2. Since H is a very chemically active element, even a very small amount of it can cause significant and synergistic effects with existing He atoms and dpa damages. Therefore, theoretical and experimental study of radiation damage evolution under multi-beam irradiation are both scientifically and technically important.

1.6 Scope of the dissertation

The primary objective of this dissertation is to develop a new computational model to investigate the evolution of complex radiation damage produced under multi-beam irradiation conditions, relevant to those exist inside nuclear fission/fusion reactors and accelerated material testing facilities. In Chapter 2, we introduce the stochastic cluster dynamics (SCD) model and the underlying theory, and main features of the model are also provided. In Chapter 3, computational enhancements to SCD model such as the implementation of the dynamic reaction network update and expansion, the τ-leaping method or the volume rescaling method are described, these enhancements allow SCD to handle radiation damage simulations that are otherwise prohibitively expensive when using current simulation methods. An application of the model is presented, the accuracy and the computational performance of the enhanced SCD model are examined. In Chapter 4, we discuss the observations from simulations of simultaneous irradiation of Fe^{3+}, He^{+} and H^{+} ions in pure bcc-Fe using SCD models and propose hypothesis for the cause of synergistic effects developed in Tanaka's experiments. In Chapter 5, using SCD, we investigate the feasibility of replacing triple-beam irradiation of Fe^{3+}, He^{+} and H^{+} ions by pulsed single/dual-beam irradiations in which, unlike the triple-beam irradiation case, Fe^{3+}, He^{+} and H^{+} ions are implanted in alternate pulses instead of simultaneously. This study is motivated by the fact that there are very few triple-beam irradiation facilities around the world available for nuclear material research while experiments carried out using sequential irradiation often overlook the synergies developed due to the interaction of transmutation gases and heavy ion damages. Through this study, we propose modification suggestions to the configurations of current dual-beam irradiation facilities that can allow them to produce similar results to those from triple-beam irradiation facilities. Chapter 6 concludes the present dissertation on computational modeling of complex ra-

diation damage evolution under multi-beam irradiation using SCD models, and related future research is briefly discussed.

Chapter 2

A new model for simulation of complex radiation damage evolution in materials

2.1 Limitations of current computational models

The production and accumulation of defects in materials subjected to irradiation is a multiscale problem spanning multiple orders of magnitude in time and space. For the last several decades, the rate theory (RT) method for solving coupled ordinary differential equation (ODE) systems has been the workhorse for irradiation damage simulations [12], mostly owing to its much greater computational efficiency compared to more detailed methods such as molecular dynamics (MD) or kinetic Monte Carlo (kMC). RT involves solving a set of coupled ODEs such as:

$$\frac{dC_\nu}{dt} = \dot{\mathcal{F}}_\nu - \dot{\mathcal{L}}_\nu, \qquad (\nu = 1, ..., N) \tag{2.1}$$

where each equation describes the time evolution of the average concentration of a particular type (species) of defect cluster denoted by index ν. The terms on the right hand side are the loss rate $\dot{\mathcal{L}}_\nu$ of species ν due to various kinetic processes, and the production rate $\dot{\mathcal{F}}_\nu$ of species ν due to irradiation and reactions involving defect cluster species other than ν. RT models achieve a high level of simulation efficiency at the cost of drastic simplifications in the underlying physical model, chief of which is the mean-field approximation that neglects spatial correlations and finite volume fluctuations. Another significant reduction in computational complexity is gained by limiting the number of species considered. In practice, the number of admissible defect species (and ODEs in the system) is truncated to achieve a satisfactory balance between accuracy and available computational resources. Large defect clusters not explicitly included in the set are accounted for only approximately (if at all) using a truncation model for the tail of the defect size distribution [91, 92] [1]. Once defined, the number of ODEs in the set must remain the same through

[1] Existing truncation schemes are ad hoc and unlikely to correctly capture the statistic of extreme values in the defect size distribution believed to be important for understanding material degradation

the simulation. To allow simulations to realistically high irradiation doses, this number may need to be as high as 10^6 even in the simplest materials, e.g. pure Fe. Furthermore, the number of distinct ODEs that need to be included in the set grows exponentially with increasing number of complex defect cluster types, e.g. simulations of V_mHe_n complexes of m vacancies and n He atoms requires $(m \times n)$ equations to be included. This is yet another case of combinatorial explosion where the number of equations to be solved is far too large for practical numerical simulations. Consequently, current RT models have been limited to defect populations having no more than two and, in most cases, only one size dimension. This need to allocate an ODE for every possible defect cluster type even before the simulation starts is a serious limitation of the ODE-based RT method.

To overcome these limitations, Marian and Bulatov recently introduced the stochastic cluster dynamics (SCD) model to model defect evolution in irradiated materials [15] which will be briefly described in the following subsections for clarity. The SCD model is based on the stochastic simulation algorithm (SSA) proposed originally by Gillespie for simulations of chemical kinetics in well-stirred systems [1]. Whereas RT is formulated in terms of average species concentrations that can take arbitrary fractional values, SSA considers integer-valued species populations in a finite volume and interprets the ODEs defining the RT model as a set of stochastic master equations (MEs). The so-defined species population is then evolved stochastically, one reaction at a time, following a standard kMC algorithm. SSA method has been widely used in the chemical engineering and biochemistry communities [2, 3, 4] but is still relatively unknown to computational materials scientists. SCD achieves additional efficiency through the use of dynamic data handling mechanisms where only defect clusters with non-zero populations are kept track of throughout the simulation time. This is a major advantage over traditional RT in which every admissible defect cluster must be allocated a variable and an equation that persist through all stages of the ODE integration. Importantly, the computational complexity of a SCD simulation is controlled by the value of the simulation volume and does not depend on the complexity (number of size dimensions) of admissible defect cluster types. Thus, SCD does not suffer from combinatorial explosion and can handle cluster populations with arbitrary number of size attributes.

Several proof-of-principle studies have been carried out to demonstrate the applicability of the SCD model to simulation of radiation damage evolution in irradiated materials [15]. Beside application in radiation damage simulation, our model can be easily adopted to simulate systems where diffusion-reaction processes are of interest such as advanced fuels [13], nuclear waster management [13], and ion-beam synthesis and transmutation doping of nano-structures [93].

---

under irradiation

2.2 The stochastic cluster dynamics (SCD)

2.2.1 Theory

The origins of standard RT and the SSA can be traced to the same fundamental reaction–diffusion master equation (ME) which has been widely used in the fields of biochemistry and cell biology [30, 31]. The mean-field assumption permits a drastic reduction of the ME, leading to a set of non-linear ODEs for the individual components of the species population in the reaction volume. Along the way, in order to obtain the needed equations for species concentrations, all spatial correlations among these species are ignored, and finite-volume fluctuations are deliberately suppressed by taking the limit of an infinite volume. The resulting ODEs for the average species concentrations then have the following forms:

$$\frac{dC_\nu}{dt} = \Gamma_\nu - \sum_\mu R\left(\nu \to \mu\right) C_\nu + \sum_\mu R\left(\mu \to \nu\right) C_\mu \\ - \sum_{\lambda\mu} K\left(\mu + \nu \to \lambda\right) C_\nu C_\mu + \sum_{\lambda\mu} K\left(\lambda + \mu \to \nu\right) C_\nu C_\mu \quad (2.2)$$

where, in the context of irradiation damage, the first term on the r.h.s, Γ_ν, represents the insertion or production rate (i.e. source term) of defect cluster ν due to external irradiation sources. The second and third terms correspond to single-species (1^{st}-order) reactions of conversion to and from defect of type μ, respectively. The fourth and the fifth terms correspond to two-species (2^{nd}-order) reactions leading to removal and creation of defect of type ν, respectively.

Here, species index ν is a shorthand notation for arbitrarily complex defect cluster $\nu = ijkl...$ in which index $i = 0,\ \pm1,\ \pm2, ...$ is the number of self-interstitial atoms (SIA) (+) or vacancies (-) in cluster ν, and indices $j,\ k,\ l, ... = 0,\ 1,\ 2,\ 3, ...$ are the number of atoms of some other elements contained in this cluster, e.g. He, H, C, etc. Given that C_ν's are expressed in unit of concentration, i.e. the average number of defect cluster ν per unit volume, the reaction rate constants must be expressed in the following units: $\text{m}^{-3}\text{s}^{-1}$ for Γ, s^{-1} for R, and m^{-3} for K.

2.2.2 The stochastic simulation algorithm (SSA)

SSA was first proposed by Gillespie in the 70s [1]. The key difference between the standard RT and the SSA is that, instead of solving the rate equations (i.e. the ODE system) for average concentrations of defects in an infinite volume, only integer-valued populations N_ν of chemical species in a finite volume V are considered in SSA. Then, rather than integrating the ODE system forward in time, SSA evolves the defect population in a stochastic manner, one reaction at a time by sampling the next reaction event and the time

it takes place. Over the years, Gillespie has presented substantial theoretical justification for his method [16, 31]. In particular, he showed that the SSA is equivalent to standard RT when the reaction volume under consideration is large enough, or in other words, the system is well-mixed, i.e.

$$\lim_{V\to\infty} \frac{N_\nu}{V} = C_\nu \tag{2.3}$$

Gillespie has also argued that his method is more faithful to the underlying ME than standard RT models in the sense that the system evolution given by the SSA is stochastic in nature. Therefore, SSA reproduces finite volume variations (fluctuations) in species population that otherwise have been averaged out in standard RT models. According to Gillespie, SSA is only accurate when the chemical components present in volume V are well-stirred, i.e. it is only valid for systems driven by reaction controlled kinetics. This assumption is generally accurate for bimolecular reactions in gaseous mixtures of reactants. However, in condensed matter systems the overall bi-molecular reaction rate is often diffusion-controlled which is limited by slow diffusion of species that react instantly upon collision. As a result, the applicability of SSA in its original form to systems where diffusion plays an important role is not guaranteed. At the same time, as we show in Section 2.3, it is possible to recast the RT formulation into a form of stochastic algorithm that reproduces the solution of standard RT in the limit of infinite volume, $V \to \infty$. Thus, the accuracy (or lack thereof) of resulting stochastic method in the context of irradiation damage derives from that of standard RT, which in turn, largely relies on the validity of the mean-field approximation for diffusion-controlled reactive systems representing irradiated materials.

The key step in our reformulation is to convert the reaction rates appearing in the standard RT into rates that are usable in a stochastic setting. To illustrate this rate conversion, it is sufficient to multiply both sides of Eq. 2.2 by the volume V and express the concentrations in terms of integer numbers of reactant species according to Eq. 2.3, i.e. $N_\nu = VC_\nu$. The resulting converted rate equations will then have the following forms:

$$\begin{aligned}\frac{dN_\nu}{dt} = \Gamma_\nu V - \sum_\mu R\left(\nu \to \mu\right) N_\nu + \sum_\mu R\left(\mu \to \nu\right) N_\mu \\ - \sum_{\lambda\mu} \frac{K\left(\mu+\nu\to\lambda\right)}{V} N_\nu N_\mu + \sum_{\lambda\mu} \frac{K\left(\lambda+\mu\to\nu\right)}{V} N_\nu N_\mu\end{aligned} \tag{2.4}$$

If we redefine the rates as: $\widetilde{\Gamma} = V\Gamma$, $\widetilde{R} = R$, and $\widetilde{K} = K/V$, then

$$\frac{dN_\nu}{dt} = \widetilde{\Gamma}_\nu - \sum_\mu \tilde{R}\left(\nu \to \mu\right) N_\nu + \sum_\mu \tilde{R}\left(\mu \to \nu\right) N_\mu \\ - \sum_{\lambda\mu} \tilde{K}\left(\mu + \nu \to \lambda\right) N_\nu N_\mu + \sum_{\lambda\mu} \tilde{K}\left(\lambda + \mu \to \nu\right) N_\nu N_\mu \quad (2.5)$$

We can consider Eq. 2.5 as the physical representation of a collection of possible reaction events characterized by reaction coefficients $\left\{\tilde{\Gamma},\ \tilde{R},\ \tilde{K}\right\}$ that can be sampled using any exact kMC algorithm, such as BKL [17]. In fact, Gillespie independently proposed an algorithm essentially identical to BKL that correctly samples stochastic trajectories from the distributions implied by Eq. 2.5. Other kMC algorithms developed for exact sampling of ME may also be used such as in Ref. [18]. Here we want to emphasize that regardless of the kMC algorithm chosen, the species population will be evolved stochastically, one reaction at a time. In Chapter 3, we will discuss the implementation of the τ-leaping method that allows us to leap through multiple reactions in one single simulation time step.

It will be evident in the subsequent discussion that the most important advantage of the SSA is that, at any given point in the simulation, only species with nonzero populations, i.e. those that actually exist in the finite volume V, are kept track of. By contrast, all possible species whose evolution is included in the ODE system must be dealt with at all stages of the ODE integration in standard RT models, thus causing a huge computational cost as a consequence. Therefore, the major advantage of the SSA method is that the number of existing species is controlled by the simulation volume V rather than by the combinatorial complexity of the defect clusters considered in the RT model. This situation is just another manifestation of the power of the Monte Carlo method that was originally proposed for efficient numerical calculations of multi-dimensional integrals, i.e. rather than covering the whole multi-dimensional space with a grid, the Monte Carlo method obtains a converging estimate of the integral by sparse sampling of the integrand values in randomly selected points [18].

2.2.3 Selection of reaction event and time to the next reaction

For clarity, we briefly summarize the SSA method developed by Gillespie for simulations of chemical reactions in well-stirred systems. The reader is referred to the original papers [1, 16] for more details of the method and the theory behind it. Consider a population containing N defect-clusters $S_1,\ S_2, ..,\ S_N$ that can participate in M reaction channels $\{\mathbb{R}_1,\ \mathbb{R}_2, ...,\ \mathbb{R}_M\}$. Let $\overrightarrow{X}(t)$ be the dynamic state vector of the system at an arbitrary time t, $\overrightarrow{X}(t) = \{X_1(t),\ X_2(t),\ ...,\ X_N(t)\}$, where $X_i(t)$ is the number of defect clusters of type S_i at time t. Each reaction channel is characterized by its reaction rate R_j and by its state change vector $\overrightarrow{\nu}_j = (\nu_{1j}, \nu_{2j},\ ..., \nu_{Mj})$. The probability that a reaction of

type j will take place within the next infinitesimal time interval $[t,\, t+dt)$ is given by the product $R_j dt$ whereas ν_{ij} specifies the change in the population of species S_i after a single reaction event along channel $\mathbb{R}_j$. The evolution of so-defined reaction network obeys the following chemical master equation (CME):

$$\frac{\partial P(\overrightarrow{x},\, t|\overrightarrow{x_0}, t_0)}{\partial t} = \sum_{j=1}^{M} [R_j(\overrightarrow{x} - \overrightarrow{\nu_j}) P(\overrightarrow{x} - \overrightarrow{\nu_j},\, t|\overrightarrow{x_0}, t_0) - R_j(\overrightarrow{x}) P(\overrightarrow{x},\, t|\overrightarrow{x_0}, t_0)] \quad (2.6)$$

where $P(\overrightarrow{x},\, t|\overrightarrow{x_0}, t_0)$ is the conditional probability that $\overrightarrow{X}(t) = \overrightarrow{x}$ at time t if $\overrightarrow{X}(t_0) = \overrightarrow{x_0}$ at time t_0. The above CME defines a stochastic process referred to as a continuous time Markov chain. Rather than attempting to solve this CME equation directly, individual stochastic time trajectories of the state vector $\overrightarrow{X}(t)$ can be obtained using an appropriate kinetic Monte Carlo algorithm. In particular, in the following algorithm two random numbers r_1 and r_2 uniformly distributed in $[0, 1)$ are generated. The time to the next reaction event is then given by:

$$\Delta t = -\frac{1}{\sum_j R_j} log\left(\frac{1}{r_1}\right) \quad (2.7)$$

and the index of the same reaction event, R_k, is taken to be he smallest integer k that satisfies the following condition:

$$\sum_{j=1}^{k} R_i > r_2 \sum_{j=1}^{M} R_j = r_2 R_{tot} \quad (2.8)$$

where R_{tot} is the total reaction rate, $R_{tot} = \sum_j^M R_j$. Once the next reaction event and its time increment are selected, the simulation time and the state vector are updated accordingly, $t = t_0 + \Delta t$ and $\overrightarrow{X}(t + \Delta t) = \overrightarrow{X}(t_0) + \overrightarrow{\nu_j}$. The simulation proceeds to the next reaction event until the desired simulation time is reached.

2.3 Recasting the rate theory of damage accumulation in stochastic terms

2.3.1 0^{th}-order reactions

In the context of irradiation damage, 0^{th}-order reactions represent the source of initial defect clusters or implanted species. Generally, the rate of insertion of a given defect subspecies is expressed in terms of displacements per atom per second (*dpa s*), whereas ion insertion (e.g. He, H, etc.) is simply given in terms of number of ions per second. These processes are all considered as stochastic Poisson events with the corresponding

rates. More detailed description of how damage is inserted in SCD simulations is provided in Section 2.3.4.

2.3.2 1st-order reactions

1st-order reactions represent emission events of component monomers from clusters or absorption of defect at sinks. Cluster dissociation is usually taken to proceed according to classical nucleation theory, that is via a quasi-equilibrium exchange of monomers with the remote (mean-field) monomer atmosphere [19]. It is also possible to obtain the rate of monomer emission from considerations not involving quasi-equilibrium, as shown below. The monomer emission rates used in the mean-field RT calculations are effective, which means that the rate value entering the mean-field equations must be adjusted to reflect the fact that some monomers emitted from a parent cluster, will return to the same cluster even if there is no cluster-monomer attraction. This correlation effect is purely geometrical: a point-like random walker placed at a standoff distance d away from the surface of spherical cluster, will return to the same cluster with probability $r/(d+r)$ [20]. Therefore, even though the rates of monomer emission events should be approximately proportional to the surface area of the cluster ($4\pi r^2$), the effective rate at which the cluster supplies monomers to the remote atmosphere should be corrected by the fraction of non-returning monomers $d/(d+r)$. As a result, the effective rate of monomer emission for a cluster of size n can be written as:

$$R_n = \frac{d}{d+r}\frac{4\pi r^2}{\alpha a_0^2}\nu_0 exp\left(-\frac{E_b(n)+E_m}{k_b T}\right) \tag{2.9}$$

where d is the first nearest-neighbor jump distance, and the term $4\pi r^2/\alpha a_0^2$ is an approximate count of all distinct locations on the cluster surface from which a monomer may be emitted. Here, α is a dimensionless geometric parameter of unit order, and a_0 is the lattice parameter. Also, ν_0 is the attempt frequency, $E_b(n)$ is the binding energy of a monomer to a cluster of size n, E_m is the monomer migration barrier, k_B is Boltzmann's constant and T is the temperature of the system. Obviously, the effective monomer emission rate scales as $\sim d/r$ for large clusters ($r \gg d$), as is the case when quasi-equilibrium is assumed.

Defect absorption at sinks such as dislocations, grain boundaries, precipitate particles and other elements of the material microstructure, is traditionally included into sink terms of the following form:

$$R = SD_\nu C_\nu$$

where S is the so-called sink strength parameter that represents the efficiency of a given sink in removing mobile species ν, and D_ν and C_ν are the diffusion coefficient and the concentration of the species ν. The appropriate defect absorption rate for our discrete-valued implementation is simply:

$$R = SD_\nu N_\nu$$

Here we consider only dislocation and grain boundary sinks, whose contribution to S is, respectively,

$$S = S_d + S_g = \rho + 6\sqrt{\rho}/L$$

where ρ is the dislocation density, and L is the average grain size. The values of S_d and S_g for interstitial and vacancy-type defects can be obtained by multiplying with appropriate bias factors. Alternatively, the same sinks can be included in the model more explicitly, i.e. in the form of 2$^{\text{nd}}$-order reactions, as described in the following section. Which of the two alternative forms —1$^{\text{st}}$ or 2$^{\text{nd}}$-order— used to describe sinks can have an effect on model accuracy and computational efficiency.

2.3.3 2$^{\text{nd}}$-order reactions

The 2$^{\text{nd}}$-order reaction term in RT accounts for the various mechanisms that involve collisions of two species. In the irradiation damage context, the possible reactions are SIA-vacancy annihilation, SIA absorption by an interstitial cluster, vacancy aggregation, etc. The terms describing such binary reactions are often taken directly from Smoluchowski's stationary solution for the collision rate between two spherical particles [21]:

$$R = 4\pi \left(r_\mu + r_\nu\right)\left(D_\mu + D_\nu\right) C_\mu C_\nu$$

where r_μ and r_ν are the reaction radii of the reacting species ν and μ. D_ν and D_μ are the corresponding diffusion coefficients, and C_ν and C_μ are the respective concentrations. For our discrete valued model, the 2$^{\text{nd}}$-order reaction is given as:

$$R = \frac{4\pi \left(r_\mu + r_\nu\right)\left(D_\mu + D_\nu\right)}{V} N_\mu N_\nu$$

For more accurate description of binary association mechanisms in irradiated materials, the 2$^{\text{nd}}$-order terms sometimes include correction terms to account for possibly different (non-spherical) shapes of interacting clusters, their mutual attraction or repulsion, and for the one-dimensional diffusion characteristic of some clusters [22, 23], for example SIA clusters are known to migrate one-dimensionally in metals. In our discrete SCD model, the binary terms are written as:

$$\frac{4\pi r_{\mu\nu} f_{\mu\nu}}{V} N_\mu N_\nu,\ if\ \nu \neq \mu$$

$$\frac{4\pi r_{\mu\nu} f_{\mu\nu}}{V} \frac{N_\nu \left(N_\nu - 1\right)}{2},\ if\ \nu \equiv \mu$$

where $r_{\mu\nu}$ is an interaction radius that reflects the shapes of one or both collision species as well as their possible attraction or repulsion, and the factor $f_{\mu\nu}$ takes a different form

depending on the dimensionality of motion of the species involved. Three distinct cases relevant for simulations of radiation damage accumulation can be considered here:

(i) Both species μ and ν diffuse isotropically in 3D (e.g. reactions between vacancies, vacancy clusters).

(ii) One species μ diffuses one-dimensionally and species ν diffuses isotropically in 3D (e.g. reactions of SIAs/SIA clusters with vacancies/vacancy clusters or other gas bubbles).

(iii) Both species diffuse in 1D along two non-parallel directions (e.g. reactions between SIAs or SIA clusters).

In our current study, we limit our attention to the first case (i) so that $f_{\mu\nu} = (D_\mu + D_\nu)$ and $r_{\mu\nu} = (r_\mu + r_\nu)$. As discussed above, it is possible to treat defect absorption at sinks as a 2^{nd}-order reaction. More specifically, consider the species μ (which can be mobile or immobile) such that its number count N_μ is not affected by collisions with defect species ν. Such a 2^{nd}-order reaction term can be written as:

$$\frac{4\pi r_{\mu\nu} f_{\mu\nu} N_\mu D_\mu}{V} D_\nu N_\nu$$

and its effect on the kinetics of species ν will be precisely the same as that of a first order sink term with an ideal (constant) sink strength represented by:

$$S = \frac{4\pi r_{\mu\nu} f_{\mu\nu} N_\mu D_\mu}{V}$$

Because the number count of species μ remains unchanged in this case, it is more efficient to treat such reactions as 1^{st}-order reactions. However, even when N_μ does change in collisions with species ν, their reaction can be approximately treated as first order for computational efficiency, for as long as variations in N_μ remain small compared to the species number count itself, $\delta N_\mu / N_\mu \ll 1$. Species μ should be updated if and when the accumulated change δN_μ reaches a certain fraction of N_μ. Conversely, some of the elements of material microstructure traditionally treated as ideal sinks such as dislocations or grain boundaries may be more accurately described as non-ideal sinks whose properties (and strength) are changing as a result of reactions with other defect species. Such a sink requires that its strength parameter S be occasionally updated, or loss at sinks may even deserve to be treated as a second order binary reaction.

2.3.4 Damage source term

Due to its stochastic nature, SCD can also treat collision cascades generated by ions and gas implantation as stochastic processes. In our current implementation, the ion implantation and cascade damage are modeled as sequences of discrete Poisson events

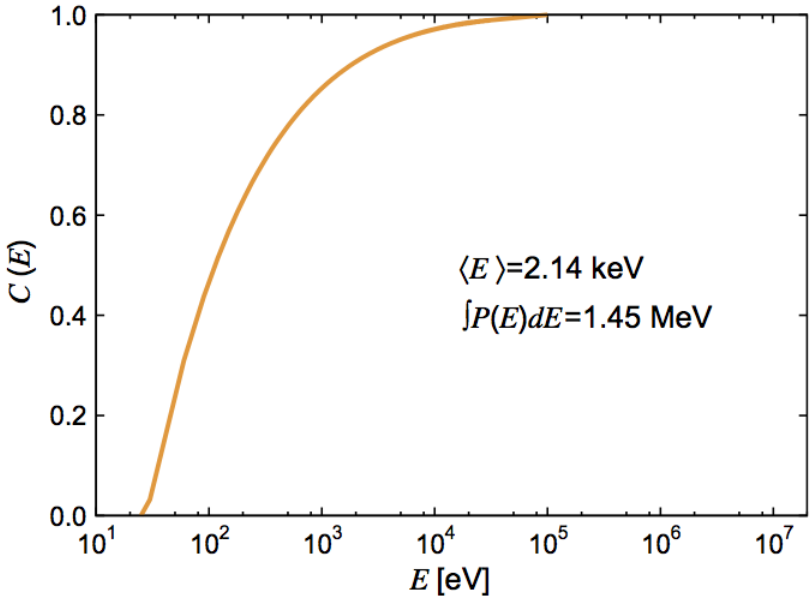

Figure 2.1: Cumulative Fe recoil distribution as obtained from SRIM for 10.5-MeV Fe-ion irradiation assuming a threshold displacement energy of 25 eV. $C(E)$ is used to obtain random samples of the primary knock-on atom (PKA) energies E by solving $E = C^{-1}(\xi)$, where ξ is a random number uniformly distributed in [0,1). Note that $C(E) = \int_0^E \|P(E)\| dE$, where $P(E)$ is the recoil energy spectrum [15].

with ion insertion rates adjusted to the nominal damage dose rate in $dpa\ s^{-1}$ and to the gas implantation rate in unit of $appm/dpa$. In our reported simulations of bcc-Fe under multi-ion irradiation, the primary displacement damage is generated from a Fe-recoil distribution obtained using the SRIM software package [24] for approximately 1000 Fe ions with the same incident energy of 10.5MeV which is the energy of incident Fe^{3+} ions in the Tanaka's experiments [14]. According to SRIM calculations, only about 14% or 1.45 MeV of the total incident energy is converted to actual lattice damage production while the rest is lost in ionization via electronic stopping. The available 1.45 MeV are partitioned according to the cumulative probability distribution function (*cpdf*) shown in Fig. 2.1, which results in an average recoil energy of 2.14 keV.

Once an ion insertion event is selected in the main simulation cycle described in Eq. 2.8, this *cpdf* is used to randomly sample the energies of multiple recoils, one PKA energy at a time, until the sum of all these sampled recoil energies reaches the 1.45 MeV threshold. For each individual PKA, further randomization is performed to account for statistical variations in the number of defects and defect clusters generated in a collision cascade with a given recoil energy. Then, defect species are generated randomly on demand at each simulation step by sampling from discrete distributions parameterized to reproduce sub-cascade statistics collected by Malerba *et al.* [25]. In this fashion, the inserted defect

populations originate from a rich statistical database constructed from hundreds of MD cascade simulations covering a wide range of recoil energies and temperatures. For the cases of He or H implantation, a He or H atom is inserted into the reaction volume and a Frenkel pair will be produced, consequently. H or He atoms will occupy interstitial sites in these cases.

2.4 Conclusion

In this chapter, we briefly describe the stochastic simulation algorithm (SSA) introduced by Gillespie and show how to recast the existing ODE-based RT models into the context of SSA. Within the mean-field RT formulation for investigation of damage accumulation kinetics in irradiated materials, a number of numerical and physical issues are dealt with that are more consistently and/or conveniently within the SCD framework than in the standard ODE-based implementations. The key advantage of SCD over ODE-RT is that computational cost is defined principally by the size of simulation volume. For ODE-RT models, on the other hand, cost is defined mostly by the resolution of the ODE grid and, if defect populations are of complex structures (i.e. consist of more than one component species), by the dimensionality of the cluster size-space. Thus, computational complexity scales exponentially with the number of size dimensions, leading to combinatorial explosion, i.e. too many equations that need to be solved in ODE-based RT models. This situation is not at all unfamiliar in computational sciences, for example numerical evaluation of multi-dimensional integrals often encounters similar computational challenges. The solution originally proposed by Gillespie in the context of chemical reaction networks [1, 16] draws on the general strength of the Monte Carlo method, in which, rather than computing the integrand on every grid point, the integral is estimated by averaging random samples of the integrand. Now widely recognized and rigorously justified mathematically, a key advantage of the Monte Carlo method is that such random sampling does not have to be dense for computing the integral to an acceptable accuracy. Similarly in SCD, accurate predictions of damage accumulation can also be obtained by sparse random sampling of the evolving defect cluster populations.

Although various aspects of cascade production and cluster migration fluctuations in RT models have been accounted for in the past [26, 27, 28, 29], SCD is better suited than ODE-based RT to deal with the probabilistic aspects of irradiation damage thanks to its intrinsically stochastic nature. Furthermore, the persistent issue of non-conservation of species populations associated with RT-models never arises in SCD model because species populations always carry integer values. Thus, there is no size distribution tails that need to be concerned in SCD for the same reason. SCD model, in fact, is remarkably close in its spirit to kMC. The only, but essential, difference between kMC and SCD is that the SCD is a mean-field method and does not deal with the spatial distribution of species populations. This close affinity of SCD and kMC has opened door to direct comparisons between the two methods on identical reaction–diffusion models, and it may prove useful for the development of both approaches.

Chapter 3

Enhancements to the existing SCD model

3.1 Motivation

In this chapter, we present an improved version of a recently developed stochastic cluster dynamics (SCD) model [15] as an alternative to rate theory (RT) methods for solving coupled ordinary differential equation (ODE) systems for irradiation damage simulations. SCD circumvents by design the curse of dimensionality of the variable space that renders traditional ODE-based RT approaches inefficient when handling complex defect population comprised of multiple (more than two) defect species.

Although SCD sidesteps combinatorial explosion, the method relies on a kMC algorithm to sample stochastic evolution trajectories from the master equation. Thus, SCD simulations face the usual computational challenges characteristic of kMC simulation methods, such as stiffness caused by a wide spectrum of event rates. Further applications of SCD to technologically relevant materials and irradiation conditions require improvements to make the method more robust and computationally efficient.

Several improvements introduced here enable efficient and accurate simulations of irradiated materials up to realistic (high) damage doses characteristic of next-generation nuclear systems. The first improvement is a procedure for efficiently updating the defect reaction-network and event selection in the context of a dynamically expanding reaction-network. Next is a novel implementation of the τ-leaping method that speeds up SCD simulations by advancing the state of the reaction network in large time increments when appropriate. Lastly, a volume rescaling procedure is introduced to control the computational complexity of the expanding reaction-network through occasional reductions of the defect population while maintaining accurate statistics. The enhanced SCD model is then applied to model defect cluster accumulation in iron thin films subjected to triple ion-beam (Fe^{3+}, He^{+} and H^{+}) irradiations, for which standard RT or spatially-resolved kinetic Monte Carlo simulations are prohibitively expensive.

The τ-leaping method was originally developed and has been used in SSA simulations

with fixed variable spaces [32, 33, 34]. In SCD, where the size of the reaction network varies with time, an efficient algorithm for updating noncritical reactions and noncritical species and for computing the leap time is needed to reduce the overhead associated with τ-leaping. We apply the enhanced SCD model to simulations of defect populations in pure iron subjected to triple ion-beam irradiation. The predicted damage accumulation kinetics are verified by comparing them to the original SCD algorithm predictions. The same comparisons are used to quantify gains in computational performance over the original SCD simulations.

In this chapter, we overview the theory behind the τ-leaping methods in Section 3.2. In Section 3.3, we briefly overview our original SCD algorithm, our material model for pure bcc-Fe and the types of reaction events considered in our radiation damage simulations. Improvements to the SCD model are described in Section 3.4 together with their algorithmic details. In Section 3.5, we present the numerical verification of the new improved SCD algorithm and compare its computational performance to the original algorithm. Finally, Section 3.6 summarizes our findings.

3.2 The τ-leaping method

The method described Section 2.2.3 is referred to as *direct* SSA method. The direct SSA method rigorously generates stochastic trajectories sampled for the exact (even if often unknown) solutions of the CME. Several algorithmic enhancements have been proposed to improve efficiency of the direct SSA method, including the *first reaction method* [1], the *modified direct method* [35], the *optimized direct method* [35], the *sorting direct method* [36], or the *logarithmic direct method* [37], to name a few. Any such improvements notwithstanding, simulating every reaction event one at a time is often impractical for large reaction networks of practical interest. To address this problem, Gillespie proposed the τ-leaping method that allows many reactions channels to fire in a single timestep at the expense of some minor accuracy loss [32]. Because conditions that justify the using of τ-leaping are often met in radiation damage simulations, we briefly describe τ-leaping as a way to accelerate stochastic simulations.

The τ-leaping method is based on the leap condition which assumes that a reaction channel may be fired multiple times within a small time interval [t, t + τ) if the reaction rate does not suffer significant change over that interval and is bounded by ϵR_{tot}, where ϵ is an error control parameter ($0 < \epsilon \ll 1$). Then, given the state vector of the system $\overrightarrow{X}(t) = \overrightarrow{x}$, the number of times that each reaction channel $\mathbb{R}_j$ can fire is approximated by the Poisson distribution $\mathcal{P}(R_j\tau)$.

The simulation proceeds as follows:

1. At each time-step we find a value of τ that satisfies the leap condition mentioned above;

2. For each ν_j, a Poisson random variable with mean $R_j\tau$, i.e. $\mathcal{P}(R_j\tau)$ is generated;

3. The system is updated accordingly as $\overrightarrow{X}(t+\tau) \leftarrow \overrightarrow{X}(t) + \sum_j^M \mathcal{P}(R_j\tau)\,\nu_j$, and the simulation time advances to the new time $t \leftarrow t+\tau$.

As a result, the simulation can be accelerated at a greater speed since the it can leap through multiple reactions in one single step instead of firing the reactions one by one.

3.3 More details on the stochastic cluster dynamics algorithm

3.3.1 Model representation

At any point in time the state of the model is characterized by the set of all existing clusters $\overrightarrow{S}_{all} = \{S_i\}$. Dynamic updates of state vectors are efficiently handled using hash tables with dynamic resizing. More details on the hash functions and associated operations are given in the next section. Each cluster S_i contains several associated attributes such as the number of each component species contained in the cluster, the cluster species population count, its diffusion coefficient, the binding energies among the component subspecies and the cluster, and other relevant parameters.

Mobile species with a nonzero diffusivity are regarded as a subset $\overrightarrow{S}_m$ (here m stands for mobile) of $\overrightarrow{S}_{all}$. Defect cluster species associated with a recently executed event are stored in a dynamic array whose purpose will be described in the following section. Such species can be reactants or products of a recently executed reaction event or a collection of defects and clusters that have just been introduced into the volume as a result of a defect insertion event (due to irradiation).

The evolving reaction network $\overrightarrow{\mathbb{R}} = \{\mathbb{R}_i\}$ specifies all reaction channels available for the current defect population $\overrightarrow{S}_{all}$. Each binary reaction channel $\mathbb{R}(S_1, S_2)$ represents a reaction between species of type S_1 and type S_2 with an associated reaction rate $R(S_1, S_2)$ (clusters S_1 and S_2 can be identical when the reaction involves two like species).

To implement the τ-leaping method, two more data sets will be defined. The first set $\overrightarrow{\mathbb{J}} = \{\mathbb{J}_i\}$ contains all noncritical reaction channels whose associated reactants have populations larger than a certain user-predefined value n_{cr}. Another set $\overrightarrow{P} = \{P_i\}$ contains all defect cluster species associated with the noncritical reactions, these clusters are termed noncritical clusters. Each P_i contains a parameter specifying the highest order of possible reactions species i can participate in, as explained in more details later these reaction order parameters are utilized in computing the leap time τ.

3.3.2 Types of events considered in SCD

Hereafter, V_s and I_s denote a void or a self interstitial atom (SIA) cluster of size s. In our model, we only consider clusters with a maximum of three component species, specifically the clusters only contain He and H atoms together with either vacancies or interstitials

of the host material. If desired, the model can be modified to admit defect clusters of arbitrarily complex compositions. The following reactions are currently admitted in our SCD model of iron:

0^{th}-order reactions:

- Defect insertion, e.g. generation of certain types of defects resulting from collisions of incoming energetic particles with the host matrix atoms.

1^{st}-order reactions:

- Defect absorption at sinks: mobile clusters can migrate towards sinks and become absorbed there. Sinks can be free surfaces, dislocation networks or grain boundaries.
- Emission of a monomer from a defect cluster: a cluster can emit a monomer of one of its constituent species and reducing its species count appropriately. A complex cluster cluster $V_iHe_jH_k$ can emit a vacancy, or a He monomer or a H monomer. Following emission, the initial cluster's population is reduced by one and two new defect species are created or, if one or both species already exist, their counts are increased by one. For example, emission of one vacancy V (or one He monomer) produces a smaller defect cluster $V_{(i-1)}He_jH_k$ (or $V_iHe_{(j-1)}H_k$ in case the monomer is a He atom).

2^{nd}-order reactions

- Defect annihilation: collisions of two clusters containing vacancies and self interstitial atoms result in their complete or partial recombination. For example, collision of a complex vacancy cluster $V_iHe_jH_k$ with a SIA cluster $I_{i'}$ produces $V_{(i-i')}He_jH_k$ (if $i > i'$) or $I_{(i'-i)}He_jH_k$ (if $i' > i$) or releases j monomers of He and k monomers of H monomers (if $i = i'$). He and H monomers are assumed not to bind unless vacancies and interstitials are also present.
- Defect aggregation: clusters containing like defects can combine to form larger clusters upon interaction. For example, a $V_iHe_jH_k$ cluster can collide with a $V_{i'}He_{j'}H_{k'}$ cluster producing a larger $V_{(i+i')}He_{(j+j')}H_{(k+k')}$ cluster.

3.3.3 Summary of the original SCD algorithm

The main motivation for the development of SCD was to circumvent combinatorial explosion in the number of equations encountered in traditional ODE-based RT simulations. In SCD, the simulation volume is finite and defect cluster species have integer-valued populations. In a typical initial state, relatively few (if any) defect species exist, so, rather than allocating memory for all possible defect-clusters before the start of the simulation, cluster species are added or removed from the hash table dynamically, as needed. Therefore, only defect clusters that have nonzero populations are kept track of. The hash table

is implemented as an associative array in which a hash function is used to map the identifying values –known as hash *keys*– to their associated values. The hash function maps the keys onto the index array elements (or buckets) where the associated values are stored. Operations on a hash such as adding, removing or locating buckets take constant time on average and do not depend of the size of the hash itself unlike operations on indexed arrays. In simulations of irradiated materials, the number of pre-existing defect clusters is usually small but increases rapidly after high energy particles begin to create defects. Furthermore, defect populations and their associated reaction channels change with each subsequent reaction event. It is our experience that in such conditions hashing is more efficient than using array structures for handling large and evolving data sets since defect clusters can be located and updated quickly. The original SCD algorithm consists of the following steps and are displayed schematically in Fig. 3.1:

1. Construct two hash tables: one, $\overrightarrow{S}_{all}$, to store all the existing defect clusters and another one, $\overrightarrow{S}_{m}$, to store only the mobile defects in $\overrightarrow{S}_{all}$, .

2. Construct a reaction table $\overrightarrow{\mathbb{R}}$ containing the reaction channels involving all existing defect clusters, and store $\overrightarrow{\mathbb{R}}$ in an array.

3. Calculate the total reaction rate by summing the rates of all currently existing reaction channels in the reaction table.

4. Randomly select the time increment to the next reaction as well as the type of the reaction event using Eqs. 2.7 and 2.8.

5. Execute the selected reaction event, update the hash tables accordingly and delete the reaction table $\overrightarrow{\mathbb{R}}$.

6. Return to step 2 and proceed until the total simulation time is reached.

Using an array to store the reaction channels $\overrightarrow{\mathbb{R}}$ proves to be inefficient due to the highly dynamic nature of stochastic evolution. Furthermore it is wasteful to build the reaction table anew after every reaction event since only a portion of the reaction channels is changed due to the executed event while most others are left intact. These two inefficiencies are addressed in the improved version of SCD presented in the following section.

3.4 An improved stochastic cluster dynamics algorithm

Except for massive defect insertion events representing the collision cascades, only a small number of defect clusters in the simulation volume are affected by a single reaction event. Therefore, only the reaction channels involving affected defect species need to be updated, while the rest of the reaction network remains untouched. In this enhanced version of SCD, we use hashing to maintain existing species and reaction channels and to expand the

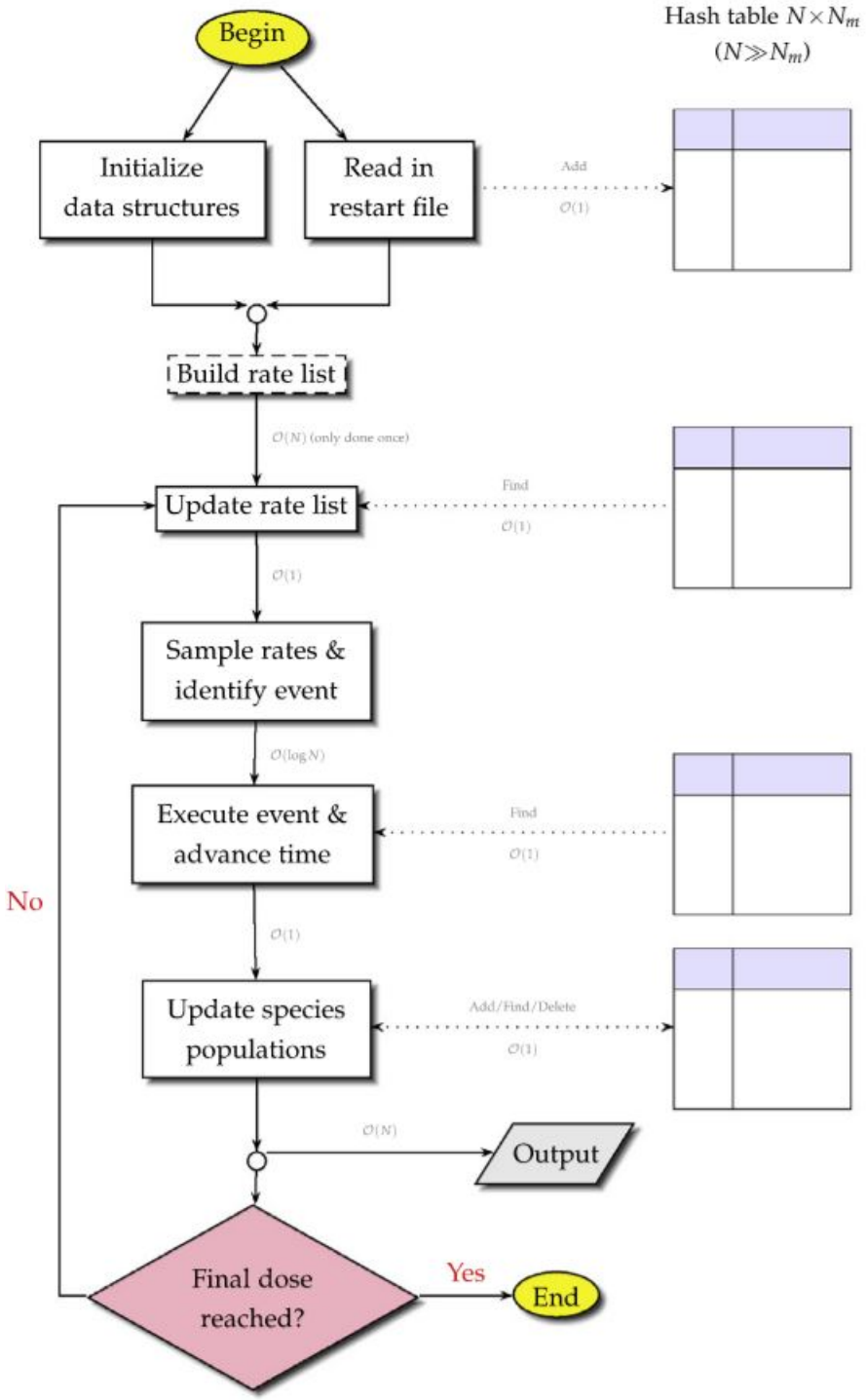

Figure 3.1: Flow chart of the initial stochastic cluster dynamics algorithm [15].

reaction network when new species are introduced by the reaction events. Such updates are typically more efficient than the reconstruction of the entire reaction table in between insertion events. Depending on the specific reaction model implemented, some defect species become quite numerous and their associated reaction channels can fire much more frequently than others. For example in our model for iron, SIAs and vacancies are observed to migrate in large numbers to defects sinks soon after irradiation commences, whereas defect insertion and defect association events are relatively infrequent. To expedite SCD simulations under such conditions, we implement a version of τ-leaping method in which several repetitive reaction events are executed at once. Lastly, we introduce and justify a volume rescaling procedure to reduce the computational complexity of SCD simulations at later stages of damage accumulation. This is when the density of defect clusters becomes high, and the diffusion length of mobile defects becomes small compared to the linear dimension of the simulation volume.

3.4.1 Dynamic reaction network updates and expansion

As follows from Eqs. 2.7 and 2.8, both the time increment to the next reaction event and the type of reaction are selected based on the total event rate summed over all existing reaction channels. In the original version of SCD, the net event rate was recomputed after each reaction event throughout the simulation. However, in a production scale SCD simulation the number of distinct reaction rates grows rapidly to thousands and even millions and yet only a small sub-set of reaction channels is directly affected by each reaction event. Enabling incremental updates requires that reaction channels affected (modified or eliminated) by the last event be located and updated in the computer's memory efficiently during the course of the simulation. We rely on hashing to quickly add, remove, locate and update reaction channels in real time.

In the improved version of SCD reported here, in addition to the two hash tables $\overrightarrow{S}_{all}$ and $\overrightarrow{S}_{m}$ used to store and reference the total and the mobile cluster populations, all existing reaction channels are stored in a reaction hash $\overrightarrow{\mathbb{R}}$. The reaction table expands or contracts as needed to accommodate new reactions associated with the creation (or extinction) of new defect species. The process for updating the affected hash tables goes as follows:

- A new hash key is created for all possible species resulting from these reactions. For each 2^{nd}-order reaction, this key is generated from the keys of its constituent reactants stored in $\overrightarrow{S}_{all}$ while for 0^{th} and 1^{st}-order reactions, dummy keys –two and one, respectively– are used as appropriate.

- Each cluster in the $\overrightarrow{S}_{all}$ hash table is assigned a parameter f_1 indexing its count change due to the recently executed event; another parameter f_2 indicates whether the defect already existed in the simulation volume in the previous time-step. These parameters let SCD know whether it should look up and update the existing reaction $\mathbb{R}(S_1, S_2)$ or add it as a newly created one into the reaction hash table $\overrightarrow{\mathbb{R}}$.

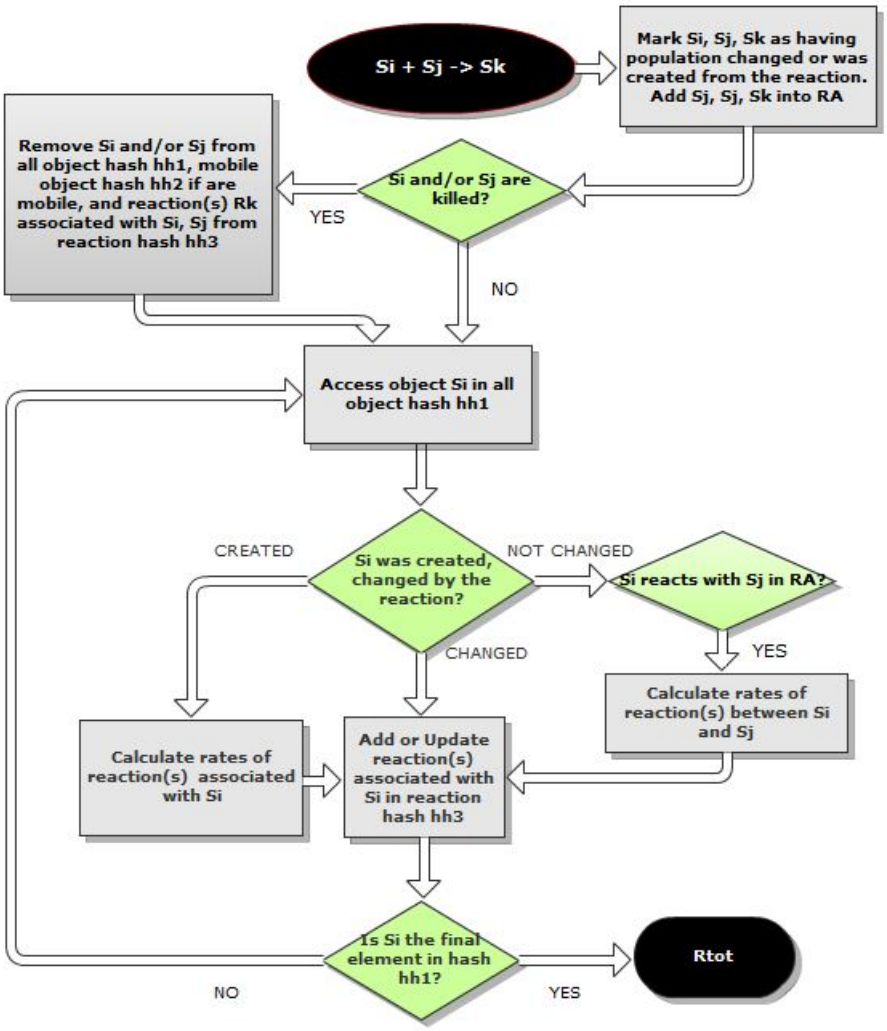

Figure 3.2: Flow chart of the dynamic reaction network update and expansion algorithm.

- As a cost-savings measure, defect clusters that have participated in a recent reaction event are stored in a dynamic array so that product species can be updated efficiently. As the number of these clusters is not very large, a dynamic array is simpler than a hash table in this case.

3.4.2 Reaction rate updating

The first step of the reaction update process is to visit each reaction in $\overrightarrow{\mathbb{R}}$ and remove those whose component reactants no longer exist due to the previous event(s). Subsequently, we visit each element S_i in $\overrightarrow{S}_{all}$ and update all the reaction channels that this cluster associates with. As a result, some existing reactions inS_i will be modified and new reactions will be added into the reaction hash table $\overrightarrow{\mathbb{R}}$.

Based on the values of f_1 and f_2 mentioned previously, it can be established whether a cluster was a reactant or product of the last reaction event. If S_i is a new defect cluster, all the reactions associated with it will be added directly into the reaction hash table because it is not necessary to check for their existence in it. On the other hand, if the cluster S_i only increases or decreases in number, all of its associated reactions will be first located in the reaction hash and updated accordingly based on the value of f_1. If f_1 is the change in population of cluster S_i and R is the rate of a reaction channel involving S_i, then the total reaction rate R_{tot} can be updated as follows:

1$^{\text{st}}$-order reaction:

$$R(S_i) \leftarrow R_0(S_i)\left[1+\frac{f_1(S_i)}{X_0(S_i)}\right], \qquad R_{tot} \leftarrow R_{tot} + R_0(S_i)\frac{f_1(S_i)}{X_0(S_i)} \tag{3.1}$$

For 2$^{\text{nd}}$-order reactions between a cluster S_i and another cluster S_j (assuming $\mathbb{R}(S_i, S_j)$ already exists):

$$\begin{cases} R(S_i,S_j) \leftarrow R_0(S_i,S_j)\left[1+\frac{f_1(S_i)}{X_0(S_i)}\right]\left[1+\frac{f_1(S_j)}{X_0(S_j)}\right] & (S_i \neq S_j) \\ R(S_i,S_j) \leftarrow R_0(S_i,S_j)\left[1+\frac{f_1(S_i)}{X_0(S_i)}\right]\left[1+\frac{f_1(S_i)}{X_0(S_i)-1}\right] & (S_i \equiv S_j) \end{cases} \tag{3.2}$$

$$\begin{cases} R_{tot} \leftarrow R_{tot} + R_0(S_i,S_j)\left[\frac{f_1(S_i)}{X_0(S_i)}+\frac{f_1(S_j)}{X_0(S_j)}+\frac{f_1(S_i)f_1(S_j)}{X_0(S_i)X_0(S_j)}\right] & (S_i \neq S_j) \\ R_{tot} \leftarrow R_{tot} + R_0(S_i,S_j)\left[\frac{f_1(S_i)}{X_0(S_i)}+\frac{f_1(S_i)}{X_0(S_i)-1}+\frac{f_1^2(S_i)}{X_0(S_i)\left[X_0(S_i)-1\right]}\right] & (S_i \equiv S_j) \end{cases} \tag{3.3}$$

where $R_0()$ and $X_0()$ are the equivalent old reaction rate and old population. Therefore, the reaction rate updates depend only on values of the f_1 parameters and the old populations of the clusters.

If both f_1 and f_2 are zero, the cluster S_i is not affected by the selected event, but we need to check whether S_i can engage in any 2$^{\text{nd}}$-order reactions with those clusters S_j that are affected by the recent reaction event. These clusters are stored in the dynamic array mentioned previously. The last step of this process is to check whether the clusters in the dynamic array can form 2$^{\text{nd}}$-order reactions with one another. Some of these reactions, which may have been skipped in previous steps because of the way the reaction *keys* are assigned, are now accounted for in this step. If any pair of defect-clusters S_i and S_j can react, the corresponding reactions –as well as the total reaction rate– can be updated accordingly using Eqs. 3.1, 3.2, and 3.3.

3.4.3 Implementation of the τ-leaping method in SCD

In this section, we describe our implementation of the τ-leaping method within SCD. The method has been previously implemented on top of the direct SSA algorithm [33, 34]. However, implementation of τ-leaping in an open system where new species are constantly

added to or removed from the reaction network, as is the case of SCD simulations of irradiated materials, has not been attempted to our knowledge. Employing hash tables, we now show how τ-leaping can be added to the SCD model to make the simulations more efficient. Several improvements have been proposed to the τ-leaping method since it was first proposed by Gillespie [38, 39], including efficient simulations of stiff reaction networks [44, 45] by replacing explicit τ-leaping formula with its implicit counterpart using deterministic numerical techniques developed for implicit ODE solver [43], or prevention of meaningless negative species populations that can be caused by leaping [40, 41, 42]. Cao *et al.* developed an efficient τ-leaping SSA algorithm that avoids having to solve a complicated set of partial differential equations suggested in Ref. [39]. For the sake of clarity and to better explain our implementation of τ-leaping in the SCD algorithm, here we briefly summarize Cao *et al.*'s algorithm. The reader is referred to the original paper for more details of the method and the underlying theory [39].

In Cao *et al.*'s approach, the set of all existing reactions is divided into two non-overlapping subsets: the critical subset includes all reactions that are within n_{cr} (a pre-defined integer) firings away from extinguishing one of the component reactants and the noncritical subset includes all the other reactions. We add all 0^{th}-order defect insertion reactions to the critical subset in which every reaction is advanced one at a time, just like in the *direct* SSA method. To enable efficient τ-leaping over the noncritical reaction subset, we make use of two more hash tables. The first one $\overrightarrow{P}$ is used to store the noncritical species, each element in $\overrightarrow{P}$ containing the species' attributes such as its *key*, population count and several additional parameters g, μ, σ^2 and O's as defined below. The second hash table $\overrightarrow{\mathbb{J}}$ contains the noncritical reactions. Similar to the regular reaction hash, each element of $\overrightarrow{\mathbb{J}}$ contains the key and the rate of a noncritical reaction. Denoting the lower number of clusters among the two reactants as X_{min}, a safe leap time τ for every noncritical reaction in $\overrightarrow{\mathbb{J}}$ is selected as:

$$\tau = \min_{P_i \in \overrightarrow{P}} \left\{ \frac{\max\{\epsilon X(P_i)/g(P_i), 1\}}{|\mu(P_i)|}, \frac{\max\{\epsilon X(P_i)/g(P_i), 1\}^2}{\sigma^2(P_i)} \right\} \tag{3.4}$$

with

$$\mu(P_i) = \sum_{\mathbb{J}_j \in \overrightarrow{\mathbb{J}}} \nu_{ij} J_j, \quad \forall i \in \overrightarrow{S}_{all} \tag{3.5}$$

$$\sigma^2(P_i) = \sum_{\mathbb{J}_j \in \overrightarrow{\mathbb{J}}} \nu_{ij}^2 J_j, \quad \forall i \in \overrightarrow{S}_{all} \tag{3.6}$$

In Cao's new approach, the fractional change in each reactant population, $\triangle_\tau X(P_i)/X(P_i)$, during the leap-time τ is bounded by an amount $\epsilon_i = \epsilon_i(\epsilon, X)$, where the function ϵ_i is chosen so that $\triangle_\tau R_j/R_j$ for every reaction$j$ is bounded by the pre-defined ϵ. The more detailed algebraic form of this ϵ_i function can be found in [39], in summary, to ensure the requirements for leaping as well as the non-negative population of participating reactants are satisfied, the following condition must be satisfied:

$$| \triangle_\tau X(P_i) | \leq max \{\epsilon_i X(P_i), 1\} \tag{3.7}$$

As can be seen from the τ-leaping formula:

$$\triangle_\tau X(P_i) = \sum_j \mathcal{P}(R_j \tau)\, \nu_j \tag{3.8}$$

therefore the value of τ provided in Eq. 3.4 is to assure that the condition imposed in Eq. 3.7 is satisfied. This condition can be adequately fulfilled if it is satisfied by both the means and variances of $\triangle_\tau X(P_i)$, where, from Eq. 3.8, $\langle \triangle_\tau X(P_i) \rangle = \sum_j \nu_{ij} (R_j \tau)$ and $var \{\triangle_\tau X(P_i)\} = \sum_j \nu_{ij}^2 (R_j \tau)$.

The value of g_i depends on the highest order O_i of any reaction in which the noncritical cluster P_i appears as a reactant. As appropriate for our model of irradiated materials, we categorize these reaction-order parameters into three different types: 1^{st}-order (O_1), 2^{nd}-order (O_2), and 2^{nd}-order with like reactants (O_3). When a reaction becomes critical or no longer exists due to exhaustion of one or both of its reactants, O_i parameters of the participating reactants are updated accordingly. The values of μ and σ^2 for each P_i are also updated every time a reaction involving a noncritical cluster is analyzed.

To determine the value of the leap time τ, our algorithm inspects all clusters P_i stored in the noncritical-reactant hash $\overrightarrow{P}$, determines the highest order of their associated reactions and calculates the corresponding values of g_i. When $O_2(P_i) = 0$, the highest order of reactions involving species P_i is 1^{st}-order, and the corresponding value of $g(P_i)$ is 1. A positive $O_2(P_i)$ indicates that P_i takes part in at least one 2^{nd}-order reaction in which case $g(P_i)$ is taken to be 2. However when a reaction exists that can involve two clusters of species P_i, $O_3(P_i)$ will also be positive and the value of $g(P_i)$ is determined instead as:

$$g(P_i) = \left[2 + \frac{1}{X(P_i) - 1}\right]$$

After a safe value of the leaping time is estimated as described above, the number of times k_i each reaction $\mathbb{J}_i \in \overrightarrow{\mathbb{J}}$ in the noncritical reaction hash will fire during this interval is computed as a Poisson random variable $\mathcal{P}(J_i, \tau)$. However the reactions are not executed immediately as it is still necessary to ensure that none of the noncritical reactant populations $\overrightarrow{P}$ becomes negative after τ-leaping is performed on all reactions in the current noncritical reaction hash $\overrightarrow{\mathbb{J}}$. To ensure that all species populations remain non-negative after τ-leaping, the total number $k^{tot}(P_i)$ of reaction events reducing the population of species P_i is obtained by summing k_j over all noncritical reactions $\mathbb{J}_j$ consuming P_i during the leap time τ. Only when the population of every noncritical cluster $X(P_i)$ is found to be larger than $k^{tot}(P_i)$, every reaction $\mathbb{J}_i$ stored in the noncritical reaction hash is executed k_i times and the f_1 and f_2 parameters of reactant clusters S_1 or S_2 are updated accordingly; otherwise, the value of τ is reduced, new firing times k_i's are determined and the previous non-negativity condition is re-examined. Should the need for

reduction in τ persist, τ-leaping is abandoned in favor of the *direct* (single-reaction) SSA algorithm for some number of SSA steps (200 steps in simulations described in Section 3.5) after which τ-leaping is resumed.

3.4.4 Controlling simulation complexity using volume rescaling

The computational complexity of SCD simulations is largely defined by the number of distinct cluster species currently present in the defect population. This number can be controlled by the size of the simulation volume. In selecting the volume, one needs to balance two conflicting requirements: (1) defect cluster populations should be statistically representative (which favors larger volumes) and (2) the computational cost of SCD simulations should remain acceptable (which favors smaller volumes). Here we introduce a method to balance these two requirements through volume rescaling.

Typically, at the start of a SCD simulation, most of defect clusters are mobile and their volume concentrations as well as the concentration and the net strength of pre-existing defect sinks (dislocations, grain boundaries, etc) are low. Under such conditions, mobile defects diffuse over long distances through the reaction volume before they meet a reaction partner. However, as time proceeds and progressively more defects are inserted by continued irradiation, clusters become more numerous while smaller mobile clusters combine and form increasingly larger clusters. Such kinetics result in a more or less steady reduction in the lifetime and diffusion length of mobile clusters defined as the average time and distance travelled by a mobile cluster from birth to death, respectively. In a given defect population, the average lifetime of a mobile cluster of species S_i is the inverse of the total rate of loss:

$$\mathcal{L}(S_i) = D(S_i) \sum_l Z_{il}\rho_l + \epsilon_m + \sum_j k_{ij} \frac{X(S_j)}{V}, \tag{3.9}$$

while the maximum diffusion length among all mobile cluster species $\overrightarrow{S'}_m$ can be estimated as:

$$l_{max} = \max_{S_i \in \overrightarrow{S'}_m} l_{S_i}, \quad l_{S_i} = \sqrt{\frac{D(S_i)}{\mathcal{L}(S_i)}} \tag{3.10}$$

where $\mathcal{L}(S_i)$ is the net rate of loss and $D(S_i)$ is the diffusion coefficient of the mobile cluster species S_i, Z_{il} is the strength of a given sink of type l with respect to the same species (the sink's ability to remove clusters S_i), ρ_l is the volume density of sinks of type l, ϵ_m is the total rate of all dissociation reactions leading to splitting clusters S_i, and k_{ij} is the reaction rate of a 2$^{\text{nd}}$-order reaction between the mobile defect S_i and the defect cluster of type S_j with a population of $X(S_j)$. Here $\overrightarrow{S'}_m$ denotes the set of all mobile species that will possibly appear in the simulation volume, not limited to only those exist at the current time-step.

The significance of parameter l_{max} is that it defines the range of distances beyond which neighboring reaction sub-volumes are no longer exchanging their reactants (defect clusters). Thus, reaction volumes with linear dimensions exceeding l_{max} can be viewed as causally isolated from each other. Typically, as a SCD simulation progresses l_{max} decreases due to a more or less steady increase in the magnitude of the last term on the rhs of Eq. 3.9. A significant reduction in l_{max} justifies an appropriate reduction in the reaction volume, $V_{new} = \gamma V_{old} \geq l_{max}^3$ (with $\gamma < 1$). The essence of our volume rescaling method is that when conditions for volume reduction conditions are satisfied, the cluster population is reduced by allowing every cluster to be randomly eliminated with probability $(1 - \gamma)$ before resuming the SCD simulation. Such a volume reduction procedure allows to maintain the size of the reaction network approximately constant even when damage accumulation increases the volume density of defects by orders of magnitude. However, volume rescaling should be avoided when there are large fluctuations in the defect population, for example right after a massive defect insertion event.

3.4.5 Algorithm implementation

In this section we present the key algorithmic elements of our improved SCD model in pseudocode format, including construction of hash tables for noncritical reactions and defect clusters and an algorithm for estimating a safe leap time τ in SCD. In the following $R(S_1, S_1)$ is the rate of a binary reaction $\mathbb{R}(S_1, S_2)$ between species S_1 and S_2. Similarly, $J(P_1, P_2)$ denotes the rate of the noncritical reaction $\mathbb{J}(P_1, P_2)$ between two noncritical species P_1 and P_2. The set of all critical reactions is represented by $\overrightarrow{\mathbb{R}}_{cr}$. For a 1^{st}-order reaction $\mathbb{R}(S_1)$ or $\mathbb{J}(S_1)$, S_1 represents its one and only reactant cluster. $X(S_i)$ denotes the population (number of units) of cluster species S_i in the reaction volume.

Algorithm 3.1 Construction of the noncritical reaction and reactant hash tables.

1. If $\mathbb{R}$ is a 2^{nd}-order reaction:

   (a) If $S_1 \equiv S_2$ (reaction between two like clusters):

      i. If $X(S_1) >= n_{cr}+2$ (reaction $\mathbb{R}$ is noncritical, and cluster S_1 is noncritical, i.e. $\mathbb{R}(S_1) \equiv \mathbb{J}(S_1) \in \overrightarrow{\mathbb{J}}$ and $S_1 \equiv P_1 \in \overrightarrow{P}$)

      - If $\mathbb{J}(P_1)$ does not exist: add $\mathbb{J}(P_1)$ into the noncritical reaction hash $\overrightarrow{\mathbb{J}}$ and update $O_{2,3}(P_1) \leftarrow O_{2,3}(P_1)+1$.
      - Else: update $J(P_1) \leftarrow R(S_1)$ and $X_{min}(\mathbb{J}) \leftarrow X(S_1)$, reset $k\left[\mathbb{J}(P_1)\right] \leftarrow 0$.
      - Locate P_1 in the noncritical cluster hash $\overrightarrow{P}$
        - If P_1 does not exist: add P_1 to $\overrightarrow{P}$ with $\mu_{tot}(P_1) \leftarrow \mu\left[J(P_1)\right]$ and $\sigma^2_{tot}(P_1) \leftarrow \sigma^2\left[J(P_1)\right]$ as determined by Eqs. 3.5 and 3.6.
        - Else: update $\mu_{tot}(P_1) \leftarrow \mu_{tot}(P_1) + \left\{\mu\left[J(P_1)\right]\right\}_{new} - \left\{\mu\left[J(P_1)\right]\right\}_{old}$ and $\sigma^2_{tot}(P_1) \leftarrow \sigma^2_{tot}(P_1) + \left\{\sigma^2\left[J(P_1)\right]\right\}_{new} - \left\{\sigma^2\left[J(P_1)\right]\right\}_{old}$.

      ii. Else ($\mathbb{R}$ is critical):

      - If $\mathbb{P}(P_1)$ exists: locate P_1 in $\overrightarrow{P}$. If P_1 exists: update $O_{2,3}(P_1) \leftarrow O_{2,3}(P_1)-1$, $\mu_{tot}(P_1) \leftarrow \mu_{tot}(P_1) - \mu\left[J(P_1)\right]$, $\sigma^2_{tot}(P_1) \leftarrow \sigma^2_{tot}(P_1) - \sigma^2\left[J(P_1)\right]$. If $O_1(P_1) = O_2(P_1) = O_3(P_1) = 0$, remove P_1 from the noncritical cluster hash $\overrightarrow{P}$.
      - Remove $\mathbb{J}(P_1)$ from the noncritical reaction hash $\overrightarrow{\mathbb{J}}$.

   (b) Else (reaction between unlike species $S_1 \neq S_2$):

      i. If $min\left\{X(S_1), X(S_2)\right\} > n_{cr}$ (reaction $\mathbb{R}$ is noncritical, and clusters S_1, S_2 are noncritical, i.e. $\mathbb{R}(S_1,S_2) \equiv \mathbb{J}(S_1,S_2) \in \overrightarrow{\mathbb{J}}$ and $S_{1,2} \equiv P_{1,2} \in \overrightarrow{P}$)

      - If $\mathbb{J}(P_1,P_2)$ does not exist: add $\mathbb{J}(S_1,S_2)$ into the noncritical reaction hash $\overrightarrow{\mathbb{J}}$, update $O_2(P_{1,2}) \leftarrow O_2(P_{1,2})+1$.
      - Else: update $J(P_1,P_2) \leftarrow R(S_1,S_2)$ and $X_{min}(\mathbb{J}) \leftarrow min\left\{X(S_1), X(S_2)\right\}$, reset $k\left[\mathbb{J}(P_1,P_2)\right] \leftarrow 0$.
      - Locate P_1 and P_2 in the noncritical cluster hash $\overrightarrow{P}$
        - If P_1 and/or P_2 do not exist: add them into $\overrightarrow{P}$ with $\mu_{tot}(P_{1,2}) \leftarrow \mu\left[J(P_1,P_2)\right]$ and $\sigma^2_{tot}(P_{1,2}) \leftarrow \sigma^2\left[J(P_1,P_2)\right]$ as determined by Eqs. 3.5 and 3.6.
        - Else: update $\mu_{tot}(P_{1,2}) \leftarrow \mu_{tot}(P_{1,2}) + \left\{\mu\left[J(P_1,P_2)\right]\right\}_{new} - \left\{\mu\left[J(P_1,P_2)\right]\right\}_{old}$ and $\sigma^2_{tot}(P_{1,2}) \leftarrow \sigma^2_{tot}(P_{1,2}) + \left\{\sigma^2\left[J(P_1,P_2)\right]\right\}_{new} - \left\{\sigma^2\left[J(P_1,P_2)\right]\right\}_{old}$.

      ii. Else: ($\mathbb{R}$ is critical):

      - If $\mathbb{J}(P_1,P_2)$ exists: locate P_1 and P_2 in $\overrightarrow{P}$. If P_1 or P_2 exists: update $O_2(P_{1,2}) \leftarrow O_2(P_{1,2})-1$, $\mu_{tot}(P_{1,2}) \leftarrow \mu_{tot}(P_{1,2}) - \mu\left[J(P_1,P_2)\right]$, $\sigma^2_{tot}(P_{1,2}) \leftarrow \sigma^2_{tot}(P_{1,2}) - \sigma^2\left[J(P_1,P_2)\right]$. If $O_1(P_{1,2}) = O_2(P_{1,2}) = O_3(P_{1,2}) = 0$, remove P_1 and/or P_2 from the noncritical cluster hash $\overrightarrow{P}$.
      - Remove $\mathbb{J}(P_1,P_2)$ from the noncritical reaction hash $\overrightarrow{\mathbb{J}}$.

2. Else: $\mathbb{R}$ is a 1^{st}-order reaction (emission or absorption of a defect cluster at sinks). Follow similar steps as described in 1(a), except that the noncritical condition for cluster S_1 is $X(S_1) > n_{cr}$ in this case.

Algorithm 3.2 Reaction update loop.

1. Remove all illegal reactions whose reactants are no longer exist from the reaction hash $\overrightarrow{\mathbb{R}}$. Starting from the first cluster S_1 in the all-cluster hash $\overrightarrow{S}_{all}$:

2. If $f_1(S_1) \neq 0$ or $f_2(S_1) \neq 0$ (S_1 is affected by the recently executed event):

   (a) If $f_1(S_1) \neq 0$ and $f_2(S_1) = 0$ (S_1 is only the reactant not the product of the previously executed event):

      i. Check if S_1 is immobile, skip to ii; else: find 1st-order reaction channels associated with S_1 and update the reaction rates using Eq. 3.1.

      ii. Loop through the mobile-cluster hash $\overrightarrow{S}_m$, determine if $key(S_1) \geq key(S_2)$ where S_2 denotes the mobile cluster and find the associated reaction channel $\mathbb{R}(S_1, S_2)$.

         A. If $\mathbb{R}$ exists: update values of $\mathbb{R}$ and the total rate R_{tot} using Eqs. 3.2 and 3.3.

         B. Else: calculate the reaction rate $R(S_1, S_2)$ between clusters S_1 and S_2, add $\mathbb{R}(S_1, S_2)$ to the reaction hash $\overrightarrow{\mathbb{R}}$ and update the total reaction rate, $R_{tot} \leftarrow R_{tot} + R(S_1, S_2)$.

   (b) Else if $f_2(S_1) \neq 0$ (the cluster has just been created): similar to 2(a), except that all reactions associated with S_1 will be added directly into the reaction hash $\overrightarrow{\mathbb{R}}$. It is not necessary to locate these reactions in $\overrightarrow{\mathbb{R}}$ since they are completely new reactions.

3. Else $f_1(S_1) = f_2(S_1) = 0$ (the cluster does not participate in the previous reaction):

   (a) Loop through the effected clusters S_2 contained in the dynamic array and evaluate these following conditions: 1) $key(S_1) > key(S_2)$ and S_1 is mobile, 2) S_1 is immobile while S_2 is mobile.

   (b) If any of those conditions is satisfied: find the associated reaction $\mathbb{R}(S_1', S_2')$ (S_1' is the larger value of S_1 and S_2, the other is S_2').

      i. If $\mathbb{R}(S_1', S_2')$ exists: update $R(S_1', S_2')$ and R_{tot} using Eqs. 3.2 and 3.3.

      ii. Else: calculate the reaction rate $R(S_1', S_2')$ between clusters S_1 and S_2, add $\mathbb{R}(S_1', S_2')$ into the reaction hash $\overrightarrow{\mathbb{R}}$ and update the total reaction rate, $R_{tot} \leftarrow R_{tot} + R(S_1', S_2')$.

4. Proceed to the next cluster in the all-cluster hash $\overrightarrow{S}_{all}$ and repeat Step 2 until reaching the last cluster.

5. Loop through the clusters contained in the dynamic array. For all possible pairs of (S_1, S_2), if at least one of the clusters in the pair is mobile: find the associated reaction $\mathbb{R}(S_1', S_2')$ (S_1' is the larger value of S_1 and S_2, the other is S_2').

   (a) If $\mathbb{R}(S_1', S_2')$ exists: update $R(S_1', S_2')$ and R_{tot} using Eqs. 3.2 and 3.3.

   (b) Else: calculate the reaction rate $R(S_1', S_2')$ between clusters S_1 and S_2, add $\mathbb{R}(S_1', S_2')$ into the reaction hash $\overrightarrow{\mathbb{R}}$ and update the total reaction rate, $R_{tot} \leftarrow R_{tot} + R(S_1', S_2')$.

6. Locate in the all-cluster hash $\overrightarrow{S}_{all}$ the same clusters S_i that are stored in the dynamic array and reset the values of f_1 and f_2: $0 \leftarrow f_1(S_i)$ and $0 \leftarrow f_2(S_i)$ and clear the dynamic array.

If the τ-leaping method is implemented, update the noncritical cluster hash $\overrightarrow{P}$ and noncritical reaction hash $\overrightarrow{\mathbb{J}}$ at the end of Steps 2, 3 and 5 above as described in Algorithm 3.1.

Algorithm 3.3 Main reaction event loop.

1. If the simulation is resumed from a pre-existing one, enter input data into the hash tables $\overrightarrow{S}_{all}$, $\overrightarrow{S}_{m}$, and $\overrightarrow{\mathbb{R}}$. Set the appropriate initial time and compute the total rate R_{tot} of all reactions associated with existing defect clusters in $\overrightarrow{S}_{all}$. Skip to Step 3.

2. Update the $\overrightarrow{S}_{all}$, $\overrightarrow{S}_{m}$ and $\overrightarrow{\mathbb{R}}$ hashes and the total reaction rate R_{tot} as described in Algorithm 4.5.2. Perform volume rescaling if the conditions in Eq. 3.10 are satisfied.

3. If SSA has run less than N_{SSA} steps: select and execute a reaction event $\mathbb{R}(S_1, S_2) \in \overrightarrow{\mathbb{R}}$ and calculate the time to next reaction event using Eqs. 2.7 and 2.8, store identities of the effected clusters in the dynamic array and return to Step 2 until the final time is reached; else: go to Step 4.

4. Reset $N_{SSA} \leftarrow 0$. If the noncritical reaction hash $\overrightarrow{\mathbb{J}}$ is empty: τ-leaping cannot be performed, return to Step 3; else:

   (a) Calculate the value of $g(P_i)$ for each cluster $P_i \in \overrightarrow{P}$ based on the values of its O_i parameters as described in Section 3.4.3.

   (b) Determine the value of the noncritical time leap τ' using Eq. 3.4.

   (c) Calculate the total reaction rate R_{cr} of all the critical reactions in $\overrightarrow{\mathbb{R}}_{cr}$ and the critical time leap τ'' using Eq. 2.7.

   (d) If τ' is less than some small n-multiple (we set n equal 10) of $1/R_{tot}$, temporarily abandon τ-leaping and return to Step 3.

   (e) Else:

      i. Take the leap time to be the smaller value of τ' and τ'', $\tau = min\{\tau', \tau''\}$.

      ii. Calculate the number of times each reaction $\mathbb{J}_i \in \overrightarrow{\mathbb{J}}$ will fire during this time interval $[t, t+\tau)$ as described in Section 3.4.3.

      iii. If $\mathcal{P}(J\tau) > X(P_1)$ (if $\mathbb{J}_i$ is a 1^{st}-order reaction) or $\mathcal{P}(J_i\tau) > min\{X(P_1), X(P_2)\}$ (if $\mathbb{J}_i$ is a 2^{nd}-order reaction): reduce τ' by half and return to Step 4(d). Else: assign $k(\mathbb{J}_i) \leftarrow \mathcal{P}(J_i\tau)$, $k(P_{1,2}) \leftarrow k(P_{1,2}) + k[\mathbb{J}(P_1, P_2)]$. If $k(P_{1,2}) > X(P_{1,2})$: reduce τ' by half and return to Step 4(d).

      iv. Execute $\mathbb{J}_i \in \overrightarrow{\mathbb{J}}$ a number of $k(\mathbb{J}_i)$ times. Store the identities of the effected clusters in the dynamic array if $k(\mathbb{J}_i) > 0$. Update $t \leftarrow t + \tau$, then return to Step 2 or stop if the final time has been reached.

      v. If $\tau'' \leq \tau'$: select and execute a critical reaction event $\mathbb{R}(S_1, S_2) \in \overrightarrow{\mathbb{R}}_{cr}$ and store identities of the effected clusters in the dynamic array. If an insertion event is selected, process the event and store the identities of the new clusters in the the dynamic array, then return to Step 2 or stop the simulation if the final time has been reached.

3.5 Verification and performance benchmarking

3.5.1 Case study: Triple-ion irradiation on pure bcc-Fe

Materials performance in nuclear fusion reactors is expected to degrade as a consequence of prolonged exposure to neutron irradiation. However, neutron irradiation experiments are costly, irradiation facilities are scarce and presently achievable neutron fluxes are low requiring years of exposure before material specimens receive a significant dose of irradiation. As a faster and more cost effective alternative for assessing irradiation-induced changes in physical and mechanical properties of materials, ion beam experiments are used for accelerated testing of material degradation because ion cascades can produce damage similar to neutron irradiation but on a much shorter time scale. In addition to the displacement damage, material exposure to fast neutrons results in simultaneous formation of He and H atoms through nuclear transmutation reactions. To mimic such specific conditions properly, triple ion beam irradiation can be used in which ions of He and H are co-implanted, either sequentially or concurrently, with the heavy ions imparting the primary (displacement) damage. Recent triple-beam experiments of this kind conducted on iron crystals have revealed pronounced synergistic effects associated with co-implantation of He and H under irradiation by self-ions of Fe [14]. Specifically, the amount of measurable swelling increased several fold when all three ion species were implanted simultaneously, relative to baseline sequential dual Fe^{3+}/ He^{+} and Fe^{3+}/ H^{+} irradiations.

As previously discussed, ODE-based simulations methods have so far proven incapable of coping with complex cluster species with more than two size attributes, as is the case of triple-beam irradiations reported in Ref. [14]. Here we show that our enhanced SCD model is capable of simulating of complex defect microstructures in pure iron subjected to simultaneous irradiation with Fe^{3+} ions and co-implantation with He^{+} and H^{+} ions. In setting up our model and SCD simulations we mimic as close as possible irradiation conditions used in the triple ion-beam experiments performed by Tanaka and coworkers. The model parameters used in SCD simulations reported here are provided in Tables 3.1, 3.2, 3.3.

3.5.2 Model parameters

Table 3.1 lists the parameters describing the host material, irradiation conditions and sink efficiencies used in all the simulations discussed in this dissertation. The diffusivities and binding energies of various defects and clusters considered here are listed in Tables 3.2 and 3.3, respectively. In both tables, literature sources for each parameter type are listed in the rightmost column. Here, diffusion coefficients of all mobile defects and clusters are computed using an Arrhenius function:

$$D(T) = D_0 exp\left(-\frac{E_m}{k_B T}\right)$$

whereas the binding energies of clusters V_n or I_n are computed using the following extrapolation law [57, 58]:

$$E_b(n) = E_f + [E_b(2) - E_f] \left[n^{2/3} - (n-1)^{2/3} \right] / \left(2^{2/3} - 1 \right)$$

For consistency with the microstructures used in Tanaka's experiment [14], here we consider only two types of sinks: grain boundaries and dislocations. Due to the relatively small grain size and high dislocation density, the combined strength of all sinks in our model material is quite high. For dislocations, we assume a bias factor of 20% favoring the absorption of SIAs over that of vacancy-type defects, whereas the grain boundaries are assumed to be neutral sinks. To parameterize our model, we use, whenever possible, available insights gained from both experiments and atomistic simulations. Regarding defect mobilities, only mono and di-vacancies are assumed to be mobile in our models. Once V_nHe_m clusters are formed, only certain combinations of n and m correspond to mobile species, as shown in Table 3.2. All clusters with more than two vacancies are considered immobile regardless of their He content, which is consistent with recent MD simulations of di-vacancy and V–He cluster diffusivity [10, 59]. Due to the lack of any data on the mobility of V_nH_m clusters, such defect complexes are considered immobile for all non-zero values of n and m. For their part, SIA clusters of all sizes are assumed to be mobile with diffusivities given in Table 3.2. At the same time, all I_nHe_m clusters with nonzero n, m values are assumed to have zero diffusivity regardless the number of He atoms contained in the complex (in substitutional or interstitial form), as suggested by two MD studies in which SIA clusters and He atoms were observed to react and form stable sessile complexes [11, 60].

In our models, H can form SIA-H and V-H complexes but these complexes are unstable, consistent with experimental observation in which hydrogen atoms can easily escape from vacancies between 423 K and 573 K [75]. In the current stage, we choose to disregard one-dimensional diffusion of SIA/SIA clusters and assume that all mobile defect species move three-dimensionally for the sake of simplicity. With respect to cluster dissociation reactions, we have assumed that all SIA–He clusters are thermally stable following Ventelon *et al.*, who have reported binding energies from 1.3 to 4.4 eV for small SIA–He clusters [11]. The numerical parameters pertaining to the mechanisms described above are given in Tables 3.1, 3.2 and 3.3.

3.5.3 Results

We have performed simulations of triple-beam irradiation and tracked the accumulation of pure vacancy (V), V-He, V-H, and V-He-H clusters in the simulation volume using first direct (exact) SCD simulations [15] and then repeated the same simulations after turning on, one by one, the various enhancements described in the preceding sections. The inset to Fig. 3.3 shows the concentrations of various types of clusters as functions of simulated irradiation time as obtained with the original (unenhanced) SCD model.

Each curve in the inset was obtained by averaging over five independent simulations

Table 3.1: Material and simulation parameters used for the multi-ion irradiation simulations

Material parameters:	Symbol		Unit
Atomic density	ρ_a	8.5×10^{28}	$[m^{-3}]$
Lattice parameter	a	2.9×10^{-10}	$[m]$
Dislocation density	ρ_d	3×10^{15}	$[m^{-2}]$
Grain size	S_g	10^{-6}	$[m]$
Irradiation parameters:			
Temperature	T	$743, 783, 873, 973$	K
dpa rate		1.6×10^{-3}	$[s^{-1}]$
Fe ion energy	E_i	10.5	$[MeV]$
He/dpa ratio		10	$[appm]$
H/dpa ratio		40	$[appm]$
Simulation parameters:			
Volume	V	10^{-19}	$[m^3]$
SIA dislocation capture efficiency	Z_{di}	1.2	
Vacancy dislocation capture efficiency	Z_{dv}	1.0	
SIA grain boundary capture efficiency	Z_{gi}	1.0	
Vacancy grain boundary capture efficiency	Z_{gv}	1.0	

starting from different random seeds. The main figure shows the relative deviation from the reference (unenhanced) simulations in the net vacancy cluster population obtained in SCD simulations with enhancements. For consistency, five independent simulations were performed for every enhancement. The error bars shown on the plot can be used as a measure of statistical significance of the observed deviations. As the figure shows, the results of enhanced SCD simulations fall within the statistical errors to the exact (reference) simulations which verifies that the approximations used here to improve computational efficiency of SCD simulations, namely τ-leaping and volume rescaling, are not distorting the simulated kinetics of damage accumulation (for simulations shown in Fig. 1 we used the following values of runtime parameters: $n_{cr} = 10$ and $\epsilon = 0.03$ for τ-leaping and γ ranging from 0.99999 to 0.9999 for volume rescaling). The ratio γ can be reduced further to achieve even greater speedup, but accuracy is what we prefer here since we have already managed to reduce the computing time significantly with the current simulations.

3.5.4 Performance

A rather significant –a factor of 20 or higher– speedup in SCD simulations is attained simply due to a greater efficiency of the incremental updates of the evolving reaction network and associated reaction rates, as described in Sections 3.4.1 and 3.4.2. This is a general improvement resulting from a better implementation of the standard SCD algorithm reported in Ref. [15]. We use the efficiency of our standard SCD simulations

Table 3.2: Diffusion coefficients of the mobile species considered for the multi-beam irradiation simulations.

Species	$D_0\,(\mathrm{m^2 s^{-1}})$	$E_m\,(\mathrm{eV})$	Reference
I_1	1.3×10^{-8}	0.25	[66]
I_2	351.6×10^{-8}	0.36	[66]
I_3	12.1×10^{-8}	0.14	[66]
I_4	12.3×10^{-8}	0.15	[66]
n >4	$9.0 \times 10^{-7}\mathrm{n}^{-0.6}$	$0.06 + 0.07\mathrm{n}^{-1.3}$	[67]
V_1	7.9×10^{-7}	0.06	[68]
V_2	3.5×10^{-8}	0.66	[69]
V_1He_2	3.3×10^{-7}	0.31	[10]
V_1He_3	3.2×10^{-8}	0.30	[10]
V_1He_4	2.1×10^{-9}	0.31	[10]
V_2He_1	4.1×10^{-8}	0.27	[70]
V_2He_3	9.9×10^{-9}	0.53	[10]
He_1	2.8×10^{-8}	0.06	[10]
He_2	3.0×10^{-8}	0.08	[10]
He_3	1.0×10^{-8}	0.07	[10]
He_4	0.1×10^{-8}	0.05	[10]
He_5	1.6×10^{-9}	0.20	[71]
He_6	3.9×10^{-9}	0.28	[71]
H_1	1.5×10^{-7}	0.09	[72]

Table 3.3: Binding energies for all species used for the triple ion-beam irradiation simulations. $E_{fi} = 3.8$ eV and $E_{fv} = 1.7$ eV are the SIA and vacancy formation energies.

Species	$E_b\,(\mathrm{eV})$	Reference
I_2	0.80	[73]
I_3	0.92	[73]
I_4	1.64	[73]
n>4	$E_{fi} - 5.06\left[\mathrm{n}^{2/3} - (\mathrm{n}-1)^{2/3}\right]$	[57]
V_2	0.30	[73]
V_3	0.37	[73]
V_4	0.62	[73]
n>4	$E_{fv} - 3.01\left[\mathrm{n}^{2/3} - (\mathrm{n}-1)^{2/3}\right]$	[57]

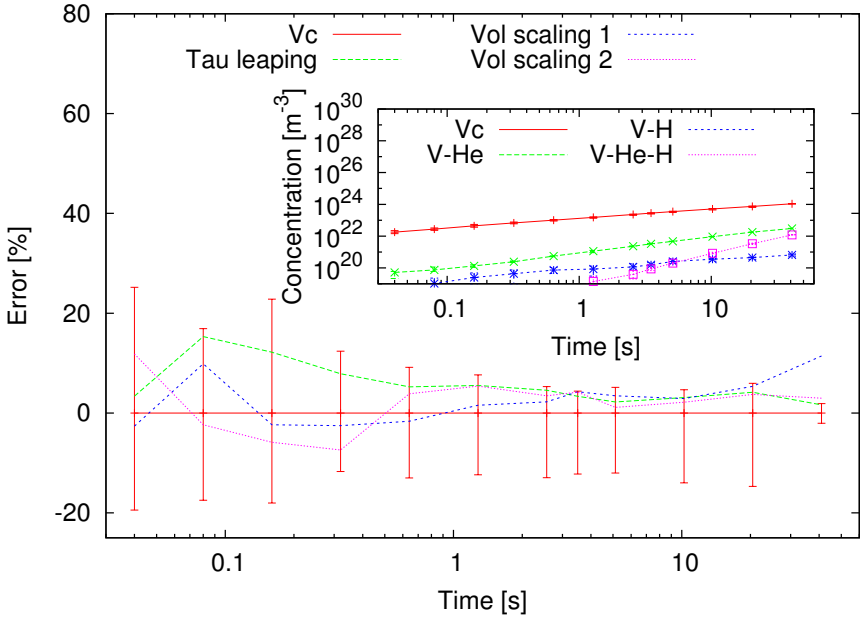

Figure 3.3: Statistical errors of various enhancement methods compared to the original SCD model. The specimen is under triple-ion irradiation of Fe^{3+}, He^{+} and H^{+}, total irradiation time is 40.96 *secs* and the temperature is 783 K. The inset shows the concentrations of various defect-cluster types as functions of irradiation time, in this case the simulation is carried out using the original SCD algorithm with no improvement. Here, Vol scaling 1 uses $\gamma = 0.9999$, and Vol scaling 2 uses $\gamma = 0.99999$.

with incremental updates as a reference comparison with further enhancements.

We find that, in our SCD simulations of irradiated iron, conditions for τ-leaping are often satisfied and many reactions can be allowed to fire at once rather than one at a time. The key condition for τ-leaping to be accurate is that the change in the defect population caused by a leaping step should not affect too much the rates of existing reactions. Whenever it is safe to perform, τ-leaping results in longer time-steps compared to the standard (one reaction at a time) SCD algorithm, as shown in Fig. 3.4(b) for the same simulation setup as described in the previous section.

It is clear that, with τ-leaping active, fewer short time-steps are taken than in the direct SCD resulting in a total reduction in the number of time-steps required to simulate the same evolution, beside that the total number of steps taken is reduced significantly, and so is the overhead cost for system updating. This is confirmed in Fig. 3.4, where a histogram of the time-step size distribution for a τ-leaping simulation is plotted and compared to the same histogram obtained from a standard SCD simulation. In addition to showing that the distribution shifts to longer time-steps due to τ-leaping, the same histogram also shows that a few specific timesteps occur much more frequently than the rest, and that they are clearly separated from each another. The observed peaks in the distribution indicate that a handful of noncritical reaction channels dominate the kinetics

in our model, and that our enhanced algorithm can identify and handle such reaction channels efficiently with τ-leaping. Specifically, the first peak in Fig. 3.4, which ranges from 89.2 ps to 123 ps is dominated by the absorption of SIA and SIA clusters by defect sinks. The second group, whose reactions with time-steps between 5.01 ns and 25.1 ns mostly consists of absorption of vacancies by sinks, and reactions in the last group from 0.87 μs to 1.19 μs are predominantly migration of vacancy clusters to defect sinks. As a result, τ-leaping is not only better for computational efficiency, but it also provides very useful physical information by identifying the reactions that control the kinetic evolution of the system. This has implications beyond efficiency improvements because it can indicate where to focus the efforts to calculate the physical parameters that matter the most with maximum accuracy. This can potentially be helpful in uncertainty quantification of the models and/or to learn where to devote efforts to improve the physical parameterization.

To quantify the speedup gained from the enhancements described in this paper, the computational cost of SCD simulations performed with and without the enhancements is plotted in Fig. 3.5 as a function of the simulated time. As the figure shows, significant gains in simulation efficiency are realized using τ-leaping and volume rescaling. τ-leaping is typically most efficient at early stages of SCD simulations but its associated speedup is subsequently negated by an increasing computational cost of updates of the growing reaction network. Under such circumstances volume rescaling is prescribed to control the size of a growing defect population. When used together, these two enhancements significantly reduce the wall clock time of a SCD simulation without detectable sacrifice in its accuracy. As an example, Fig. 3.5 shows that while it took the original SCD algorithm more than two days to achieve a trivial irradiation dose of 0.1 dpa, it only takes the enhanced algorithm only about 12 hours to reach a technologically significant dose of 50 dpa.

3.6 Conclusion

We have presented a computationally efficient implementation of the SCD algorithm originally devised as an adaptation of the well-known SSA method to simulations of complex microstructure evolution in irradiated materials. The key advantage of the SCD model is that, unlike the traditional ODE-based rate theory approaches that notoriously suffer from combinatorial explosion, SCD handles with ease multi-species populations of arbitrary complexity. However, early applications of the original SCD algorithm to irradiated materials exposed several computational bottlenecks, e.g. wide disparity in reaction rates and stiff kinetics. Enhancements presented in this paper are introduced to address some of the bottlenecks in order to achieve reactor-relevant irradiation doses at a reasonable computational cost.

Gains in computational efficiency of SCD simulations are achieved through the following: (i) a dynamic reaction-network expansion mechanism to efficiently update the reaction channels and the total reaction rate, (ii) an implementation of the τ-leaping algorithm to accelerate SCD simulations by allowing several reaction events to be leaped

over in one single time-step τ, and (iii) a volume scaling method in which the reaction volume is reduced adaptively in order to control the computational cost while preserving statistically significant defect populations.

Further enhancements to the SCD algorithm reported here are being considered, e.g. a more robust method for τ-leaping implementation into SCD simulations of stiff reaction networks with wide spectra of reaction rates [44, 45], or the implementation of slow-scale SSA (ssSSA) as suggested in Refs. [46] to [54], as well as an adaptive mechanism for deciding which method is best to use at each particular stage of an SCD simulation to optimize the overall computational performance. Efficient parallelization of the SCD algorithm is another interesting venue for further research, e.g. following replication strategies recently proposed in the context of parallel kinetic Monte Carlo algorithms [56] or parallel replica method [84]. We note that, in addition to our SCD development borrowing heavily from the SSA method ideas, algorithmic enhancements reported here can be re-used in other simulation contexts where reaction-diffusion processes with dynamic species populations are of interest, such as in combustion science, cellular process simulation, or chemical kinetics.

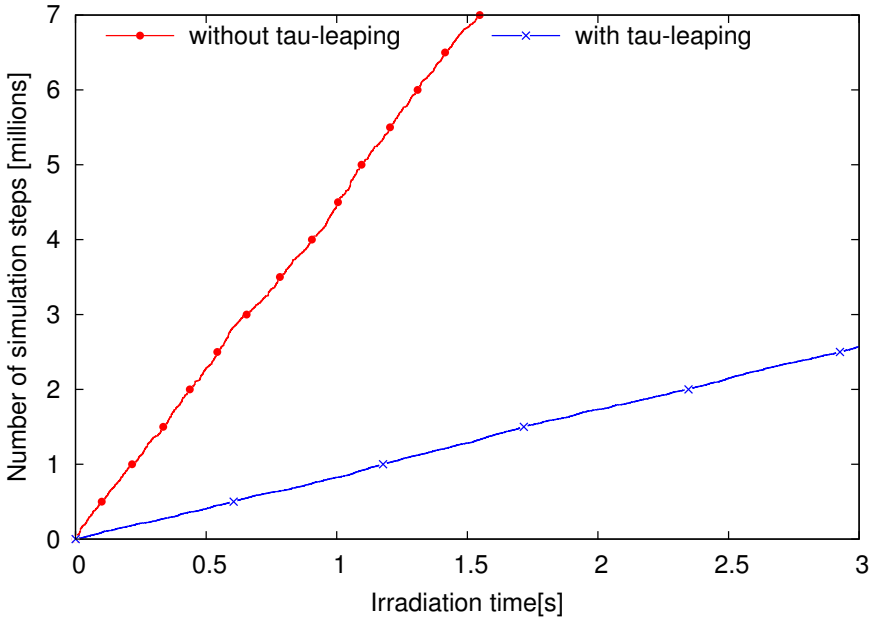

(A)

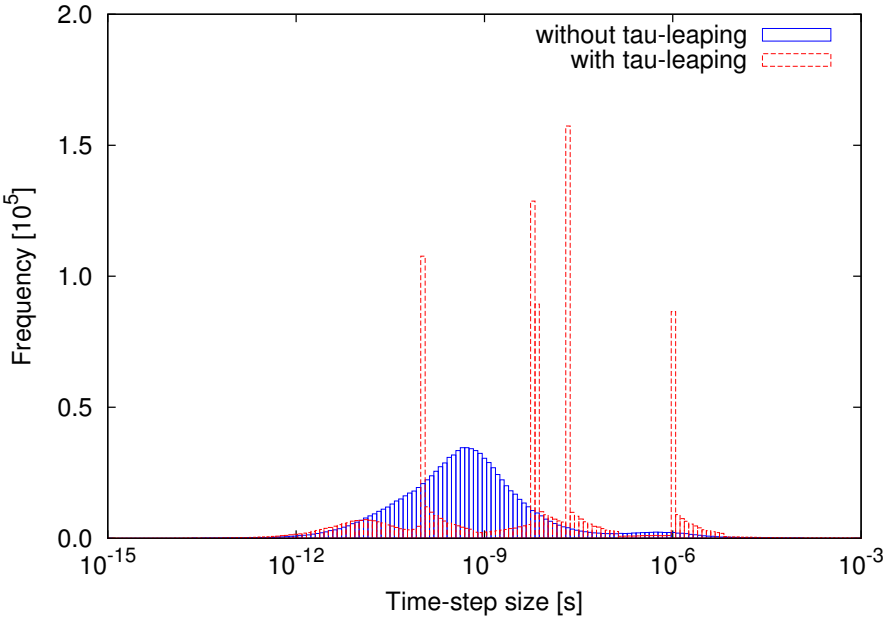

(B)

Figure 3.4: (A) Number of simulation steps as function of the irradiation time obtained from SCD simulations of triple-beam irradiation at 783 K with and without τ-leaping implementation. (B) Distribution of the time-steps in these two cases, here one millions time-steps are collected and analyzed.

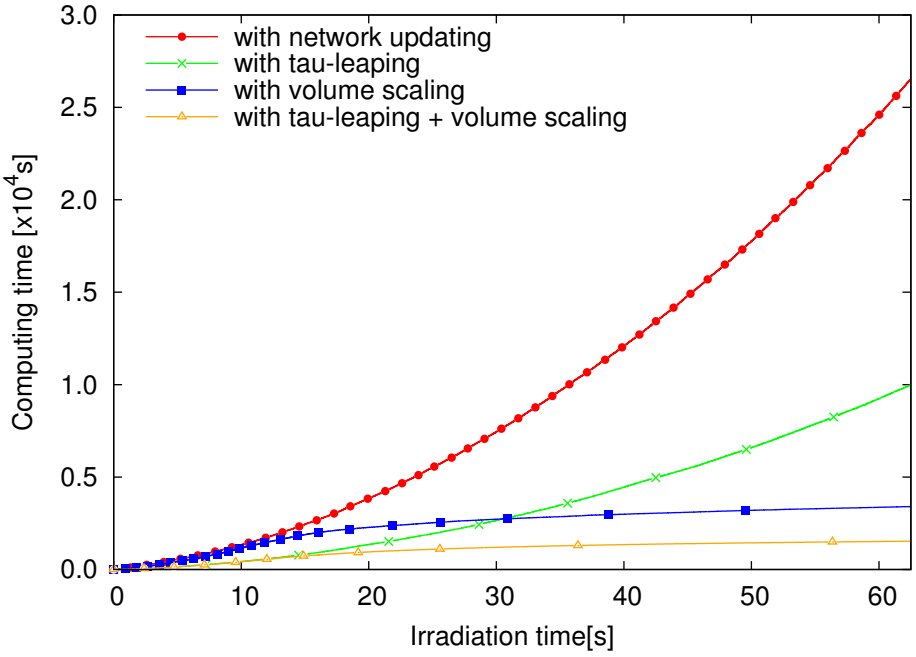

Figure 3.5: Comparison of computational cost of the SCD model with different enhancement methods, here a scaling ratio, $\gamma = 0.99999$ is used whenever the volume scaling method is implemented.

Chapter 4

Simulations of complex synergies in bcc-Fe under multi-ion irradiation

4.1 Introduction

Under multi-ion irradiation conditions present in accelerated material-testing facilities or fission/fusion nuclear reactors, the combined effects of atomic displacements with radiation products may induce complex synergies in the materials. However, limited access to multi-ion irradiation facilities and the lack of computational models that are capable of simulating complex defect evolution make it difficult to understand the physical processes actually taking place in the materials under these extreme conditions. In this chapter, we carry out simulations using our enhanced stochastic cluster dynamics (SCD) models to investigate the microstructural evolution in bcc-Fe under simultaneous Fe^{3+}, He^{+} and H^{+} triple-ion irradiation. It is shown that the observed synergistic effects may be attributed to the formation of stable V-He-H clusters, and the retention of both He and H as well as their competition for defect sinks appear to play major roles in this case. On average, the triple clusters are significantly larger than other defects and may account for the large clusters observed experimentally. Temperature influences formation and structure of these triple V-He-H clusters, leading to a temperature dependence of the overall volume swelling ratio, as well as of the size and density of cavities. However, simulation results also suggest that the synergistic effects reported in Ref. [14] might be overstated if swelling from small defect clusters were not quantified properly.

4.2 Computational models

In this study, we use our enhanced SCD models to study the evolution of defect species in pure bcc-Fe under steady dual and triple-ion irradiations. The dual beam configurations consist of Fe^{3+} in one beamline and either He^{+} or H^{+} on the other while, in the triple beam configuration, all three species are implanted into the material simultaneously. Simulation conditions applied are the same as those in Tanaka's experiments [14]. The irradiation

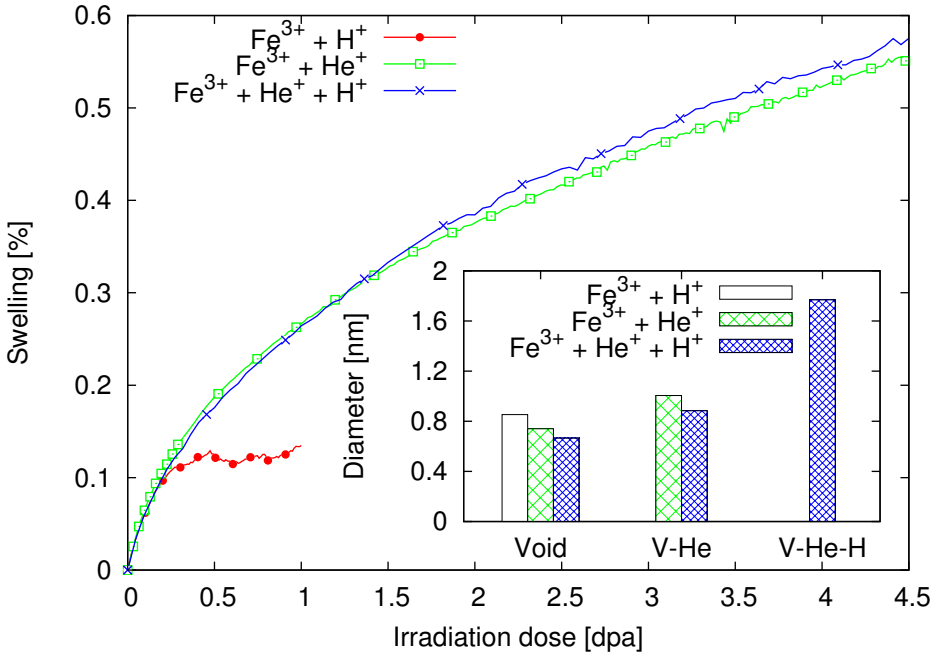

Figure 4.1: Material swelling and average sizes (inset) of defect clusters formed under dual and triple-ion irradiations in bcc-Fe at 783 K. Sizes are measured at the end of the irradiations at 1 *dpa* (for dual (Fe^{3+} + He^{+}) ion irradiation) and 4.5 *dpa* (for dual (Fe^{3+} + He^{+}) and triple-ion irradiations).

dose rate is $1.6 \times 10^{-3} dpa/s$, the co-implantation rates of He^{+} and H^{+} are 10 *appm*/*dpa* and 40 *appm*/*dpa*, respectively. The irradiation temperature varies between 743 K and 973 K. Material and simulation parameters used in the models are shown in Table 3.1, other physical properties of defect-clusters are listed in Tables 3.2 and 3.3. With SCD, we can easily modify simulation conditions such as irradiation temperature, implantation rate or dislocation density, allowing us to model different experiment scenarios. From these simulations, we will examine the evolution of defect populations, and their size distributions as functions of time and temperature and try to understand how the interaction of radiation species gives rise to different phenomena observed in the experiments described earlier.

4.3 Results and Discussion

4.3.1 Radiation damage under dual and triple-ion irradiation

Fig. 4.1 shows the average sizes of different types of defects formed in pure bcc-Fe and the corresponding swelling ratios for the three cases of dual and triple-ion irradiations described above. It can be seen that swelling is the highest under triple-ion irradiation compared to the two dual-ion irradiation cases. Also, the triple V-He-H clusters grow sig-

nificantly larger than other types of defects. Some of these simulation results qualitatively agree with were measured experimentally. Dual-ion ($Fe^{3+} + H^{+}$) irradiation seems to have insignificant effect on the overall swelling while it is most pronounced under triple ion irradiation as seen in Ref. [14]. This is understandable since at the current temperature (783 K), H atoms only loosely bind with existing defects and eventually get absorbed at sinks or free surfaces, thus playing a negligible role in this case. On the other hand, the retention of H definitely contributes to the synergies observed in the triple-ion irradiation case.

However, our simulations show only a small difference in swelling between the triple-ion and dual-ion ($Fe^{3+} + He^{+}$) irradiation cases, and the synergies of He and H gas species are not as significant as those observed experimentally. A possible reason is that every single defect, no matter how small it is, can be accounted for in our models meanwhile only large defect clusters can be resolved experimentally in the TEM micrographs. Fig. 4.2(A) shows the size distributions of cavities formed in F82H steel irradiated at 470 C to 50 *dpa* with triple and dual-ion beams under fusion condition carried out at TIARA by the same group as in Ref. [14]. Apparently, only cavities larger than 2 *nm* were counted in these cases. It can be seen in Fig. 4.2(B) that vacancy clusters totally outnumber other defect types, and most of these clusters are smaller than 2 *nm* in diameter. Our simulations also show that vacancy clusters produce over 60% of the total swelling developed in bcc-Fe under triple-ion irradiation as shown in Fig. 4.7. Therefore, it is possible that swelling was underestimated in Tanaka's experiments, especially in the ($Fe^{3+} + He^{+}$) and ($Fe^{3+} + H^{+}$) dual-ion irradiation experiments, and the reported synergistic effects might be exaggerated as a result.

As can be seen in Fig. 4.3, if we only take into account swelling due to defect clusters that are larger than 1 *nm* in diameter, the sum of swelling caused by ($Fe^{3+} + He^{+}$) and ($Fe^{3+} + H^{+}$) dual-ion irradiations is actually less than swelling caused by triple-ion irradiation. Thus, it shows that the synergistic effects observed are very sensitive to how swelling is actually measured. Besides, we only carry the simulations up to 4.5 *dpa* as compared to a total dose of 50 *dpa* in Tanaka's experiment [14]. As irradiation continues, the buildup of dislocation networks and other defect sinks indeed accelerates the swelling which will be discussed in more details later. The limited number of physical parameters available for use in our models also contributes to this discrepancy. However, SCD models have proven to be capable of capturing the underlying physics of multi-ion irradiation experiments, and the results can be further improved if more physical parameters, either obtained from experiments or atomistic calculations, are supplied to the models.

4.3.2 Effect of He^{+} : H^{+} implantation ratio

It is shown experimentally that the presence of He strongly influences the retention of H atoms in bcc-Fe [8, 76]. Due to their high mobility in bcc-Fe, H atoms will compete with He atoms for defect sinks such as dislocations, grain boundaries and existing defect-clusters. However, even when the vacancy sites are filled up by H atoms, they can be replaced by He atoms when He atoms come into contact with the V-H bubbles [74]. Results obtained

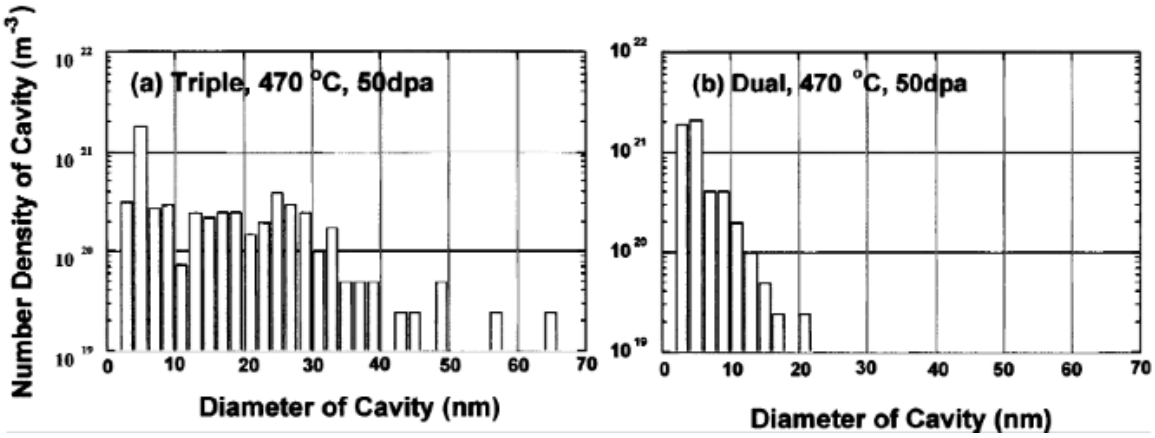

(A)

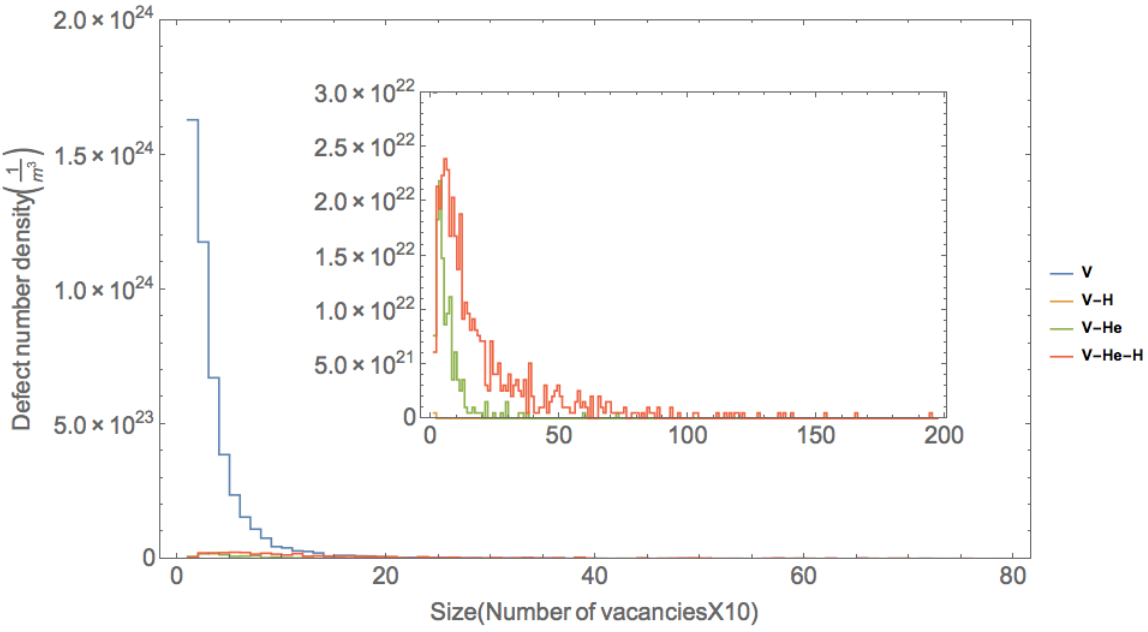

(B)

Figure 4.2: Size distributions of cavities formed in (A) F82H steel irradiated at 470 C to 50 *dpa* with triple and dual ions beams under fusion condition at TIARA [94], and in (B) bcc-Fe irradiated at 783 K up to 1 *dpa* using our SCD model, the inset shows only size distributions of V-H, V-He and V-He-H clusters.

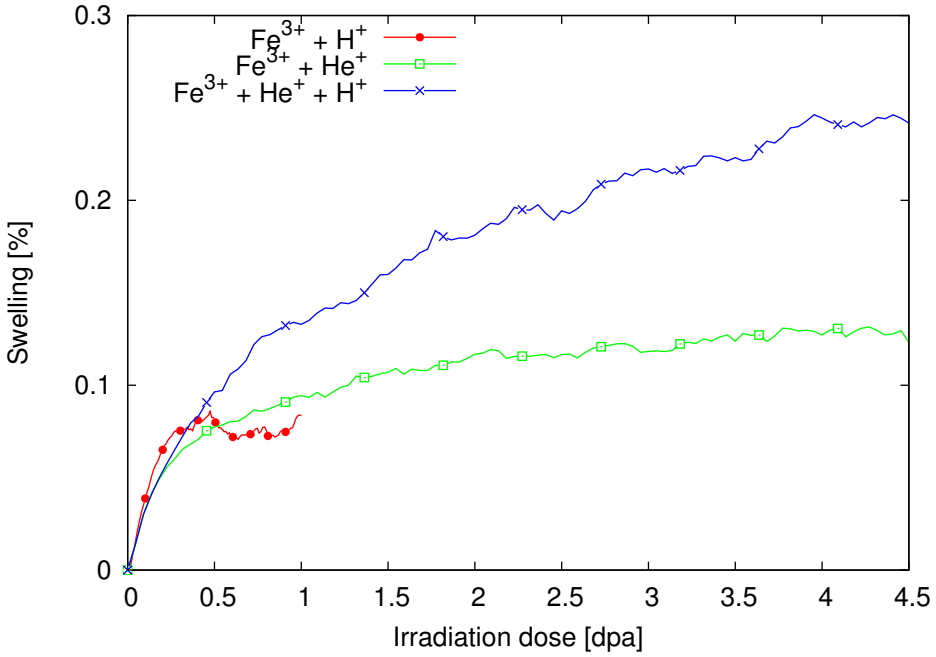

Figure 4.3: Same swelling as in Fig. 4.1 but this time only clusters larger than 1 nm in diameter are included in the swelling estimates.

from positron annihilation lifetime and coincidence Doppler broadening measurements indicate that He atoms are more effective for nano-void formation than H atoms [75]. In Fig. 4.4, our triple-ion irradiation simulations show that He forms V-He clusters with existing voids before the adsorption of H at voids takes place even though H has higher mobility and is more abundant in this case than He, in agreement with experimental observations described above. V-He-H clusters are the last to form in this case. From an experimental point of view, the growth of He bubbles due to absorption of more He and vacancies in the volume induces strong surrounding stress field that eventually attracts H atoms to migrate towards these bubbles to form V-He-H clusters. Moreover, H is usually attracted towards defects that have associated regions of reduced electron densities, which correspond to the large vacancy clusters in our case [76].

Such delayed reactions help explain the incubation period observed before the formation of major V-He-H clusters under triple-ion irradiation shown in Fig. 4.4. As we increase the implantation of He^+ ions, these triple V-He-H clusters will form even sooner. The presence of He within the material has been proven experimentally to significantly enhance the trapping of H, even for periods of years after irradiation [8, 77, 78]. Comparing the vacancy number densities in the reaction volumes for the two cases of dual ($Fe^{3+} + He^+$) ion-irradiation and triple ion-irradiation, we can see that the presence of H under triple ion-irradiation causes a reduction in the populations of voids and He bubbles. It is because a large number of these defects have been consumed to form the V-He-H clusters, and these triple clusters are expected to outnumber other types of defects as

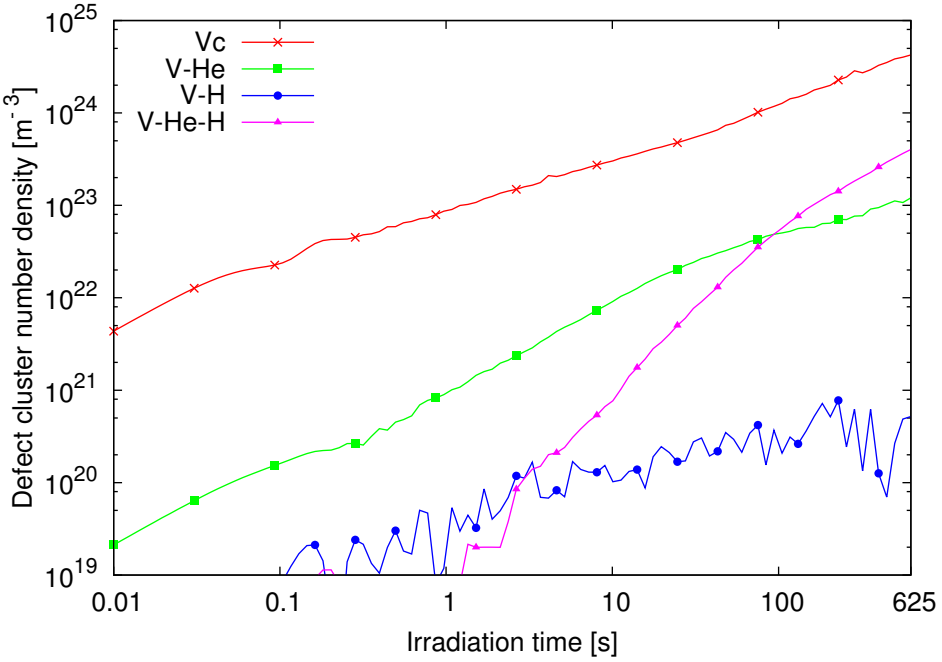

Figure 4.4: Number density of different types of defects formed in bcc-Fe under triple-ion irradiation as function of irradiation time. The material is irradiated up to 1 *dpa*.

irradiation continues.

Using molecular static simulations, Hayward and Deo show that the V-He-H clusters are formed with He atoms located at centers of the bubbles, surrounded by vacancy atoms, and H atoms attach to the outer surfaces. Hayward also points out that the presence of H makes loop punching from V-He-H clusters energetically favorable, leading to the growth of these clusters. These authors argue that, when V-He-H clusters expand, H atoms will be more tightly bound to the clusters due to the expansion of their free surfaces. On the other hand, the presence of H also increases the binding of vacancies to the clusters [79]. In our SCD models, we do not consider loop punching reaction events since the implantation rates of He^+ and H^+ gas ions (10 *appm*/*dpa* and 40 *appm*/*dpa*, respectively) in our current study are insufficient to enable such reactions. However, we also assume that these V-He-H clusters are stable in the current temperature range considered. In other words, no vacancy, He or H atoms will be emitted from these clusters. This is a reasonable assumption since, experimentally, the binding energy of H to He bubbles is very high relative to its binding energies to other defects such as vacancies or voids [76]. Once captured in a bubble, H is in its molecular form, H_2, and dissolution back into the lattice will require chemisorption and dissociation on the bubble surface. These two processes have large activation barriers, especially when O, C or other impurities poison the bubble surface [8].

So far, we can conclude that in order for V-He-H clusters to form, He bubbles must form first, and these bubbles then grow larger due to vacancy absorption and eventually attract

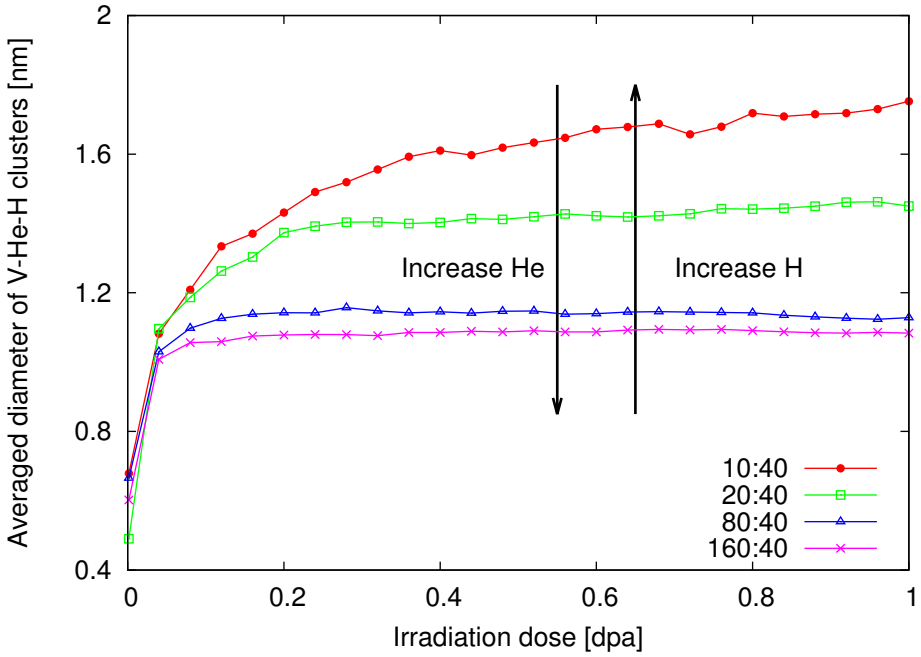

Figure 4.5: Average sizes of V-He-H clusters versus irradiation dose and ratios of He/dpa and H/dpa. The material is irradiated up to 1 *dpa* at 783 K. Implantation rates of He^+ and H^+ are measured in units of *appm*/*dpa*.

H atoms from the host material. Let us try to gain a deeper insight into the connection between the competition of He and H for defect sinks and the synergies observed in Tanaka's triple ion irradiation experiments. When we increase the He^+ implantation rate, we also see that the population of V-He-H clusters also increases, however their sizes are reduced as shown in Fig. 4.5. At the same time, swelling also decreases at increasingHe^+ implantation rate. The reason is that as more He is inserted into the volume, the number of He bubbles nucleated also increases, but these bubbles become smaller. He atoms will now form smaller V-He clusters with many distinctive voids and reduce the number of available mobile vacancies and vacancy clusters that can interact with and enlarge existing bubbles. It is confirmed experimentally that higher implantation rate of He into Fe-5.40wt% Cr causes a higher cavity density in the solid, but the mean cavity size is reduced [83].

The reactions between two defect clusters are governed by the Smoluchowski's equation, which is proportional to the sum$(r_1 + r_2)$, where r_1 and r_2 are their radii. As a result, when V-H clusters are small, their reactions with H atoms are less likely to take place, leading to the decrease of the stable V-He-H cluster population. The latter is the main cause of volume swelling in materials under triple-ion irradiation due to their large sizes. From an experimental point of view, smaller He bubbles produce weaker surrounding stress field, thus the amount of H atoms attracted to them decreases accordingly. On the other hand, loading more H into the volume causes more swelling and larger cluster

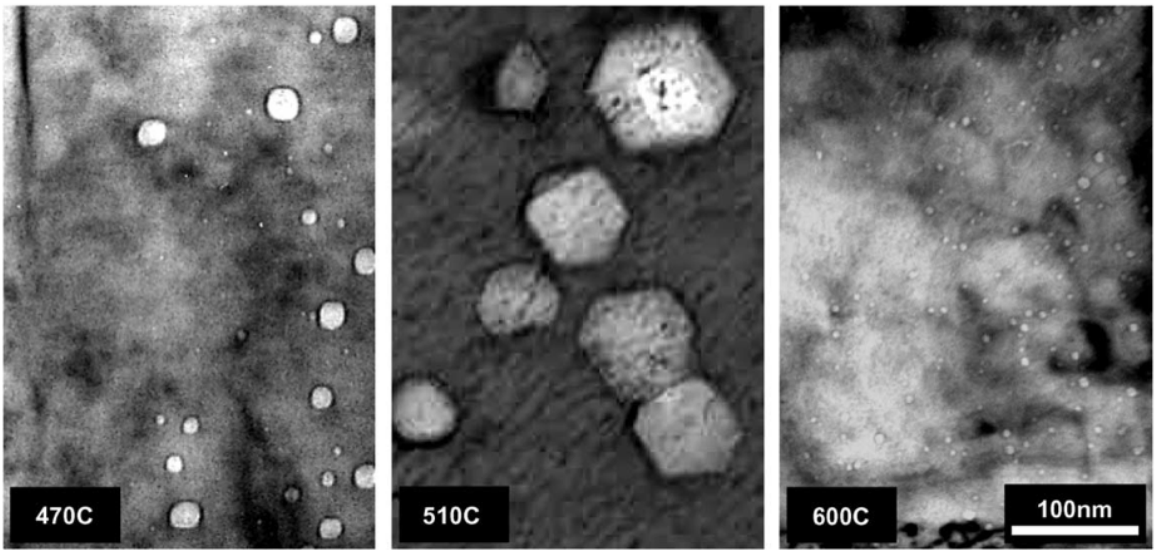

Figure 4.6: Defect structures at different temperatures in 12Cr model alloys under triple-ion irradiations at the TIARA facility [14].

sizes due to the increase in the population of large and stable V-He-H clusters, as shown in Fig. 4.5. Thus, it can be seen that the $He^+ : H^+$ implantation ratio as well as the retention of both He and H directly effect the amount of volume swelling and the formation of defect clusters in the irradiated materials.

4.3.3 Effect of irradiation temperature

In Tanaka's triple-ion experiments, it has been observed that the average size and the number density of cavities are temperature dependent. Volume swelling peaks at 783 K in Fe-12Cr model alloy, and cavities can grow as large as 100 nm in diameter as shown in Fig. 4.6.

To better understand the physics behind these observations, we carried out the above triple-ion irradiation simulations at different temperatures from 743 K to 973 K. Fig. 4.7 shows sizes and contributions to the total swelling of different defect types as function of temperature.

It can be seen that V-He-H clusters are largest in the 783 K to 873 K temperature range compared to those outside of this range. It is also shown that the contribution to the overall swelling of V-He-H clusters is higher within this temperature range while He bubbles contribute the same amount to the overall swelling regardless of the irradiation temperature. The reason is that under increasing temperature, defects become more mobile and interact more frequently to form clusters, many will accumulate at existing bubbles and cause them to grow larger. However, experiments show that defect clusters start shrinking and swelling decreases when the temperature continues to increase [14].

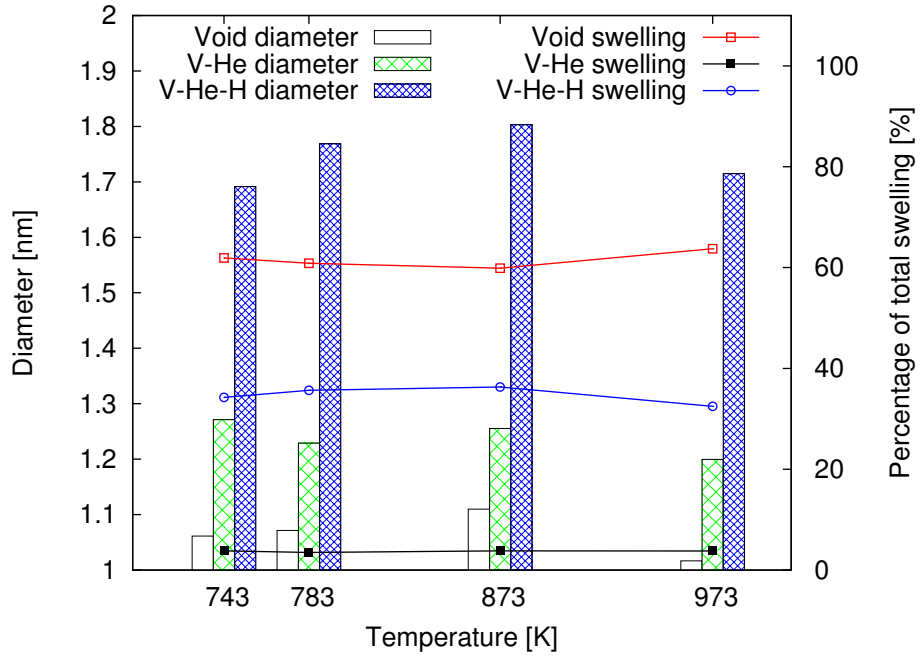

Figure 4.7: Average sizes and the contributions to swelling of various types of defects formed in bcc-Fe under triple-ion irradiations at different temperatures. Defect sizes are measured after the material is irradiated to 1 *dpa*.

In the high temperature range, H starts disassociating from the triple clusters due to its low binding energy. H has the activation energy for migration at 0.059 eV, while the V-H binding energy is 0.57 eV [80]. Thus, the binding energy of H from H-V cluster is 0.63 eV in bcc-Fe while that of He is around 3.9 eV [81]. As the temperature increases, vacancies and He atoms begin to leave the bubbles at around 1173 K [82], at the same time self-interstitial atoms (SIAs) also annihilate with vacancies in these clusters more often and reduce their sizes. As a result, V-He-H clusters shrink at high temperatures as been observed in Tanaka's experiments. On the other hand, in the low temperature range, most defects, especially vacancy clusters, are less mobile and accumulate less frequently to form large clusters, making swelling less significant as a consequence. Therefore, the temperature dependence of swelling, defect densities and defect sizes observed in the Tanaka's experiments can be directly related to the temperature dependence of diffusion coefficients as well as binding energies of the defects and defect clusters participating in the reactions.

It should be noticed that in our study, we assume that V-He-H clusters are stable and that monomers do not dissociate from these clusters in the temperature range we consider. Therefore we do not observe the significant size-reduction of these clusters when the irradiation temperature is increased above 873 K, different from what has been reported in Tanaka's experiments. However, it can be seen in Fig. 4.7 that even if we do not allow the V-He-H clusters to emit monomers in our models, high irradiation temperature still

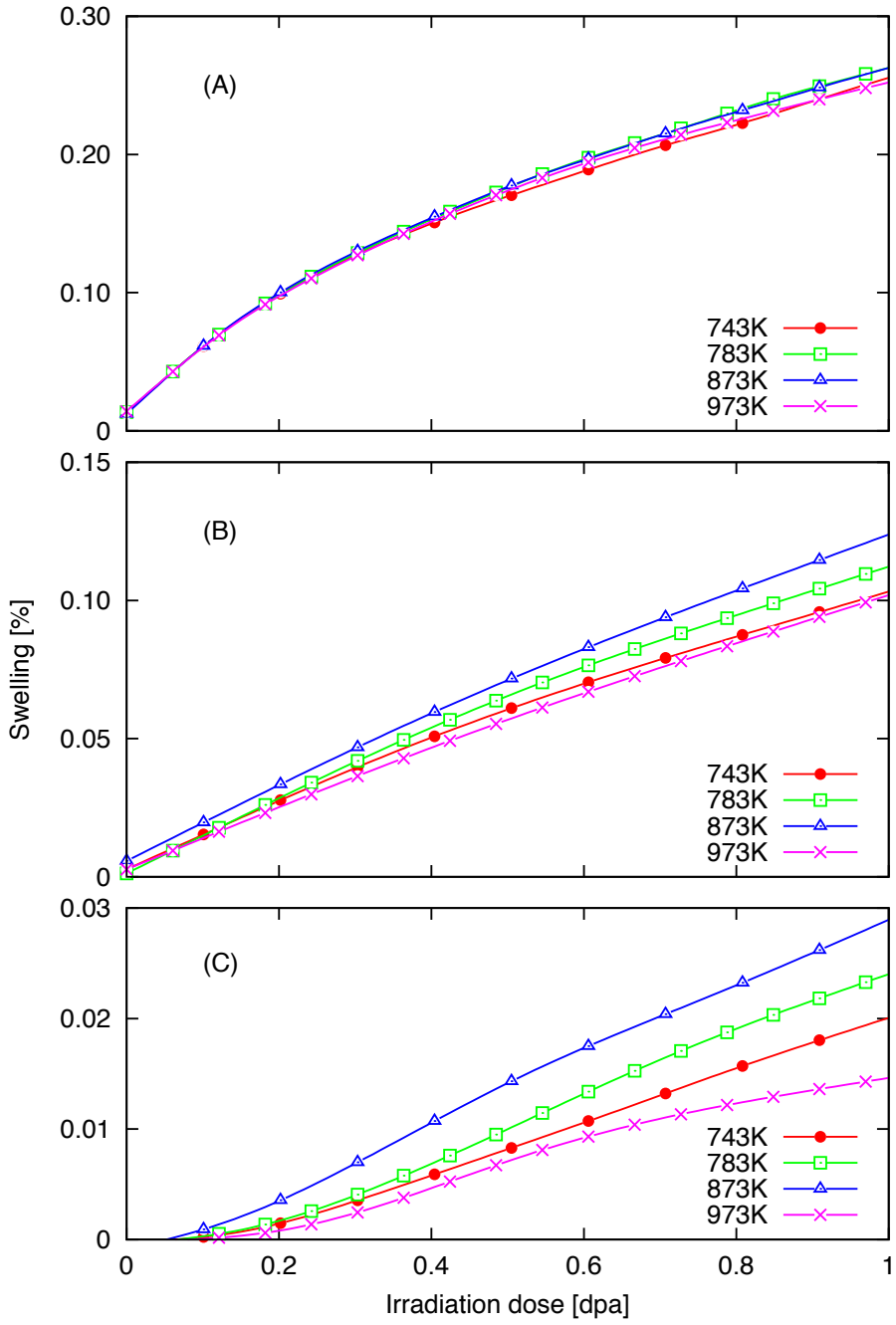

Figure 4.8: Swelling measured at different temperatures in bcc-Fe under triple-ion irradiation. The minimum sizes of defects considered are (A) 0 nm, (B) 1 nm, and (C) 2 nm.

leads to smaller cluster sizes due to the higher number of defect migrating to sinks, leaving lower populations of mobile vacancy-type defects in the volume to form large clusters. The annihilation reactions between vacancy-type and interstitial-type defects also take place more frequently, and the shrinkage of He bubbles eventually reduces the size and population of V-He-H clusters. Fig. 4.8 shows that swelling is relatively higher within the 783 K to 873 K temperature range compared to that measured under irradiation temperatures falling outside of this range. However, exactly how defects are accounted for really effects the actual amount of swelling measured as we mentioned earlier in Section 4.3.1. If we set the minimum size of resolvable defects to be 1 nm or 2 nm, the temperature dependence of swelling becomes more apparent, this may be the case in Tanaka's experiments [14]. Also, it should be noticed that we only achieve a total dose of 1 *dpa* in our simulations compared to 50 *dpa* in Tanaka's experiments, thus direct comparison between experimental and simulation results may not be appropriate.

4.3.4 Effect of defect sink density

As we increase the density of defect sinks in the material, volume swelling also increases as evident in Fig. 4.9. Therefore, it is expected that swelling rate will accelerate as irradiation continues due to the build-up of dislocation network and possible formation of other defect sinks late into the irradiation process. The formation of new defect sinks attracts large amounts of mobile defects, especially SIAs and SIA clusters. As a result, more vacancies and voids will be left behind that will eventually enhance swelling due to the increase in population of V-He and V-He-H defect clusters.

In Tanaka's experiments, dual ion (Fe^{3+} + He^{+}) irradiation causes a 0.4% volume swelling, and the swelling is enhanced to 4% with triple ion irradiation up to 50 *dpa* in 12Cr model alloy. In our simulations, dislocation density remains constant throughout, and the effects due to grain boundaries and other precipitates are ignored. As a result, volume swelling is probably underestimated in our simulations.

Our results suggest that a more consistent treatment of dislocation sink is necessary to improve the fidelity of radiation damage simulation models. Complex interactions exist between defects induced by irradiation and various material interfaces that serve as sinks for irradiation defects. These defect-sink interactions are at the basis of several major detrimental effects of irradiation such as material swelling and radiation induced creep. Due to their complexity, in the existing models such interactions are accounted for in a simplistic manner, if at all. As an example, the preferential absorption of interstitials by dislocations is treated as an effective sink term of fixed power and bias (preference) for interstitial absorption. At the same time, irradiation driven evolution of dislocations themselves is either completely ignored or included as a free adjustable knob (sink density) whose sole purpose is to tune simulation results into agreement with experimental observations. This situation leaves much to be desired, a more realistic model should treat the irradiation-induced defects and the dislocation sinks on an equal footing, as two co-evolving components of the total material microstructure. Therefore, a more physical treatment of defect sinks should be the topic of future development of the SCD model.

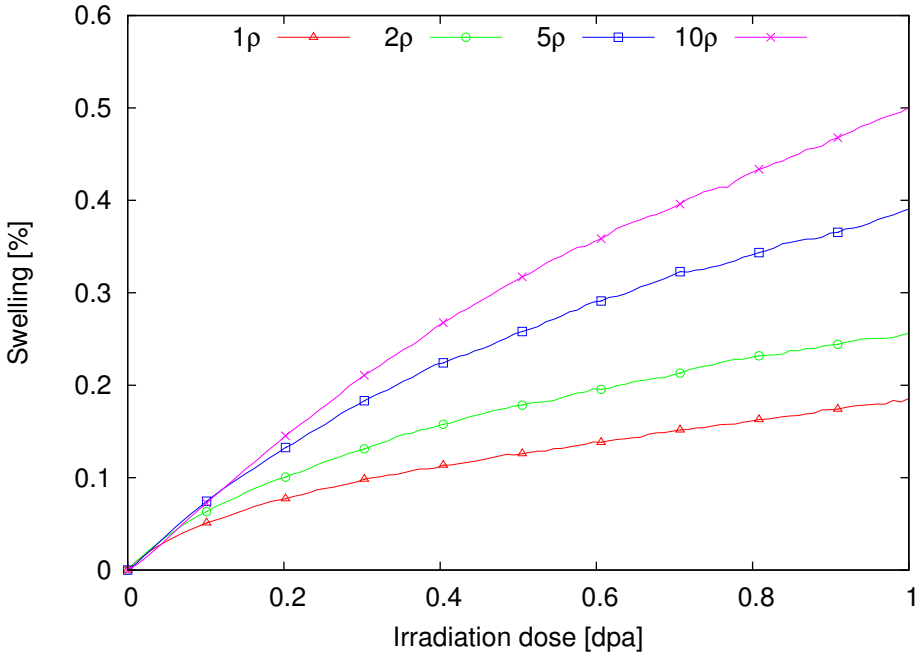

Figure 4.9: Swelling as a function of irradiation dose and dislocation density in bcc-Fe under triple-ion irradiation. The simulations are carried out at 783 K with dislocation density varying 1-10 times above the value of $1.5 \times 10^{11}[cm^{-2}]$.

However, the synergies developed between the gas species also greatly depend on the presence of other component elements in the materials. For example, the amount of chromium certainly effects the swelling ratios in Fe-Cr model alloys in Tanaka's experiments, the higher level of chromium allows more large cavities to form, but the volume swelling ratio is decreased instead [14]. Several neutron irradiations of Fe-Cr alloys have shown that swelling is generally lower for Cr contents between 3-6% [83]. A recent study shows that synergistic effects of He and H are insignificant compared to irradiation with H alone in austenitic 18Cr10NiTi stainless steel [85]. To fully understand the physics behind these phenomena, more efforts are needed to obtain a larger set of physical parameters such as diffusion coefficients and binding energies of component species that involve in the simulations. However, it can be hypothesized that the precipitates in these steels may act as sink traps for H and He atoms, prevent them from forming V-He-H clusters with existing voids in the lattice.

4.3.5 Effect of irradiation dose rate

Another important question regarding the reaction kinetics of radiation damages generated under multi-beam irradiation is whether the observed synergistic effects are rate-dependent in addition to the reported temperature-dependence, and if the effects will greatly diminish or even disappear at much lower dose rates?

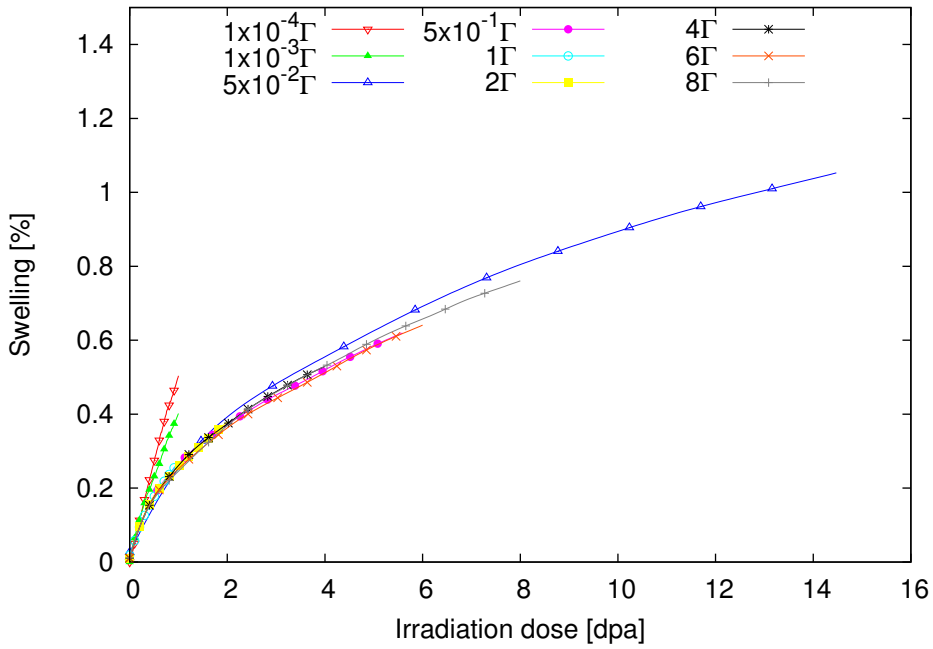

Figure 4.10: Swelling with respect to irradiation dose and dose rate in bcc-Fe under triple-ion irradiation at 783 K.

To address these questions, we carry out the earlier triple-ion irradiation simulation at different irradiation rates. The dose rate is varied between 0.05 to 8 times the current value of 1.6×10^{-3} dpa/s to examine how sensitive the system kinetics is to this change. We observe that the resulting swelling does not change much from the reference case as evident in Fig. 4.10. We also examine the average sizes of defect clusters formed under these new conditions and notice that small changes in the dose rate do not have any significant effect on the cluster sizes either. It appears that irradiation rate does not affect swelling or the synergism as significantly as does He^+ : H^+ implantation rate ratio (which was discussed in Section 4.3.2). In other words, the synergy level as well as the overall volume swelling appear to be more sensitive to the He:H ratio than to the rate at which these gas species are introduced into the material. However, it can be observed from 4.10 that swelling is relatively enhanced as irradiation rate decreases. When we lower the dose rate by three to four orders of magnitude, swelling increases significantly as a result. Fig. 4.11 shows the average sizes of various types of defects formed in bcc-Fe under triple-ion irradiation at 510 C and 1.6×10^{-6} dpa/s dose rate ($\sim 50\, dpa/year$), which are the conditions encountered in potential Generation IV fission reactors (as shown in Fig. 4.12) alongside results obtained from similar simulation but using Tanaka's experiment conditions. It is apparent that low irradiation rate enhances accumulation of mobile vacancies at other defect clusters while reducing the annihilation between vacancies and SIAs. Defects formed under low dose rates are significantly larger than those formed at higher rates which explains the significant increase in swelling.

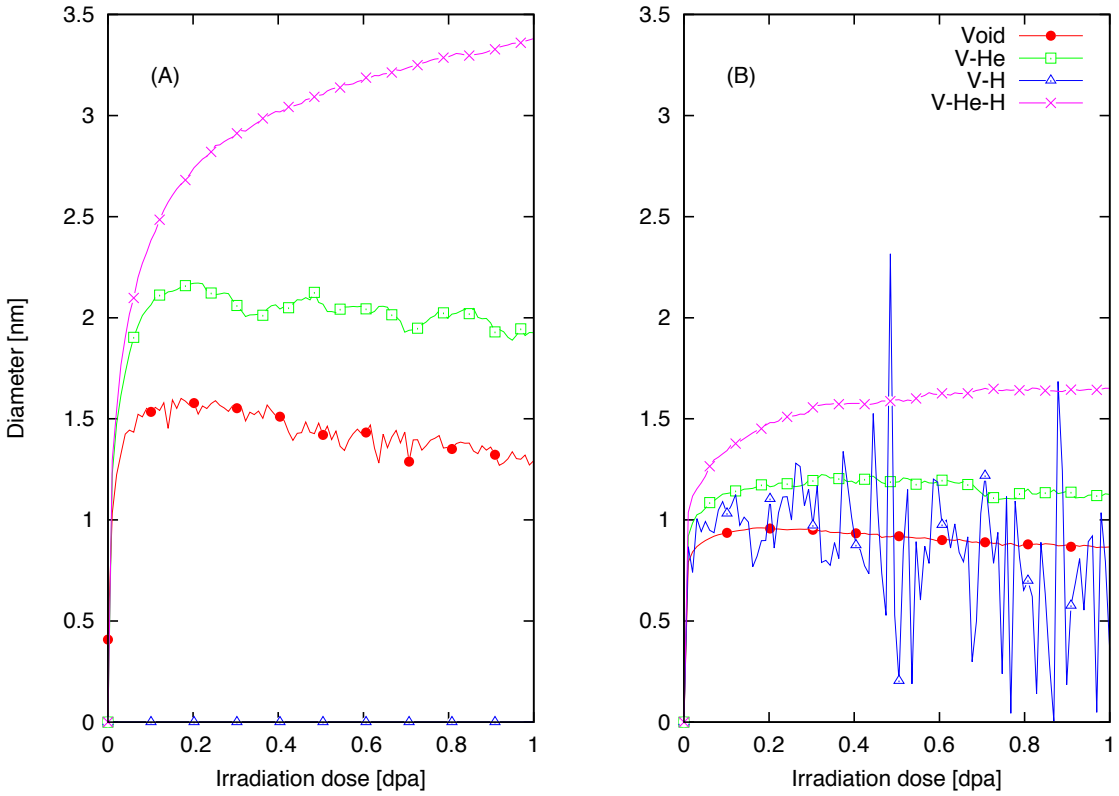

Figure 4.11: Average sizes of various defect types formed in bcc-Fe under triple-ion irradiation at different dose rates: (A) 1.6×10^{-6} dpa/s and (B) 1.6×10^{-3} dpa/s. The irradiation temperature is 783 K.

Besides, newly inserted H atoms quickly attach to large V-He and/or V-He-H clusters, producing stable V-He-H clusters instead of forming unstable V-H clusters with existing voids. From an experimental point of view, this phenomenon can be attributed to the stronger stress field surrounds these clusters and the longer mean free paths that H atoms can travel in the material.

As a result, it is safe to say that for practical dose rates normally encountered in actual accelerators or fission/fusion nuclear reactors, in which structural materials are under constant heavy ion, He and H implantation, swelling is certainly a serious concern and so are synergistic effects (if they actually exist at all).

	Fission (Gen I)	Fission (Gen IV)	Fusion (DEMO/PROTO)	Spallation (ADS)
Structural alloy T_{max}	<300 °C	300–1000 °C	550–1000 °C	140–600 °C
Max dose for core internal structures	~1 dpa	~30–200 dpa	~150 dpa	50–100 dpa
Max helium concentration	0.1 appm	~3–40 appm	~1500 appm (~10,000 appm for SiC)	~5000 appm/fpy
Max hydrogen concentration			~6750 appm	50,000–100,000 appm/fpy
Neutron Energy E_{max}	<1–2 MeV	<1–3 MeV	<14 MeV	Several hundred MeV

Figure 4.12: The dpa fluence or dpa rate encountered in various neutron technologies is shown, along with the helium and hydrogen transmutation [55].

4.4 Conclusion

In summary, we carried out simulations of defect evolution under dual and triple-ion irradiation in bcc-Fe with the goal of gaining insights into the synergistic effects observed in Tanaka's experiments with different Fe-Cr model alloys. Our results suggest that these observed effects are due to the formation and growth of the stable V-He-H clusters, these clusters are largest in size compared to other types of defects formed due to the irradiation. The retention of H appears to play a major role where H atoms are attracted to large V-He bubbles and further stabilize the clusters. The competition between He and H for defects sinks causes larger number of He bubbles (V-He clusters) to nucleate, serving as embryos for V-He-H clusters. This competition also explains the incubation time taking place before the formation of these clusters. The latter clusters are very stable under normal temperature conditions and grow larger as irradiation continues due to absorption of other vacancies. It has been shown that He:H density ratio has a strong influence on the synergy as well as on the overall volume swelling while the irradiation rate does not have much influence within small variations. However, synergistic effects is enhanced and swelling is exacerbated at very low dose rates. There exists a temperature range that allows the V-He-H clusters to grow to maximum sizes, resulting in a high level of swelling within this range. This behavior is directly related to the temperature dependence of defect diffusion coefficients and binding energies. Synergistic effects also strongly depend on the presence of other component elements in the host material which can act as sinks to the implanted gas species. However, exactly how swelling is measured can influence the actual level of synergism. We suggest additional experiments be performed to properly quantify the amount of swelling due to small defect clusters in order to validate the presence of synergistic effects in Fe under multi-ion irradiation.

Chapter 5

Replacing triple-beam irradiation by pulsed single/dual-beam irradiation

5.1 Motivation

In the previous chapter, we suggested better quantification of swelling due to small defect clusters formed under dual and triple-ion experiments to validate the presence of synergistic effects observed in Ref. [14]. Although triple-ion irradiation facilities produce conditions comparable to those encountered in actual nuclear reactors, they usually come with high construction costs so that only a few of such facilities are available around the world at present. As a result, experimental investigations of materials for nuclear applications are carried out using less expensive existing dual-ion or single-ion irradiation facilities that do not generally allow to observe possible synergistic effects of He and H gas species studied here. An interesting question arises is whether it is possible to make some modifications to the configurations of current single/dual-beam facilities that will enable them to produce experimental conditions similar to those in the scarce triple-beam irradiation facilities. A possible and inexpensive solution is to implant the heavy ions and gas species into the material in alternating pulses.

Ion-irradiation experiments in facilities equipped with fast beam-switching systems were performed earlier at ETH Zurich and University of Houston [95, 96]. Fig. 5.1 shows the plan view of the dual-source mass-analyzed low-energy ion beam system housed at University of Houston [96]. In these facilities, the length of irradiation pulses can be narrowed down to about 20 to 200 μs, the pulse repetition rate is adjustable in the range of 10 to 50 Hz, and the ion source switching can be completed within 100 ms using electromagnetic mass separation systems.

So far, most theoretical investigations of radiation damage evolution have been focused on steady irradiation with little attention paid to pulsed irradiation conditions. However, given the inherent pulsing capabilities of current and proposed irradiation facilities such the MTS at LANL, SNS at ORNL, IFMIF and ITER, both theoretical and experimental study of radiation damage under pulsed irradiations is of interest. Simulation studies have

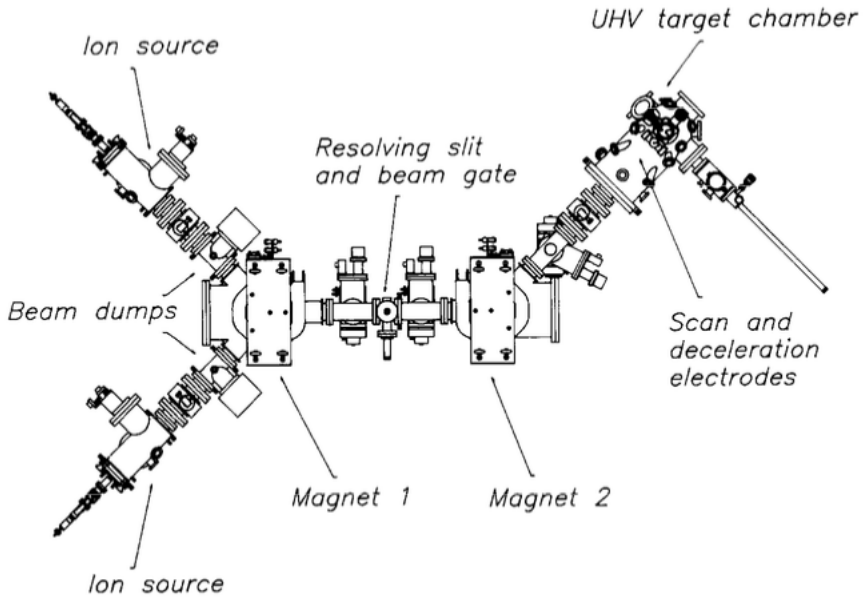

Figure 5.1: Plan view of the dual-source mass-analyzed low-energy ion beam system housed at University of Houston [96].

been reported on the impact of pulsed irradiation on defect evolution in comparison to steady irradiation. These studies show significant differences between these two types of irradiation [86, 87, 88, 89, 90]. However, these calculations were mostly performed only to very small doses, typically less than 0.1 *dpa*. Besides, these earlier studies did not go beyond single specie implantation, and complex defect populations were not considered, thus simplifying the problem significantly. With SCD, we can efficiently achieve higher irradiation doses, handle complex defects and vary simulation parameters to model a wide range of experimental conditions.

In the following section, we will use SCD models to examine if it is feasible to perform pulsed single/dual-beam irradiation to produce damage populations that are similar to those developed under steady triple-beam irradiation in pure bcc-Fe, thus suggesting cost-effective methods to verify the actual presence of synergistic effects observed in Ref. [14]. To the best of our knowledge, these types of simulations have never been attempted before.

5.2 Comparison between pulsed dual-beam irradiation and triple-beam irradiation

5.2.1 Pulse structure

In this study, the assumed dual-beam experiment configuration consists of two beamlines: one beamline consists of a steady Fe^{3+} source just like the one in the triple-beam experiment configuration, the other beamline is connected to both He^{+} and H^{+} sources

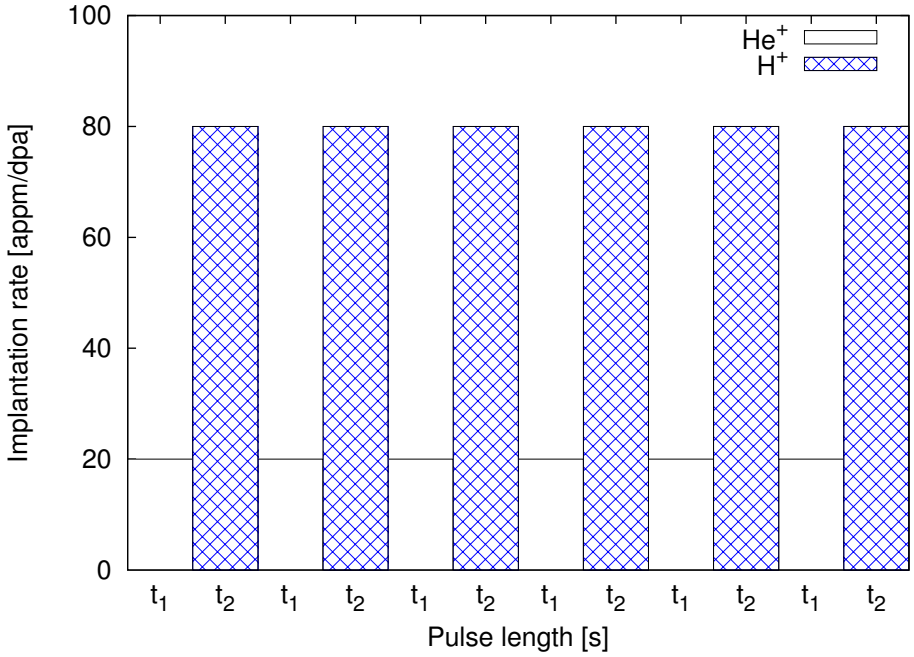

Figure 5.2: Pulsed irradiation schematic of the second beamline. In the first beamline, Fe^{3+} emits at a steady dose rate of 1.6×10^{-3} dpa/s same as in the steady triple-ion irradiation case.

and can implant gas ions in alternate pulses with length t_1 and t_2 as shown in Fig. 5.2. To compensate for the loss of He^+ and H^+fluxes due to the pulsed nature of the second beamline, we increase the implantation rates by a factor of $(t_1 + t_2)/t_1$ and $(t_1 + t_2)/t_2$, respectively.

5.2.2 Results and discussion

Fig. 5.3 shows the number densities of various types of defect species as functions of dose and pulse length and the relative differences in predicted swelling with respect to that obtained under triple-beam irradiation (in the inset). The simulation conditions are the same as in previous sections, irradiation temperature is 783 K and the total damage dose is 10^{-3} dpa. The reaction volume is increased by 1000 times compared to previous simulations in order to collect better statistics at the short irradiation time. As discussed in Section 4.3.2, defect formation in the material is sensitive to the He^+:H^+ implantation rate ratio. This ratio must be kept consistent with that of the triple-beam irradiation to produce the same results. We start with short pulse simulations to examine if pulsed dual-beam irradiation can reproduce results obtained from the reference steady triple-beam irradiation case before pursuing the more expensive simulations with longer and more practical pulses. Another advantage of carrying out pulsed simulations with short pulses is that they allow us to verify the fidelity of our model, i.e. with very short pulses,

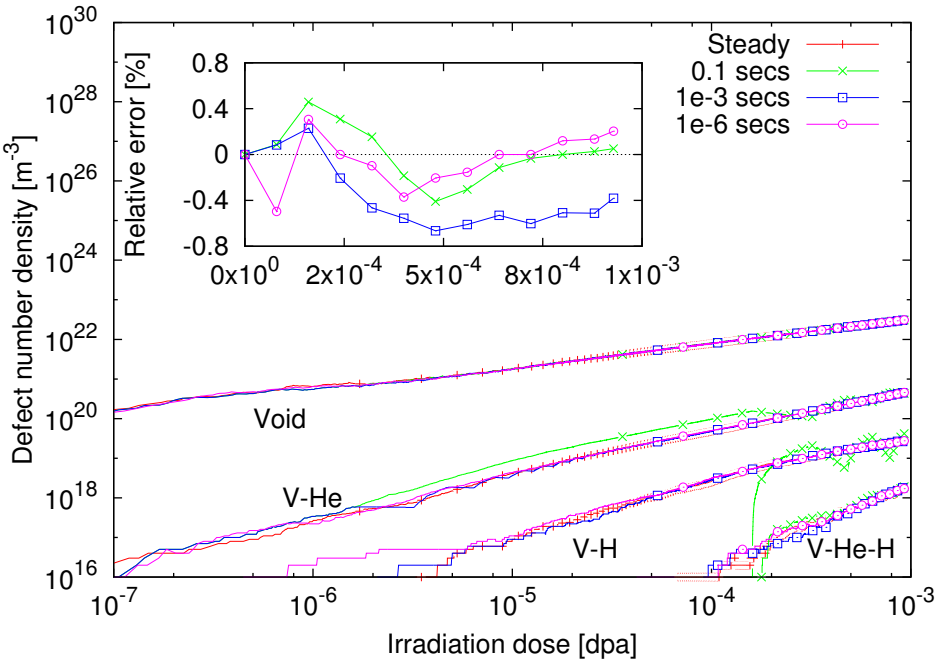

Figure 5.3: Number density of various types of defects formed under pulsed dual-beam and steady triple-beam irradiations. The inset shows relative differences in swelling between pulsed dual-beam irradiations and the steady triple-beam irradiation.

results obtained from pulsed simulations must converge to the steady irradiation case. In these simulations, we set t_1 and t_2 both equal to 1 μs, 1 ms or 0.1 s, respectively. As a consequence, the implantation rates of He^+ and H^+ gas ions in each of these pulses are doubled compared to the corresponding values in the steady triple-ion irradiation case, to 20 $appm/dpa$ and 80 $appm/dpa$, respectively.

As can be seen, pulsed dual-beam irradiations produce results similar to those obtained from steady triple-beam irradiation. As we shorten the pulse duration t_1 and t_2, the results are seen to converge closer to the reference triple-ion irradiation case. It can be seen from the inset of Fig. 5.3 that the differences in predicted swelling are within 0.5% relative to that of the triple-beam case. The average sizes of defect clusters are also observed to be nearly identical between these two irradiation methods.

Even though dual-beam irradiations with short pulses produce results closest to those obtained in steady triple-beam irradiation, they are not quite practical since designing and implementing rapidly switching ion sources can pose significant technical challenges. Therefore, we examined if it would be possible to extend the duration of the irradiation pulses, thus, increase the switching times of He^+, H^+ ion sources. Fig. 5.4 shows the swelling and average sizes of various defect types obtained in bcc-Fe under pulsed dual-beam irradiations with longer pulses, up to 45 s, compared to the reference steady triple-beam case. It can be seen that, even with long pulses, results obtained from these two different irradiation methods are still in good agreement. Therefore, on the basis of our

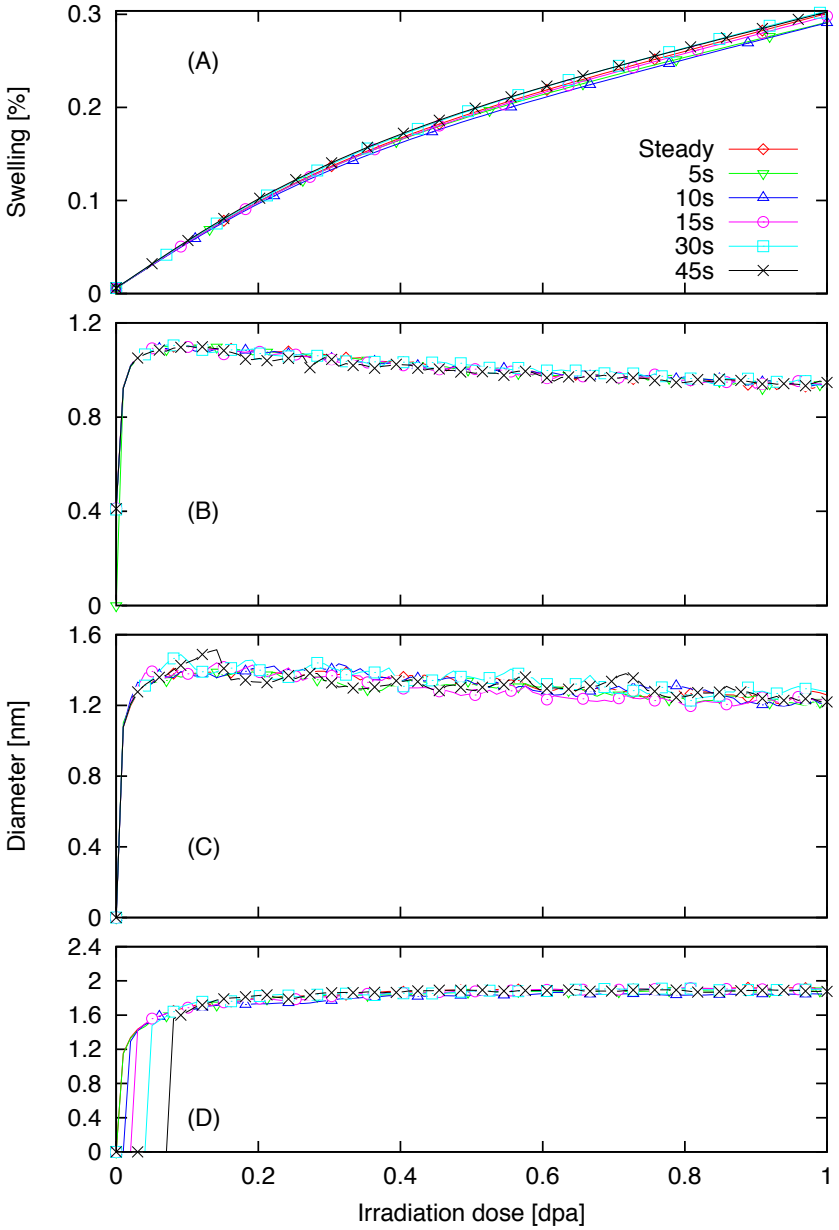

Figure 5.4: Swelling (A) and average sizes of various types of defects, such as voids (B), V-He clusters (C), and V-He-H clusters (D), formed in bcc-Fe under pulsed dual-beam and steady triple-beam irradiations at 783 K.

SCD simulation results, we suggest that pulsed dual-beam irradiations can be used in place of of triple-beam irradiation for investigation of radiation damage evolution. To justify our suggestion, experimental validation will be of great value.

5.3 Comparison between pulsed single-beam irradiation and triple-beam irradiation

Beside pulsed dual-beam irradiation, here we investigate if it is possible to reduce the complexity of the experiment configuration even further by reducing the number of beamlines to one. We performed SCD simulations of pulsed single-beam irradiations in place of triple-beam irradiation in which Fe^{3+}, He^{+} and H^{+} ions are implanted in separate pulses. Similar to the pulsed dual-beam irradiation case, the dose rate of incident ion in each pulse has been adjusted to compensate for the loss of flux during the pulse switched-off periods. The new irradiation dose rate of Fe^{3+} is:

$$\Gamma' = \frac{(t_1 + t_2 + t_3)}{t_1}\Gamma$$

and the new implantation rates of He^{+} and H^{+} gas ions are also increased by a factor of $(t_1 + t_2 + t_3)/t_2$ and $(t_1 + t_2 + t_3)/t_3$, respectively. Here, t_1, t_2, and t_3 is the duration of the Fe^{3+}, He^{+} and H^{+} pulse, subsequently, and Γ is the irradiation dose rate in the steady triple-beam case. The simulation conditions are the same as those applied in the previous pulsed dual-beam simulations, irradiation temperature is 783 K and total damage dose is 10^{-3} *dpa*. Here, the Fe^{3+}, He^{+} and H^{+} pulse durations are set to be the same, thus the corresponding irradiation fluxes are tripled in this case. Similar to the pulsed dual-beam irradiation case, we start with short pulse simulations to examine if pulsed single-beam irradiation can reproduce results obtained from the reference steady triple-beam irradiation case before pursuing the more expensive simulations with longer and more practical pulses. Besides, these simulations allow us to verify the fidelity of our model.

As can be seen in Fig. 5.5, pulsed single-beam irradiation indeed reproduces results obtained from steady triple-beam irradiation. It is apparent that defect populations formed under pulsed single-beam irradiations approach those from the steady triple-beam irradiation reference case. Better agreement between these two irradiation methods is achieved when the length of irradiation pulses is reduced. Similar to the pulsed dual-beam irradiation case, we examine if this agreement still holds at longer pulse lengths. Fig. 5.6 shows the swelling and average sizes of various defect types obtained in bcc-Fe under pulsed single-beam irradiation with longer pulses, up to 5 s. Compared to pulsed dual-beam irradiation results shown in Fig. 5.4, the curves in Fig. 5.6 exhibit some periodic oscillations, larger amplitudes with longer pulses, but they still do not deviate from the steady triple-beam curves. Therefore, it is reasonable to conclude that pulsed single-beam irradiation can be used in place of steady triple-beam irradiation or at least

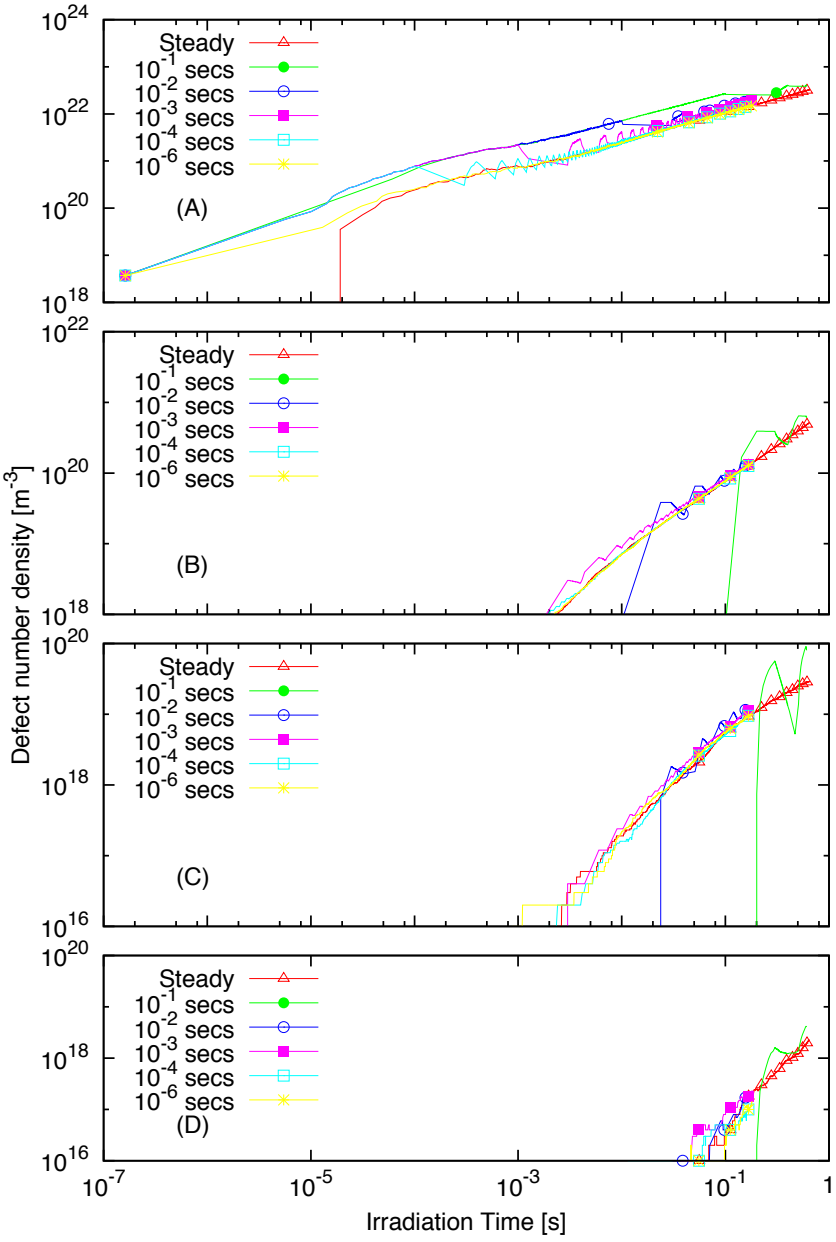

Figure 5.5: Number densities of various types of defects, such as voids (A), V-He clusters (B), V-H clusters (C), and V-He-H clusters (D) formed in bcc-Fe under pulsed single-beam with various short pulse durations compared to those obtained under steady triple-beam irradiation.

can provide us estimates of the results that may be obtained from the steady triple-beam irradiation experiments.

5.4 Conclusion

In this chapter, we have employed our SCD models to understand if pulsed single/dual-beam irradiation can potentially be used in place of steady triple-beam irradiation when testing materials used for nuclear applications. These findings provide us alternative options to investigate the complex kinetics talking place in actual nuclear materials under different irradiation conditions, whenever access to triple-beam testing facilities is limited. For the pulsed dual-beam configuration, He^+ and H^+ gas ions are implanted into the material in alternating pulses whereas the Fe^{3+} ion source is kept steady as in the reference steady triple-ion irradiation case. With pulsed single-beam configuration, Fe^+, He^+ and H^+ ions are all implanted in alternating pulses. The most important requirement is that Fe^+, He^+ and H^+ implantation rates must be adjusted accordingly to compensate for the loss of irradiation fluxes due to the pulsed nature of the beamlines. The pulse length is also important, short pulses provide results that are closer to the steady triple-beam reference case. Our main goal here is to explore if less expensive ion-beam configurations can substitute the expensive and limited-access triple-beam accelerators for studying of complex microstructure evolution in nuclear materials, especially suitable for validating experimental results report by Tanaka *et al.* in Ref. [14]. Exactly how other parameters such as irradiation dose rate, temperature or pulse order, duration and frequency eventually effect the defect populations or the synergy between gas ions are the subjects of ongoing research. However, results reported in this chapter support our hypothesis that the synergistic effects reported in Tanaka's experiments might be overstated since we manage to obtain practically the same results either with simultaneous or sequential irradiation of Fe^+, He^+ and H^+ in bcc-Fe.

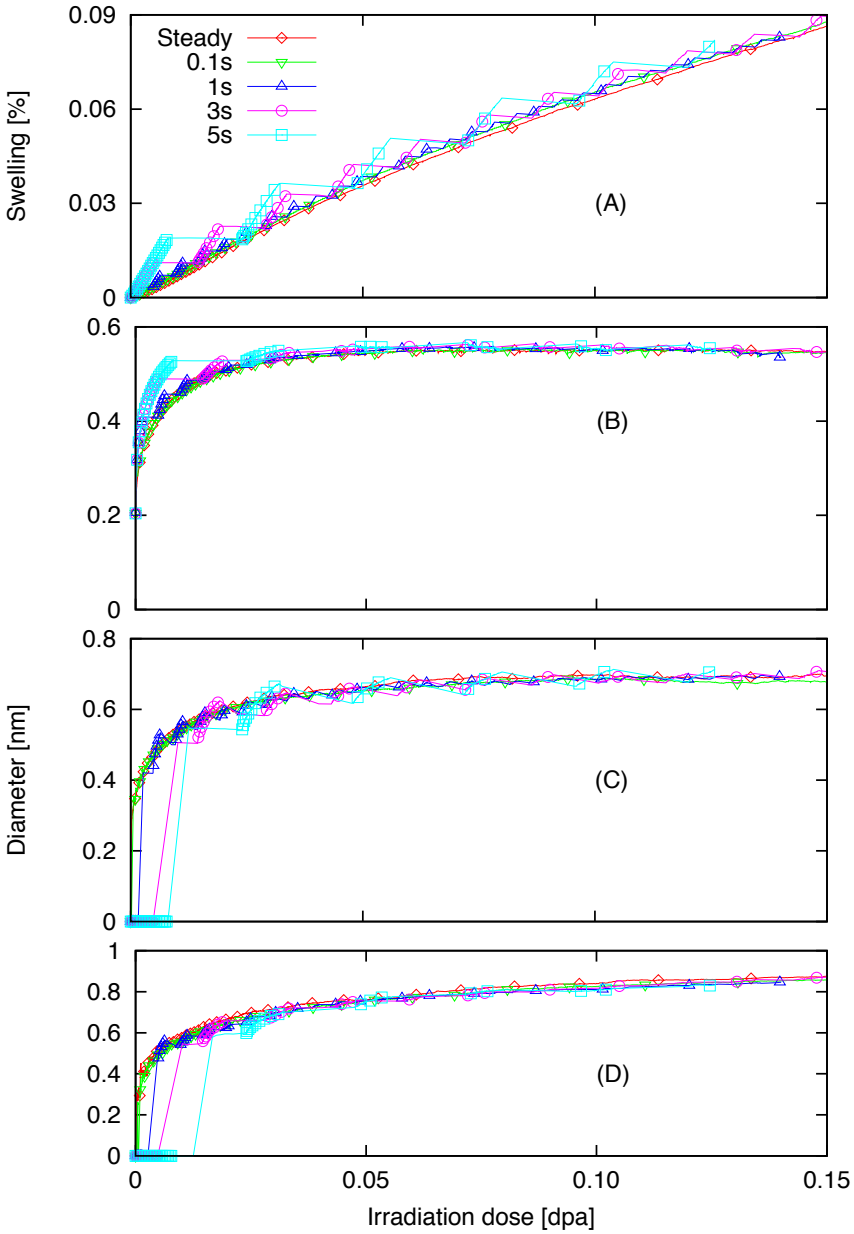

Figure 5.6: Swelling (A) and average sizes of various types of defects, such as voids (B), V-He clusters (C), and V-He-H clusters (D), formed in bcc-Fe under pulsed dual-beam and steady triple-beam irradiations at 783 K.

Chapter 6

Conclusion

Computational models can be used to bridge experimental results obtained from accelerated testing facilities with material behavior in actual nuclear reactors. Mean-field ODE-based reaction rate theory (RT) has been the workhorse for more than 40 years and remains one of the most widely used mesoscale material simulation methods. RT models can simulate damage accumulation over the time scales of accelerated irradiations and reactor lifetimes. However, to handle defect clusters with such complexity as those formed under the multi-ion irradiation conditions, RT models must be modified to expand the size-dimension of defect clusters and to avoid the combinatorial explosion of defect variables.

To address these intrinsic disadvantages of ODE-based RT-models, we introduce the stochastic cluster dynamics (SCD) model that enables efficient simulation of complex damage accumulation in materials irradiated to practical damage doses with reasonable computing time and resources. The key advantage of SCD over ODE-RT is that computational cost is defined principally by the size of simulation volume, meanwhile, with ODE-RT models, the cost is defined mostly by the resolution of the ODE grid and, if defect populations are of complex structures (i.e. consist of many component species), by the dimensionality of the cluster size-space. In ODE-based RT models, computational complexity scales exponentially with the number of size-dimensions, leading to combinatorial explosion, i.e. too many equations that need to be solved. Beside application in radiation damage simulation, our model can be easily adapted to simulate systems where reaction-driven processes are of interest such as advanced fuels, nuclear waster management, and ion-beam synthesis and transmutation doping of nano-structures.

Using SCD models, we investigate the evolution of defects formed under dual and triple-ion irradiation in bcc-Fe in order to gain insights into the development of synergistic effects observed in Tanaka's experiments with several Fe-Cr model alloys. We believe that the observed effects are due to the formation and growth of the V-He-H clusters which formed after an incubation period. These clusters are largest in size in comparison to other types of defects formed due to irradiation. The retention of H appears to play a major role, H atoms are attracted to the large V-He bubbles and further stabilize these clusters. These clusters are very stable under normal temperature conditions and grow

larger as irradiation continues due to the absorption of mobile vacancies in the volume. It has been shown that He:H density ratio has a strong influence on the synergy as well as the overall swelling. There exists a temperature range in which V-He-H clusters can reach maximum sizes, resulting in a high level of swelling within this range. This behavior is directly related to the temperature dependence of defect diffusion coefficients and binding energies. Synergistic effects also strongly depend on the presence of other component elements in the material which can act as sinks for the implanted gas elements. Our results also suggest better quantification of swelling due to small defect clusters formed under dual and triple-ion experiments in order to validate the presence of synergistic effects observed in Tanaka's experiments.

With SCD models, we also suggest that pulsed single/dual-beam irradiation can be used in place of steady triple-beam irradiation to test materials used for nuclear applications, in particular, to study the evolution of defects formed in bcc-Fe under multi-ion irradiations. These studies provide us alternative options to investigate the complex kinetics talking place in materials under different irradiation conditions whenever access to triple-beam testing facilities is limited.

Bibliography

[1] D. T. Gillespie, J. Comput. Phys. **22** (1976) 403–34 1.1, 1.6, 1.6, 1.6, 1.6, 3.2

[2] H. H. McAdams, A. P. Arkin, Proc. Natl. Acad. Sci. USA **94** (1997) 814–19 1.1, 1.6

[3] A. P. Arkin, J. Ross, H. H. McAdams, Genetics **149** (1998) 1633–48 1.1, 1.6

[4] M. B. Elowitz, A. J. Levine, E. D. Siggia, P. S. Swain, Science **297** (2002) 1183–86 1.1, 1.6

[5] J. A. Brinkman, Amer. J. Phys. 24 (1956) 251 (document), 1.1

[6] D. R. Olander, Fundamental Aspects of Nuclear Reactor Fuel Elements: Prepared for the Division of Reactor Development and Demonstration, Energy Research and Development Administration. Oak Ridge, Tenn.: Technical Information Center, Office of Public Affairs, Energy Research and Development Administration, 1976. Print. 1.2

[7] G. S. Was, Fundamentals of Radiation Materials Science Metals and Alloys. Berlin: Springer, 2007. Print. 1.2

[8] F. A. Garner, E. P. Simonen, B. M. Oliver, L. R. Greenwood, M. L. Grossbeck, W. G. Wolfer, P. M. Scott, J. of Nucl. Mater. **356** (2006) 122-135. 1.3, 1.4, 4.3.2, 4.3.2

[9] K. Morishita, R. Sugano, B. D. Wirth, J. of Nucl. Mater. **323** (2003) 243-250. 1.3

[10] D. Terentyev, N. Juslin, K. Nordlund, N. Sandberg, J. Appl. Phys. **105** (2009) 103509. 1.3, 3.5.2, 3.2

[11] L. Ventelon, B.D. Wirth, C. Domain,J. of Nucl. Mater. **351** (2006) 119. 1.3, 3.5.2

[12] A. D. Brailsford, R. Bullough, J. of Nucl. Mater. **44** (1972) 121. 1.6

[13] M. J. Fluss, G. Bench, Accelerated Nuclear Energy Materials Development with Multiple Ion Beams, Fusion-Fission Reasearch Gaithesburg, MD, United States September 30, 2009 through October 2, 2009 1.1, 1.5, 1.5, 1.6

[14] T. Tanaka, K. Oka, S. Ohnuki, S. Yamashita, T. Suda, S. Watanabe, E. Wakai, J. of Nucl. Mater. **329–333** (2004) 294-298. (document), 1.2, 1.5, 1.6, 3.5.1, 3.5.2, 4.1, 4.2, 4.3.1, 4.3.1, 4.6, 4.3.3, 4.3.3, 4.3.4, 5.1, 5.1, 5.4

[15] J. Marian, V. V. Bulatov, J. of Nucl. Mater. **415** (2011) 84-95. (document), 1.6, 2.1, 3.1, 3.1, 3.5.3, 3.5.4

[16] D. T. Gillespie, J. Phys. Chem. **81** (1977) 2340–61. 1.6, 1.6, 1.6

[17] A. B. Bortz, M. H. Kalos, J. L. Lebowitz, J. Comput. Phys. **17** (1975) 10. 1.6

[18] A. F. Voter, Introduction to the kinetic Monte Carlo method, in: K.E. Sickafus, E.A. Kotomin (Eds.), Radiation Effects in Solids, Springer, The Netherlands, 2005. 1.6

[19] N. M. Ghoniem, J. of Nucl. Mater. **179–181** (1991) 99. 1.6

[20] S. Redner, A Guide to First-passage Processes, Cambridge University Press, 2001, p. 214. 1.6

[21] M. von Smoluchowski, Zeitschrift fur Physik **17** (1916) 557. 1.6

[22] U. Gösele, A. Seeger, Phil. Mag. **34** (1976) 177. 1.6

[23] S. L. Hardt, Biophysical Chemistry 10 (1979) 239. 1.6

[24] http://srim.org 1.6

[25] L. Malerba, J. of Nucl. Mater. **351** (2006) 28. 1.6

[26] K. Kitajima, J. of Nucl. Mater. **133–134** (1985) 64. 1.6

[27] Chou, N.M. Ghoniem, J. of Nucl. Mater. **137** (1985) 63. 1.6

[28] N. M. Ghoniem, Phys. Rev. B **39** (1989) 11810. 1.6

[29] A. A. Semenov, C. H. Woo, J. of Nucl. Mater. **205** (1993) 74. 1.6

[30] D. McQuarrie, J. Appl. Probab. **4** (1967) 413–78. 1.6

[31] D. T. Gillespie, Physica A **188** (1992) 404–25. 1.6, 1.6

[32] D. T Gillespie, J. Chem. Phys. 115 (2001) 1716–33. 3.1, 3.2

[33] Cain: Stochastic Simulations for Chemical Kinetics (http://cain.sourceforge.net) 3.1, 3.4.3

[34] StochKit: a Stochastic Simulation Toolbox for Biology (http://www.cs.ucsb.edu/~cse/index2.php?software.html) 3.1, 3.4.3

[35] Y. Cao, H. Li, L. R. Petzold, J. Chem. Phys. **121** (2004) 4059–4067. 3.2

[36] J. M. McCollum, G. D. Peterson, C. D. Cox, M. L. Simpson, N. F. Samatova, Comput. Bio. Chem. **30** (2006) 39–49. 3.2

[37] H. Li, L. R. Petzold. Logarithmic Direct Method for Discrete Stochastic Simulation of Chemically Reacting Systems. Technical Report (2006). 3.2

[38] D. T. Gillespie, L. R. Petzold, J. Chem. Phys. **119** (2003) 8229–8234. 3.4.3

[39] Y. Cao, D. T. Gillespie, L. R. Petzold, J. Chem. Phys. **124** (2006) 044109. 3.4.3, 3.4.3

[40] T. Tian, K. Burragex, J. Chem. Phys. **121** (2006) 10356–10364. 3.4.3

[41] A. Chatterjee, D. Vlachos, M. Katsoulakis, J. Chem. Phys. **122** (2005) 024112. 3.4.3

[42] Y. Cao, D. T. Gillespie, L. R. Petzold, J. Chem. Phys. **123** (.2005) 054104. 3.4.3

[43] U. M. Ascher, L. R. Petzold, Philadelphia: Soc. Ind. Appl. Math. (1998). 3.4.3

[44] M. Rathinam, L. R. Petzold, Y. Cao, D. T. Gillespie, J. Chem. Phys. **119** (2003) 12784–94. 3.4.3, 3.6

[45] Y. Cao, L. R. Petzold, Proc. Found. Syst. Biol. Eng. (FOSBE 2005), pp. 149–52 3.4.3, 3.6

[46] E. L. Haseltine, J. B. Rawlings, J. Chem. Phys. **117** (2002) 6959–6969. 3.6

[47] C. Rao, A. P. Arkin, J. Chem. Phys. **118** (2003) 4999–5010.

[48] Y. Cao, D. T. Gillespie, L. R. Petzold, J. Chem. Phys. **122** (2005) 014116.

[49] Y. Cao, D. T. Gillespie, L. R. Petzold, J. Comput. Phys. **206** (2005) 395–411.

[50] A. Samant, D. G. Vlachos, J. Chem. Phys. **123** (2005) 144114.

[51] Y. Cao, D. T. Gillespie, L. R. Petzold, J. Chem. Phys. **123** (2005) 144917.

[52] E. L. Haseltine, J. B. Rawlings, J. Chem. Phys. **123** (2005) 164115.

[53] E. Weinan, D. Liu, E. Vanden-Eijnden, J. Chem. Phys. **123** (2005)194107.

[54] H. Salis, Y. Kaznessis, J. Chem. Phys. **123** (2005) 214106. 3.6

[55] Workshop on Science Applications of a Triple Beam Capability for Advanced Nuclear Energy Materials, LLNL Report (2009). (document), 1.5, 4.12

[56] E. Martinez, P. R. Monasterio and J. Marian, J Comput Phys. **230** (2011) 1359-1369. 3.6

[57] N. Soneda, T. Díaz de la Rubia, Phil. Mag. A **78** (1998) 995–1019. 3.5.2, 3.3

[58] A. Hardouin Duparc, C. Moingeon, N. Smetniansky-de-Grande, A. Barbu, J. Nucl. Mater. **302** (**Year**) 143–155. 3.5.2

[59] F. Djurabekova, L. Malerba, R. C. Pasianot, P. Olsson, K. Nordlund, Phil. Mag. **90** (2010) 2585. 3.5.2

[60] G. Lucas, R. Schäublin, Journal of Physics: Condensed Matter **20** (2008) 415206. 3.5.2

[66] N. Anento, A. Serra, Yu N. Osetsky, Model. Simul. Mater. Sc. **18** (2010) 025008. 3.2

[67] J. Marian, B. D. Wirth, A. Caro, B. Sadigh, G. R. Odette, J. M. Perlado, T. Diaz de la Rubia, Phys. Rev. B **65** (2002) 144102. 3.2

[68] M. I. Mendelev, Y. Mishin, Phys. Rev. B **80** (2009) 144111. 3.2

[69] F. Djurabekova, L. Malerba, R. C. Pasianot, P. Olsson, K. Nordlund, Phil. Mag. **90** (2010) 2585. 3.2

[70] C. -C. Fu, F. Willaime, Phys. Rev. B **72** (2005) 064117. 3.2

[71] D. M. Stewart, Yu N. Osetsky, R. E. Stoller, S. I. Golubov, T. Seletskaia, P. J. Kamenski, Phil. Mag. **90** (2010) 935. 3.2

[72] D. E. Jiang, E. A. Carter, Phys. Rev. B **70** (2004) 064102. 3.2

[73] C. -C. Fu, J. Dalla Torre, F. Willaime, J. -L. Bocquet, A. Barbu, Nature Mater **4** (2005) 68. 3.3

[74] V. V. Kirsanov, M. V. Musina, V. V. Rybin, J. of Nucl. Mater. **191–194** (1992) 1318-1322. 4.3.2

[75] T. Ishizaki, Q. Xu, T. Yoshiie, S. Nagata, T. Troev, J. of Nucl. Mater. **307–311** (2002) 961-965. 3.5.2, 4.3.2

[76] E. Abramov, D. Elizer, J. Mater. Sci. Lett. **7** (1988) 108-110. 1.3, 1.4, 4.3.2, 4.3.2

[77] G. D. Tolstolutskaya, V. V. Ruzhytskiy, I. E. Kopanets, S. A. Karpov, V. V. Bryk, V. Voyevodin, F. A. Garner, J. Nucl. Mater. 356 (2006) 136–47. 4.3.2

[78] F. A. Garner, B. M. Oliver, L. R. Greenwood, M. R. James, P. D. Ferguson, S. A. Maloy, W. F . Sommer, J Nucl. Mater. **296** (2001) 66-82. 4.3.2

[79] E. Hayward, C. Deo, J. Phys.: Condens. Matter **24** (2012) 265402. 4.3.2

[80] W. A. Counts, C. Wolverton, R. Gibala, Acta Materialia **58** (2010) 4730. 4.3.3

[81] D. J. Reed, Rad. Eff. **31** (1977) 129. 4.3.3

[82] T. Tanabe, H. Hirano, D. Imoto, J. Nucl. Mater. **151** (1987) 38. 4.3.3

[83] D. Brimbal, E. Meslin, J. Henry, B. Decamps, A. Barbu, Acta Materialia **61** (2013) 4757. 4.3.2, 4.3.4

[84] A. F. Voter, Phys. Rev. B **57** (1998) R13985–R13988. 3.6

[85] O. V. Borodin, V. V. Bryk, A. S. Kalchenko, V. V. Melnichenko, V. N. Voyevodin, F. A. Garner, J. Nucl. Mater. **442** (2013) S817–S820. 4.3.4

[86] N. M. Ghoniem, G. L. Kulcinski, J. Nucl. Mater. **69&70** (1978) 816. 5.1

[87] N. M. Ghoniem, J. Nucl. Mater. **89** (1980) 359. 5.1

[88] N. M. Ghoniem, H. Gurol, Radiation Effects **55** (1981) 209. 5.1

[89] E. P. Simonen, N. M. Ghoniem, N. H. Packan, J. Nucl. Mater. **122&123** (1984) 391. 5.1

[90] S. I. Golubov, R. E. Stoller, A. V. Barashev, ORNL Report. 5.1

[91] M. Koiwa, Journal of the Physics Society of Japan **37** (1974) 1532. 1.6

[92] A. E. Sand, S. L. Dudarev, K. Nordlund, EPL **103** (2013) 46003. 1.6

[93] Kögler, A. Mücklich, L. Vines, D. Krecar, A. Kuznetsov, W. Skorupa, Nucl. Instrum. Meth. B **257** (2007) 161-164 1.6

[94] E. Wakai, T. Sawai, K. Furuya, A. Naito, T. Aruga, K. Kikuchi, S. Yamashita, S. Ohnuki, S. Yamamoto, H. Naramoto, S. Jistukawa, J. Nucl. Mater. **307-311** (2002) 278-282. (document), 4.2

[95] S. Martin, R. Balzer, G. Bonani, W. Wölfli, Nucl. Instr. and Meth. B **5** (1984) 242-246. 5.1

[96] J. S. Gordon, D. G. Armour, S. E. Donnelly, J.A. van den Berg, D. Marton, J.W. Rabalais, Nucl. Instr. and Meth. B **59/60** (1991) 312-315.

(document), 5.1, 5.1